

District of Ucluelet Coastal Flood Mapping

Appendix A: Coastal Flood Hazard Analysis (Cascadia Coast Research)



CASCADIA COAST
RESEARCH LTD.

Coastal Flood Hazard Analysis: The District of Ucluelet, BC.

Clayton Hiles, P.Eng
Roy A Walters, PhD
Ignacio Beya, B.Eng
Cascadia Coast Research, Ltd.

June 19, 2020



Client

Ebbwater Consulting
Unit 510 119 West Pender St.
Vancouver, BC V6B 1S5

Disclaimer

This document has been prepared by Cascadia Coast Research Ltd. for the exclusive use and benefit of Ebbwater Consulting Inc. and the District of Ucluelet for specific application to *District of Ucluelet Coastal Floodplain Mapping*. No other party is entitled to rely on the contents of this document and associated digital files, in whole or in part, without specific written authorization from Cascadia Coast Research Ltd.

This document was prepared in accordance with generally accepted engineering practices and represents the best professional judgement of Cascadia Coast Research Ltd. based on the information available at the time of its completion and as appropriate for the project scope of work. No warranty, express or implied, is made.

This document and associated materials are copyright Cascadia Coast Research Ltd, 2020.

Revision History

Rev.	Date	Authour	Description	Signature
0	2020-05-17	Clayton Hiles	First Draft	
1	2020-05-27	CH, RW, IB	Draft to DOU	
2	2020-06-19	CH	Final	Original signed by Clayton Hiles

Summary

Cascadia Coast Research Ltd. was retained as a sub-consultant to Ebbwater Consulting Inc. to conduct the coastal analyses necessary for the estimation of flood construction levels (FCLs) in the District of Ucluelet (DOU). Flood construction level defines the elevation of the underside of a wooden floor system or top of concrete slab for habitable buildings and is calculated as the flood construction reference plane (FCRP) plus an appropriate freeboard allowance. FCRP is calculated as the maximum water elevation during the design flood event including allowance for future sea level rise and vertical land movement. In this work, both storm and tsunami flood hazards were assessed considering a range of sea level rise scenarios.

Relative sea level rise (RSLR) is the rise in mean sea level relative to a fixed land reference. Included is both the effect of rising sea levels and vertical land movement. The BC Provincial Guidelines for Coastal Flood Hazard Land Use suggest planning for 1.0 m of sea level rise by 2100. This study considers RLSR scenarios of 0.0, 0.5, 1.0, and 2.0 m independent of any specified year of occurrence. This range of scenarios enables short to long term planning and provides the necessary inputs for future risk assessments.

Storm flooding hazard was assessed using a response-based approach. A combination of measured and modelled data was used to synthesize a hind-cast of water levels and waves in the DOU over the past 40 years (1979-2018). This hind-cast includes: tides, storm surge (PDO/ENSO), local wind setup, wave setup, and runup. The hind-cast was then used to calculate the response of interest: the total elevation of the 2% exceedance wave runup. Extreme value analysis of the hind-cast total runup elevation was then used to calculate the frequency-magnitude curves for each of 48 shorelines reaches. The hind-cast and extreme value analysis procedure was repeated for RSLR = 0.0, 0.5, 1.0, and 2.0 m and corresponding FCRP estimates were derived.

The project budget allowed only a limited scope of tsunami hazard assessment so a conservative approach was adopted. Two tsunami sources were considered, the Cascadia Subduction Zone (CSZ), and the Aleutian Subduction zone. Based on the available literature, it is assumed that a rupture of the CSZ poses the greatest hazard to the DOU. Tsunami simulations were executed for six different candidate CSZ fault rupture models (one *traditional*, one buried rupture, two splay, and two trench-breaching). FCRPs from these simulated events were calculated based on the estimated maximum water elevation during the event, including the influence of tide and sea level rise. The impact of the 1964 Alaska earthquake at the was also considered based on the available literature and community accounts of the event. A full probabilistic tsunami hazard assessment was not within the scope of this work.

The estimated tsunami FCRPs are larger than the storm FCRPs. The tsunami FCRPs are defined mostly by one of the splay rupture scenarios, which generates inundation levels of almost twice the buried rupture scenario. Only in areas with steep shoreline, exposed to high energy waves, are storm and tsunami FCRPs estimates similar. For the RSLR = 1 m scenario, the FCRP varies from about 12 to 16 m on the exposed outer coast of the Ucluelet Peninsula. Inside Ucluelet Inlet the FCRP decreases to about 10 m between Lyche Island and Kvarno Island. At the head of the Inlet the FCRP increases again to about 12 m.

The freeboard allowance in the calculation of flood construction levels is intended to account for uncertainties in the hazard analysis. While a freeboard value of 0.6 m is generally accepted for storm flood hazard, there is no such generally accepted value for tsunami flood hazard. Uncertainties exist in the tsunami flood estimates due to the deformation model, bathymetry and most significantly because the analysis was limited to a small set of events. A 50% *factor for public safety* has been applied when defining tsunami hazard elevations in other BC jurisdictions. A similar factor for public safety may be applied at the DOU, however, it is acknowledged that this may not be practical to do so, given the very large estimated inundation levels. At minimum, when defining the tsunami hazard line, all available data concerning potential tsunami inundation should be considered, including all simulations from this work and others.

Contents

List of Figures	7
List of Tables	10
List of Acronyms	11
1 Introduction	12
2 Background	13
2.1 Site Description	13
2.2 Coastal Storm Exposure	16
2.3 Tsunami Exposure	16
3 Methods	18
3.1 Relative Sea Level Rise	18
3.2 Storm Hazard Assessment	18
3.3 Tsunami Hazard Assessment	20
4 Geo-Spatial Analysis	21
4.1 Vertical Datum	21
4.2 Digital Elevation Model	21
4.3 Shoreline Geometry	25
5 Storm Hazard Assessment	26
5.1 Coastal Hind-cast	26
5.1.1 Tides	26
5.1.2 Storm Surge	27
5.1.3 Local Winds	27
5.1.4 Wind Setup	28
5.1.5 Wave Conditions	28
5.1.6 Wave Effect	30
5.1.7 Total Wave Runup Elevation	31
5.2 Hind-cast Evaluation	32
5.3 Extreme Value Analysis	33

6	Tsunami Hazard Assessment	35
6.1	1964 Alaska Earthquake	35
6.2	Cascadia Subduction Zone Eathquake	36
6.3	Tsunami Simulation	37
6.3.1	Grid generation	37
6.3.2	Initial and boundary conditions	40
6.3.3	Numerical model	41
6.4	Tsunami Results	42
7	Results and Discussion	48
7.1	Flood Construction Reference Plane	48
7.2	Uncertainties and Freeboard Recommendations	50
8	References	51
	Appendices	54
A	Inlet Resonance Analysis	54
B	Cascadia Subduction Zone Fault Rupture Models	56
C	Tsunami Hazard Results	58
C.1	G2018-B	58
C.2	G2018-S-A	62
C.3	G2018-S-B	65
C.4	G2018-T-50	68
C.5	G2018-T-100	71
C.6	W2003	74
D	Wave model evaluation	77
E	Wave Runup Hind-cast Evaluation	84
F	Storm Hazard Results	88
G	Hydrodynamic Model Description	92
G.1	Time discretization	93

G.2 Space discretization	93
G.3 Wetting and drying algorithm	94

List of Figures

1	Screenshot of CHS navigation chart covering the Ucluelet. NOT FOR NAVIGATION.	14
2	GoogleEarth satellite image of the DOU.	15
3	Bathymetric and topographic data used in constructing the DEM	23
4	Bathymetric and topographic data used in constructing the DEM, detail of the DOU.	24
5	Location of reaches and representative transects.	25
6	A schematic showing the relationship between data (grey), models (blue) and results (yellow) in the coastal hind-cast.	27
7	Wind rose of wind direction and intensities as measured on at the La Perouse Weather Buoy. Colour indicates wind speed, the spoke orientation indicates the direction the wind is blowing to, the dotted concentric circles indicate frequency of occurrence.	28
8	Average element length of the wave model grid. Triangles indicate locations of wave measurement buoys.	29
9	Scatter of measured and modelled (WavewatchIII) significant wave height at the La Perouse weather buoy.	31
10	Wave impacting the Amphitrite Lighthouse. Estimated observed elevation is 9.3 m, modelled runup elevation is 10.3 m. Photo credit: John Towgood.	32
11	Average element length of the Tsunami model grid.	38
12	Average element length of the Tsunami model grid, detail of the DOU.	39
13	The G2018-S-A fault deformation model, interpolated onto the tsunami model grid.	41
14	Maximum tsunami amplitude for the G2018-S-A fault rupture model.	43
15	Time series of tsunami water elevation for the G2018-S-A rupture (relative to mean sea level). Transect numbers indicated in legend.	44
16	Time series of tsunami water elevation for all simulated ruptures, at transect 38 (relative to mean sea level).	44
17	Maximum tsunami amplitude for G2018-S-A rupture, detail of the DOU. Ambient water level = 2 m (2 m tide + 0 m RSLR).	45
18	Maximum tsunami current speed for G2018-S-A rupture, detail of DOU. Ambient water level = 2 m (2 m tide + 0 m RSLR).	46
19	Inlet amplification factor at Ucluelet for each of the simulated tsunami.	55
20	Inlet amplification factor at Ucluelet based on synthesized spectral forcing.	55
21	Fault rupture models used in tsunami modelling. Only vertical component of rupture is considered.	57
22	Maximum tsunami amplitude during for each fault rupture scenario. Ambient water level = 2 m (2 m tide + 0 m RSLR).	59

23	Maximum tsunami amplitude for rupture G2018-B, relative to ambient water level. Ambient water level = 2 m (2 m tide + 0 m RSLR).	60
24	Maximum tsunami current speed for rupture G2018-B. Ambient water level = 2 m (2 m tide + 0 m RSLR).	61
25	Maximum tsunami amplitude for rupture G2018-S-A, relative to ambient water level. Ambient water level = 2 m (2 m tide + 0 m RSLR).	62
26	Maximum tsunami current speed for rupture G2018-S-A. Ambient water level = 2 m (2 m tide + 0 m RSLR).	63
27	Maximum tsunami amplitude for rupture G2018-S-B, relative to ambient water level. Ambient water level = 2 m (2 m tide + 0 m RSLR).	65
28	Maximum tsunami current speed for rupture G2018-S-B. Ambient water level = 2 m (2 m tide + 0 m RSLR).	66
29	Maximum tsunami amplitude for rupture G2018-T-50, relative to ambient water level. Ambient water level = 2 m (2 m tide + 0 m RSLR).	68
30	Maximum tsunami current speed for rupture G2018-T-50. Ambient water level = 2 m (2 m tide + 0 m RSLR).	69
31	Maximum tsunami amplitude for rupture G2018-T-100, relative to ambient water level. Ambient water level = 2 m (2 m tide + 0 m RSLR).	71
32	Maximum tsunami current speed for rupture G2018-T-100. Ambient water level = 2 m (2 m tide + 0 m RSLR).	72
33	Maximum tsunami amplitude for rupture W2003, relative to ambient water level. Ambient water level = 2 m (2 m tide + 0 m RSLR).	74
34	Maximum tsunami current speed for rupture W2003. Ambient water level = 2 m (2 m tide + 0 m RSLR).	75
35	Modelled and measured H_{m0} time-series at Amphitrite Bank.	77
36	Modelled and measured H_{m0} scatter at meds336.	78
37	Modelled and measured H_{m0} quantile-quantile plot at Amphitrite Bank.	78
38	Modelled and measured T_p time-series at Amphitrite Bank.	79
39	Modelled and measured H_{m0} time-series at Florencia Bay.	79
40	Modelled and measured H_{m0} scatter at Florencia Bay.	80
41	Modelled and measured H_{m0} quantile-quantile plot at Florencia Bay.	80
42	Modelled and measured T_p time-series at Florencia Bay.	81
43	Modelled and measured H_{m0} time-series at Long Beach.	81
44	Modelled and measured H_{m0} scatter at Long Beach.	82
45	Modelled and measured H_{m0} quantile-quantile plot at Long Beach.	82
46	Modelled and measured T_p time-series at Long Beach.	83

47	Wave wash as viewed from a lookout up-shore of Melfort Pass. Estimated observed elevation is 9.6 m, modelled runup elevation is 7.75 m. Photo credit: John Towgood.	84
48	Erosion of an engineered shoreline at Terrace Beach. Estimated observed elevation is 4.5 m, modelled runup elevation is 5.5 m. Photo credit: John Towgood.	85
49	LiDAR contours over ortho photo showing logs on the rocky beach slope of reach 1.	86

List of Tables

1	Data sources for the digital elevation model.	21
2	Evaluation statistics comparing SWAN wave model estimates to observations at the La Perouse weather buoy (c4606)	30
3	Comparison of the observed and modelled runup elevation during the Jan 18, 2018 storm.	33
4	Estimated FCRP (m) for 1 m RSLR associated with the 0.5% and 0.2% AEP events. L, M and U indicate lower (5%), maximum likelihood and upper (95%) confidence estimates.	34
5	Fault models used for tsunami simulation.	40
6	Tsunami results for all simulated ruptures, at transects for the RSLR = 0 m scenario.	47
7	Comparison of FCRP estimates based on tsunami and 0.2% AEP storm flooding hazard at each transect.	49
8	Tsunami results for G2018-B rupture, at transects, for each RSLR scenario. ΔZ is the local subsidence, <i>Amp</i> is the tsunami amplitude.	58
9	Tsunami results for G2018-S-A rupture, at transects, for each RSLR scenario. ΔZ is the local subsidence, <i>Amp</i> is the tsunami amplitude.	64
10	Tsunami results for G2018-S-B rupture, at transects, for each RSLR scenario. ΔZ is the local subsidence, <i>Amp</i> is the tsunami amplitude.	67
11	Tsunami results for G2018-T-50 rupture, at transects, for each RSLR scenario. ΔZ is the local subsidence, <i>Amp</i> is the tsunami amplitude.	70
12	Tsunami results for G2018-T-100 rupture, at transects, for each RSLR scenario. ΔZ is the local subsidence, <i>Amp</i> is the tsunami amplitude.	73
13	Tsunami results for W2003 rupture, at transects, for each RSLR scenario. ΔZ is the local subsidence, <i>Amp</i> is the tsunami amplitude.	76
14	Details of wave measurement buoys used in model evaluation.	77
15	Comparison of hind-cast runup elevation for 10 largest events to observed evidence of storm activity for different shoreline reaches.	87
16	Estimated FCRP (m) for 0.0 m RSLR associated with 6.67%, 2%, 1%, 0.5% and 0.2% AEP (return periods of 15, 50, 100, 200 and 500 years). L, M and U indicate lower (5%), maximum likelihood and upper (95%) confidence estimates.	88
17	Estimated FCRP (m) for 0.5 m RSLR associated with 6.67%, 2%, 1%, 0.5% and 0.2% AEP (return periods of 15, 50, 100, 200 and 500 years). L, M and U indicate lower (5%), maximum likelihood and upper (95%) confidence estimates.	89
18	Estimated FCRP (m) for 1.0 m RSLR associated with 6.67%, 2%, 1%, 0.5% and 0.2% AEP (return periods of 15, 50, 100, 200 and 500 years). L, M and U indicate lower (5%), maximum likelihood and upper (95%) confidence estimates.	90
19	Estimated FCRP (m) for 2.0 m RSLR associated with 6.67%, 2%, 1%, 0.5% and 0.2% AEP (return periods of 15, 50, 100, 200 and 500 years). L, M and U indicate lower (5%), maximum likelihood and upper (95%) confidence estimates.	91

List of Acronyms

AEP	Annual Exceedance Probability
CD	Chart Datum
CFSR	Climate Forecast System Reanalysis
CHS	Canadian Hydrographic Service
cph	Cycles per hour
CSZ	Cascadia Subduction Zone
DEM	Digital Elevation Model
DFL	Designated Flood Level
DIM	Direct Integration Method
EC	Environment Canada
ENC	Electronic Navigation Chart
ENSO	El Nino Southern Oscillation
EGBC	Engineers and Geoscientists of BC
EVA	Extreme Value Analysis
FCL	Flood Construction Level
FCRP	Flood Construction Reference Plane
FEMA	Federal Emergency Management Agency
GD	Geodetic Datum
GFS	Global Forecast System
HHWLT	Higher High Water Large Tide
IPCC	Intergovernmental Panel on Climate Change
LiDAR	Light Detection And Ranging
MSL	Mean Sea Level
NCEP	National Centers for Environmental Prediction
PDO	Pacific Decadal Oscillation
DOU	District of Ucluleet
RSLR	Relative Sea Level Rise
SLR	Sea Level Rise

1 Introduction

The District of Ucluelet has recognized the importance of understanding their exposure coastal flood hazard especially in the context of rising sea levels. They have engaged Ebbwater Consulting Inc. and Cascadia Coast Research Ltd. to conduct the coastal analyses and mapping necessary to produce a set of modern coastal flood hazard maps.

Cascadia Coast Research Ltd., working as a sub-consultant to Ebbwater Consulting inc., was responsible for the ocean analyses necessary for the estimation of flood construction levels. This work generally follows the various BC guidelines for coastal flood hazard assessment [5, 6, 7, 3, 8] and includes:

- Assessment of storm induced flooding hazard, including the effects of sea level rise, vertical land movement, tides, storm surge, wind setup, wave setup and wave runup.
- Assessment of tsunami induced flooding hazard due to a Cascadia Subduction Zone rupture event, including the effects of sea level rise, vertical land movement, tsunami runup and subsidence.

This report is structured as follows:

- Section 2 provides background on the study location as well as tsunami and storm flooding exposure.
- Section 3 summarizes the methods used for tsunami and storm flooding hazard assessment.
- Section 4 summarizes the geo-spatial analysis required to enable the storm and tsunami ocean modelling.
- Section 5 details the process of the storm hazard assessment.
- Section 6 details the process of the tsunami hazard assessment.
- Section 7 presents and compares the results of of each hazard assessment.

2 Background

2.1 Site Description

The District of Uclulet (DOU) is a small community on the West Coast of Vancouver Island, on the Western extent of Barkley Sound (see Figures 1 and 2). It covers the Ucluelet Peninsula, is bordered to the North by the territory of the Yuułuʔiłʔath (Ucluelet) First Nation, and is south-west of the Pacific Rim National Park. The DOU has about 1,700 permanent residents, however the population increases significantly during the summer months as thousands of tourists visit the area's many beaches and other natural attractions.

Given the DOU's geography on a small peninsula, most of the population and infrastructure is in close proximity to the shore. Steep rocky shorelines are prevalent through much of the District and provide a measure of protection against coastal flooding. However the magnitude of the potential storm and tsunami forces are considerable at Ucluelet.

The scope of the present work includes the exposed Pacific shores of the DOU, and the more protected shores inside Ucluelet Inlet, including all areas of the inlet, even those which are outside of the DOU's borders.

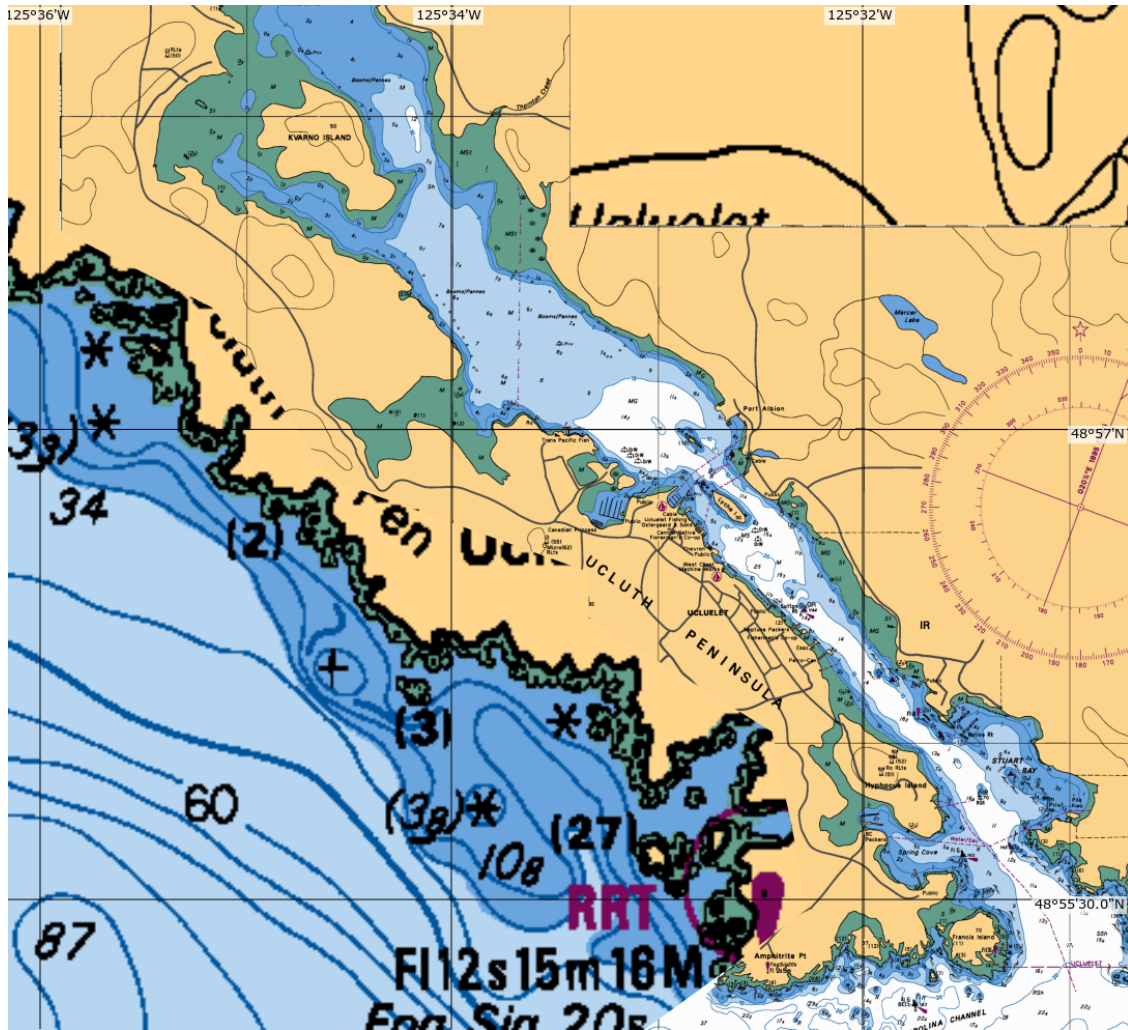


Figure 1: Screenshot of CHS navigation chart covering the Ucluelet. NOT FOR NAVIGATION.

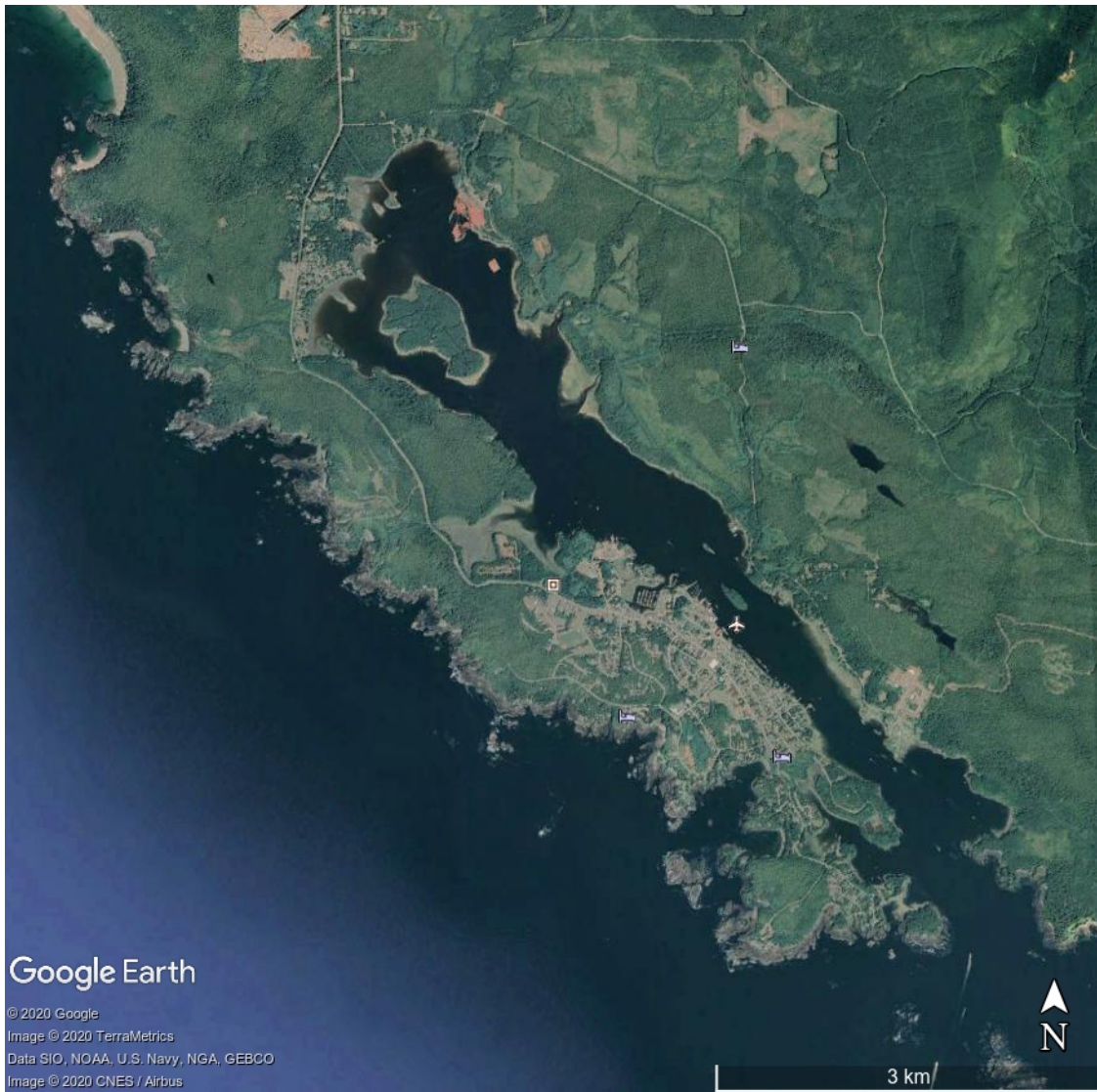


Figure 2: GoogleEarth satellite image of the DOU.

2.2 Coastal Storm Exposure

A number of physical processes, or 'components', combine to produce coastal storm flooding. Each component can be categorized as short term processes, acting over a period of a few minutes to a few months (tides, storm surge, wind setup, wave setup), or long term processes, acting over months or more (El Nino, the Pacific Decadal Oscillation, sea level rise, subsidence/uplift).

Tides in the DOU are mixed semi diurnal with a range of about 4.0 m and a maximum elevation of 2.0 m GD. Tides are larger in the winter and smaller in the summer. The maximum tidal elevation occurs once every 18.6 years, but comes close for a few tides each year. These yearly large tides are often referred to as King Tides. Tides are often the largest contributor to high water events within Ucluelet Inlet.

Storm surge events observed at the DOU are usually associated with low pressure systems that propagate off the Pacific into BC coastal waters. Water levels associated with storm surge usually peak at less than 0.5 m but can be greater than 1.0 m on top of ambient water levels and persist for a few hours to a few days. Within Ucluelet Inlet, storm surge is usually the second largest contributor to high water events.

The DOU is directly exposed to the Pacific Ocean on the south west shore. Large wave breaking on the beach causes both a static increase in water level (wave setup) and a dynamic, oscillating variation in water level (wave runup). Wave setup and runup are primarily proportional to incident wave height but also depend on wave period, shore slope, direction relative to shore and other characteristics. Wave runup is generally the largest contributor to high water level events on the west shore of the DOU.

Wind setup is associated with strong local onshore winds blowing over shallow water. While wind setup impacts all shores of the DOU, it is significant for coastal flooding only inside Ucluelet Inlet. Wind setup will endure as long as high winds blow onshore over the shallow fetch, typically not more than a few hours. Wind setup is generally the water level component with the smallest magnitude.

Inter-annual climate variations including the Pacific Decadal Oscillation (PDO) and El Nino Southern Oscillation (ENSO) also affect water levels in the DOU. Variations of sea level with these oscillations are mostly due to fluctuations in water temperatures which cause thermal expansion and contraction of the sea water. These effects have been reported to influence water levels by as much as 40 cm [2]. In practical applications the effect of these longer term variations is often lumped in with storm surge.

Of the physical processes which affect water level, only the tides are deterministic. This means that we can calculate the specific level of the tides at a certain time well into the future. When water level measurements are made at tide stations, the measurements contain both the deterministic component of the tides and probabilistic component due to storm surge and wind setup.

2.3 Tsunami Exposure

Tsunami are long-period surface waves generated by earthquakes, volcanic eruptions, landslides or other sudden movement of the earth-ocean interface. In the deep ocean, tsunami travel very fast but may not be large in height. As the tsunami wave reaches shallower water near shore, the wave slows down and increases in height dramatically. As the wave reaches shore it usually looks more like a sudden increase in water level inundating the shore than it does a typical surf wave.

The DOU's is positioned on the edge of the Pacific Ocean within the "Ring of Fire"¹, named for the abundant earthquakes and volcanic eruptions in the region. As such the DOU is exposed to hazard from many remote, regional and local tsunami sources. Available literature suggest that a megathrust fault of the Cascadia Subduction Zone (CSZ) poses the largest hazard to the DOU [1]. This fault occurs where the Explorer,

¹<https://earthquake.usgs.gov/learn/glossary/?termID=150>

Juan de Fuca and Gorda Plates subduct under the North America Plate. The fault stretches from Northern California to British Columbia. The last known major earthquake from this fault occurred in 1700 and caused a large tsunami which impacted North America and Japan.

3 Methods

The purpose of this analysis is to provide the basis for calculation of *flood construction levels (FCLs)* throughout the DOU. Flood construction levels are estimated based on the flood hazard at the study location. The West Coast of Vancouver Island is vulnerable to both storm flooding and tsunami flooding, so both must be considered in a hazard analysis [3].

Flood construction level defines the elevation of the underside of a wooden floor system or top of concrete slab for habitable buildings and is calculated as the flood construction reference plane (FCRP) plus an appropriate freeboard allowance. FCRP corresponds to the estimated elevation of the future natural boundary and is calculated as water elevation during the design flood event plus allowance for future sea level rise and vertical land movement.

3.1 Relative Sea Level Rise

Sea level rise due to global climate change is an important factor driving this coastal hazard study. Relative sea level rise (RSLR) is the rise in mean sea level relative to a fixed land reference. Included is both the effect of rising sea levels and vertical land movement.

According to the IPCC (2013) report, global sea levels have been rising at a rate of 3.2 mm/year since 1993 and about 1 mm/year over the last 100 years [4]. The BC Provincial Guidelines for Coastal Flood Hazard Land Use [5, 6, 7, 3, 8] suggest planning for 1m of sea level rise by 2100, however estimates in the literature vary considerably, with studies since 2013 tending to revise towards larger values [9].

Due to residual glacial isostatic effects and tectonic activity in the British Columbia Coast, relative sea level rise (RSLR) has been significantly less than the global mean. At nearby Tofino, tide gauge measurements have been used to estimate a RSLR rate over the last 60+ years as decreasing at approximately 0.9 mm/year [10]. The same study estimated an uplift rate of 2.6mm/year, and a resultant absolute sea level rise of 1.7mm/year.

In this study, we consider RSLR scenarios of 0, 0.5 1.0 and 2.0 m independent of any specified year of occurrence. This range of scenarios will enable short to long term planning.

While a range of RSLR scenarios are considered, the potential associated morphological changes are not. For this work the current bathymetry/topography of the region is assumed to remain constant in the future despite sea level rise.

3.2 Storm Hazard Assessment

For storm driven coastal flooding, the FCL is based on an estimated extreme flooding condition which includes the effects of:

- Future relative sea level rise
- Tides
- Storm surge
- Wave effect
- Freeboard

The BC Flood Hazard Land Use Guidelines [3] and EGBC Professional Practice Guidelines for Flood Mapping in BC [8] suggest that FCLs for storm flooding be based on an annual exceedance probability (AEP) of 0.5% or 0.2% (200 or 500 year return period) depending on the application. To aid in the planning and risk evaluations process, this work calculates flood magnitude at 6.67%, 2%, 1%, 0.5% and 0.2% AEP (return periods of 15, 50, 100, 200 and 500 years).

In Canada, the historical record is rarely long enough to contain a storm with the target level of probability. In this case, it is required to estimate the conditions of the design storm from the available data. There are many methods to do this but most rely in some way on extreme value analysis.

Extreme value analysis (EVA) is a branch of statistics addressing extreme deviations from the median of probability distributions. It seeks to assess, from an ordered sample of a random variable, the probability of events that are more extreme than any previously observed. Independent extreme events contained within the historical record are ordered and fit with a theoretical extreme value distribution. The magnitude of events with probability beyond the extent of the historical record can then be estimated with the fit distribution.

A key assumption in EVA is that the climate is statistically stationary, meaning that it is not changing with time. Based on assessment of annual maximum wave records in the North East Pacific, Erikson [12] concludes that stationarity is an acceptable assumption for 1979 to 2009. Weather patterns in the Eastern North Pacific will change with global climate change, and these changes will be different from region to region. Studies to date do not predict a large change in storm activity in the region of the DOU over the next century [12, 13, 14], however, future research may suggest otherwise.

An event based approach to flood hazard assessment is often applied in BC. In this approach, one or more designated storms are specified based on the analysts' knowledge of local coastal weather patterns and storm responses. If storm surge was thought to be the most important component to coastal flooding, an analyst may, for example, seek a storm surge event with a particular probability of occurrence, then estimate wind and wave conditions which are likely to accompany that surge event. The design storm is then combined with a high tide and relative sea level rise to enable calculation of the FCRP. This approach has the benefit that it can be very efficient and works reasonably well where the shoreline under study is similarly exposed to storm conditions and one flooding component tends to dominate the others. The drawback of this approach is that usually multiple flooding components are important and to different degrees at different locations. To address these issues a larger set of design storms may be specified, but even so assigning a probability to these storms with confidence remains a challenge [15].

Alternatively, a response-based approach to flood hazard analysis may be used. In this approach, all factors affecting water flooding are hindcast over a long period (40+ years). The benefit of this approach is that there is no need to assign a probability to each of the individual water level components; the joint probability of the individual sea level components is inherently contained within the hindcast. Extreme value analysis can be performed directly on the response of interest. While this approach is computationally expensive it is less reliant on the judgement of the analyst to determine extreme flooding levels. The response-based approach is advocated by FEMA for coastal flood hazard analysis on the Pacific Coast [15].

In this work a response-based approach was applied. A combination of measured and modelled data has been used to synthesize a hind-cast of water levels and waves in the DOU over the past 40 years (1979-2018). This hindcast includes: tides, storm surge (PDO/ENSO), local wind setup and wave setup and runup. The response of interest, the total elevation of the 2% exceedance wave runup, was extracted from the hind-cast and extreme value analysis was applied to calculate the frequency-magnitude curves for each of 48 shoreline transects. The hind-cast and extreme value analysis procedure was repeated for RSLR=0, 0.5, 1.0 and 2.0m.

3.3 Tsunami Hazard Assessment

The BC Flood Hazard Land Use Guidelines require that tsunami hazard be assessed for areas outside the Strait of Georgia [3]. The document provides the following guidance on the required assessment:

"At a minimum, building conditions should protect improvements from damage from a tsunami of equal magnitude to the March 28, 1964 tsunami that resulted from the Prince William Sound, Alaska earthquake and a possible Cascadia Subduction Zone earthquake."

The project budget allowed only a limited scope of tsunami hazard assessment so a conservative approach is adopted. Based on the available literature, it is assumed that a fault of the Cascadia Subduction Zone (CSZ) poses the greatest hazard to the DOU [1]. Tsunami FCRPs are calculated based on the estimated maximum water elevation during a small set of the tsunami events, which includes both tsunami and tidal influence. The tsunami hazard associated with a potential fault of the CSZ is investigated using a sophisticated hydrodynamic model based on the shallow water equations [11]. The hazard from the 1964 Alaska tsunami is assessed based on literature review.

A full probabilistic tsunami hazard assessment is not within the scope of this work.

4 Geo-Spatial Analysis

4.1 Vertical Datum

Unless noted otherwise, all elevations are in meters with respect to the CGVD28 vertical datum. According to Natural Resources Canada², elevations in CGVD28 may be converted to CGVD2013 with a simple offset:

$$H_{CGVD2013} = H_{CGVD28} + \beta_a \quad (1)$$

where the local value of β_a in the DOU is approximately ranges from about 15 to 20 cm.

Similarly elevations in chart datum may be converted to CGVD28:

$$H_{CGVD28} = H_{CD} + \beta_b \quad (2)$$

where, based on surveys at the Ucluelet tide station³, β_b in this case is -2.05m.

4.2 Digital Elevation Model

A digital elevation model was assembled from a variety of sources including: single and multi-beam bathymetric survey data from the Canadian Hydrographic Service (CHS), electronic navigation charts (ENCs) from the CHS, a high water data-set for the Pacific from the CHS⁴, the General Bathymetric Chart of the Oceans⁵, LiDAR derived topographic contours from the DOU and topographic contours from the CanVec data-set⁶. The input data-sets are summarized in Table 1 below.

Table 1: Data sources for the digital elevation model.

Data Description	Coverage	Source
Bathymetry/Topography DEM	Global	General Bathymetric Chart of the Oceans
ENC soundings and contours	Mid-Island Coastal Waters	Canadian Hydrographic Service
High Water Contour	BC Coastal Waters	Canadian Hydrographic Service
Bathymetry Survey data	DOU and surrounding waters	Canadian Hydrographic Service
0.3m Topographic Contours	District of Ucluelet	District of Ucluelet
20m Topographic Contours	Canada	CanVec Database

The DEM was assembled as follows:

- Electronic Navigation Charts:
 - Extract contour and sounding data as xyz points.
 - Convert elevations from chart datum to CGVD28.
 - Merge the data from each chart, preferencing data from higher resolution charts.
 - Trim some data points where LiDAR contours are available.

²https://www.nrcan.gc.ca/earth-sciences/geomatics/geodetic-reference-systems/9054#_Toc372901507

³<http://www.meds-sdmm.dfo-mpo.gc.ca/isdm-gdsi/twl-mne/benchmarks-reperes/station-eng.asp?T1=8615®ion=PAC&ref=maps-cartes>

⁴<http://www.charts.gc.ca/data-gestion/index-eng.asp>

⁵www.gebco.net

⁶<https://open.canada.ca/data/en/dataset/8ba2aa2a-7bb9-4448-b4d7-f164409fe056>

- High Water Data-set:
 - Extract xyz points from high water data-set.
 - Convert elevations from chart datum to CGVD28.
 - Trim high water data where LiDAR contours are available.
- Bathymetry Survey data:
 - Extract xyz points from bathymetry survey data-set.
 - Convert elevations from chart datum to CGVD28.
- GEBCO DEM:
 - Extract subset of global DEM (see Figure 3).
 - Trim points which are covered by ENCs.
- DOU 0.3m LiDAR Contours:
 - Extract contours from files as xyz points. Downselect points at 1:10.
 - Remove points below 0.65m (remove influence of the sea surface).
 - Remove points above 25m (unneeded for ocean models)
- CanVec Topographic Contours:
 - Extract subset of Canadian vector maps (see Figure 3).
 - Extract xyz points from contours.
 - Trim points above 50m (unneeded for ocean model).
- Merge xyz points from all sources.
- Triangulate points using Delaunay triangulation to create TIN.

The data sources used in the DEM are shown graphically in Figures 3 and 4.

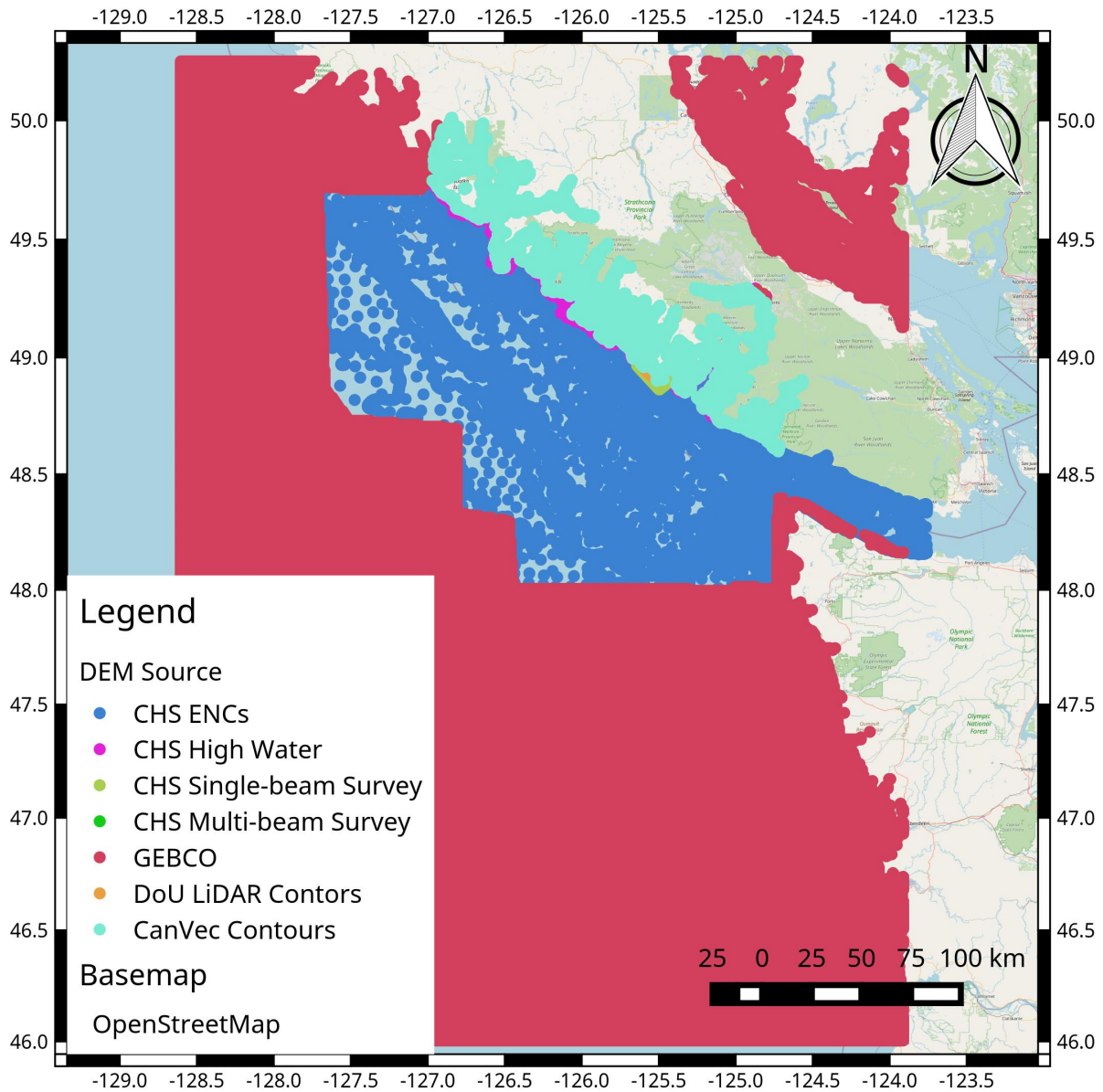


Figure 3: Bathymetric and topographic data used in constructing the DEM

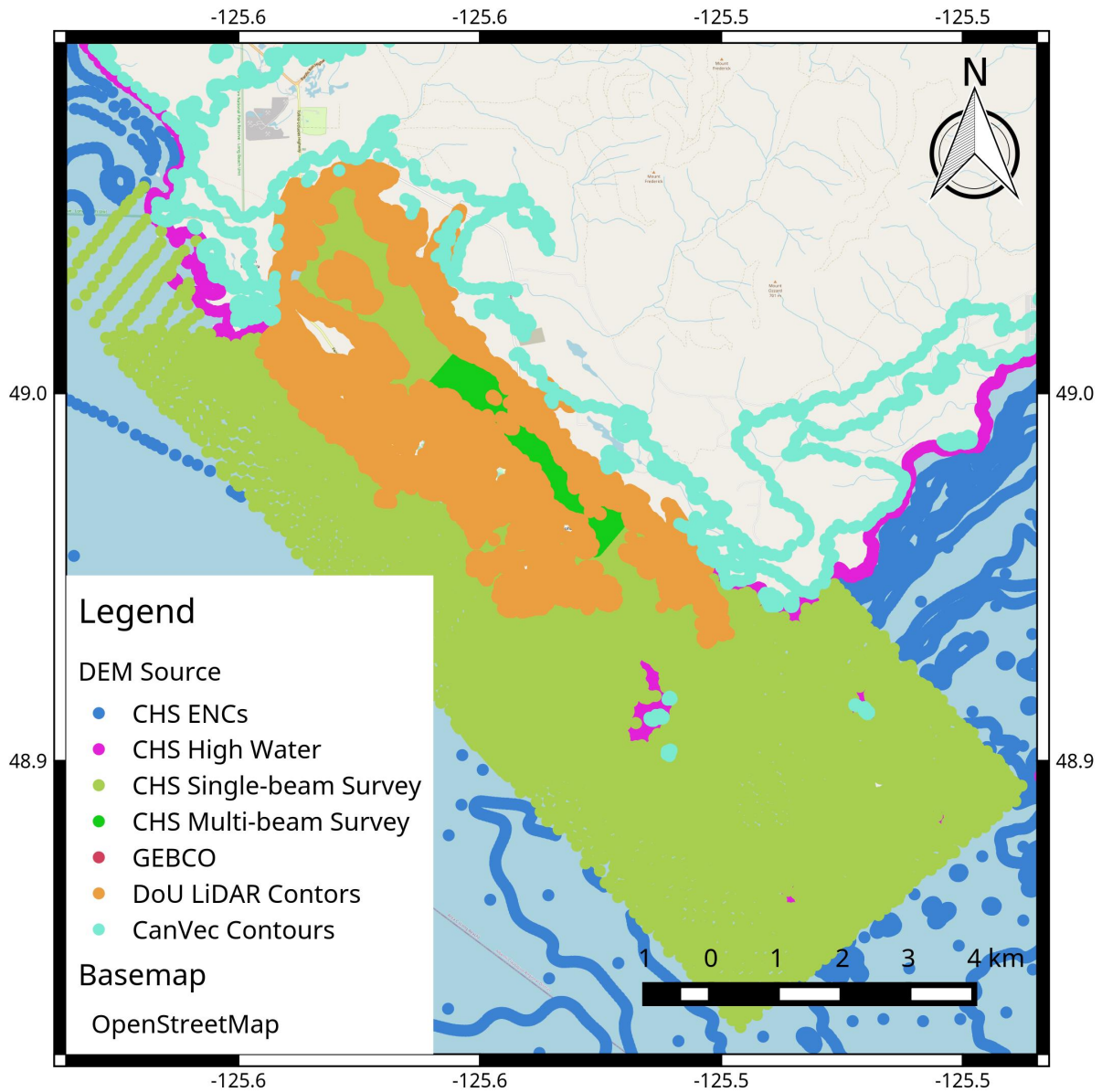


Figure 4: Bathymetric and topographic data used in constructing the DEM, detail of the DOU.

4.3 Shoreline Geometry

For analysis the shoreline is split into a series of along-shore "reaches" of approximately 500 m. For each reach a representative cross-shore transect was constructed. The surface elevation along the transect is interpolated from the DEM and the transect line segment is simplified down to approximately 10 nodes using the Douglas-Peucker Algorithm [16]. The reaches and transects are shown in Figure 5.

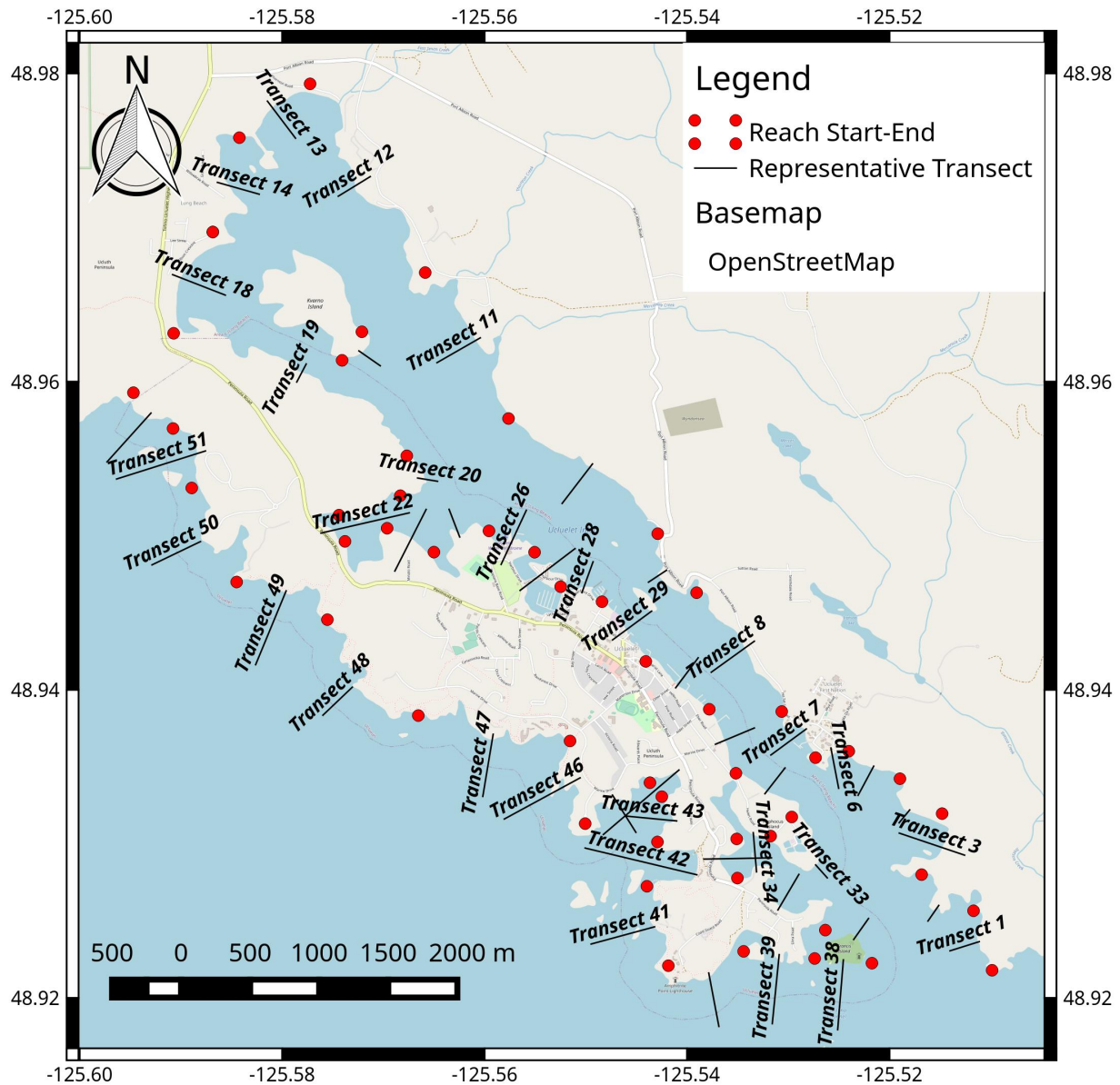


Figure 5: Location of reaches and representative transects.

5 Storm Hazard Assessment

This section describes the work conducted to assess the coastal flooding hazard due to weather driven storm events, including the development of a coastal hind-cast which is used as the statistical basis for future flooding estimates.

5.1 Coastal Hind-cast

A combination of measured and modelled data has been used to synthesize a hind-cast of water levels and waves in the DOU over the past 40 years (1979-2018). This hind-cast accounts for waves, tides, storm surge, local wind setup and wave runup. Effects of the PDO and ENSO are contained within the storm surge data.

The DOU was divided into 48 shoreline reaches based on the prevailing coastal and shoreline conditions. These reaches are shown in Figures 5. Note that the transects are not labelled continuously.

Tidal water levels were calculated based on harmonic constituents for the Ucluelet tide station available from the Canadian Hydrographic Service. Storm surge was calculated as the difference between the calculated tidal water level and the measured water level at the Ucluelet tide station. Where data was not available from the Ucluelet tide station, storm surge calculated at the Tofino tide station was used. Wind setup was modelled using the RiCOM 2D hydrodynamic model software[11]. Wave conditions were modelled using the SWAN 2D wave modelling software. Wave setup and runup was calculated at 25 shoreline transects using 1D parametric models.

A schematic of the modelling approach is provided in Figure 6. Tide and storm surge data are provided as a still water level to the SWAN wave model. Wind estimates from the ECMWF ERA5 model [31] are used to drive the SWAN wave model and the RiCOM wind setup model. Wave boundary conditions for the SWAN wave model are sourced from the NCEP WavewatchIII model[32]. At each shoreline transect wave runup is calculated using 1D parametric models based on: the ambient water level (due to RSLR, tide, storm surge and wind setup) and incident wave conditions (sourced from SWAN wave model outside the breaking zone). All components were calculated or interpolated to 15 minute intervals throughout the hind-cast period. The response of interest is the total runup elevation which includes the effects of all components. More details on the DOU coastal hind-cast are provided in the following sub-sections.

5.1.1 Tides

Tides are a deterministic process resulting from the gravitational interaction of the sun, the moon and the earth and may be accurately described by a set of harmonic constituents (each consisting of amplitude and phase). The tides may be predicted by summing the sinusoids resulting from each of the harmonic constituents.

Tides were calculated using constituents obtained from the Canadian Hydrographic Service and the T_tide tidal analysis and prediction software [33]. At the Ucluelet tide gauge, higher high water large tide (HHWLT) is 2.0 m.

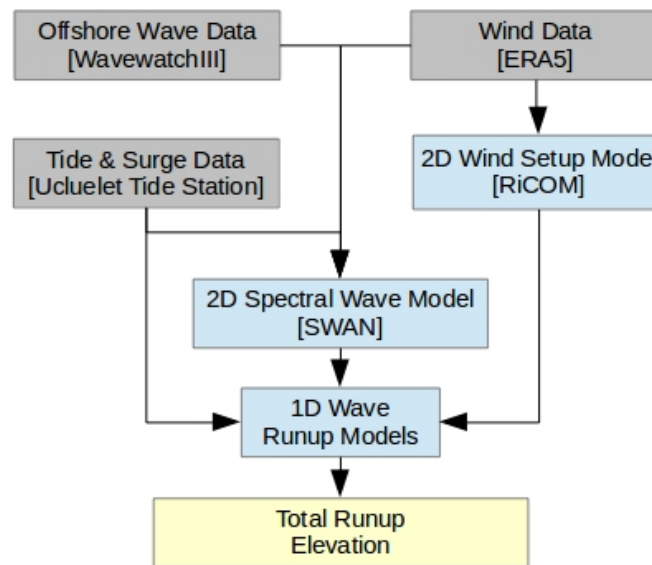


Figure 6: A schematic showing the relationship between data (grey), models (blue) and results (yellow) in the coastal hind-cast.

5.1.2 Storm Surge

Storm surge accounts for local atmospheric and steric effects on water elevation as well as water level variations which propagate off Pacific Ocean. Storm surge as defined here includes the effect of local wind setup.

Tide gauges measure ambient water level and are usually setup to filter the effect of waves. Storm surge can be estimated as the the difference between the measured water elevation and the elevation predicted by the tidal constituents, a quantity also known as the tidal residual.

In the coastal hind-cast, storm surge was represented as spatially uniform. The hind-cast time-series was calculated based on the tidal residual at the Ucluelet and Tofino tide gauges. In this calculation method, the storm surge component also includes the effects of the PDO and ENSO.

The largest storm surge event found in the hind-cast period (1979-2018) is 1.06 m.

5.1.3 Local Winds

Wind data from the European Centre for Medium-Range Weather Forecasts (ECMWF) ERA5 global reanalysis model were used to drive waves and local wind-surge within this coastal hind-cast. Wind data from this reanalysis model is available from 1950 to 2019 and has a 0.25° spatial resolution (see Figure 8). The advantage of this data-sets over measurements or other more coarse models, is that the record is complete over the hind-cast period, and full spatial coverage is available for our Ucluelet domain.

Large winds typically follow the Vancouver Island coastline in the NW or SE as shown in Figure 7. The largest wind speed recorded at the La Perouse weather buoy) is 23 m/s from SE.

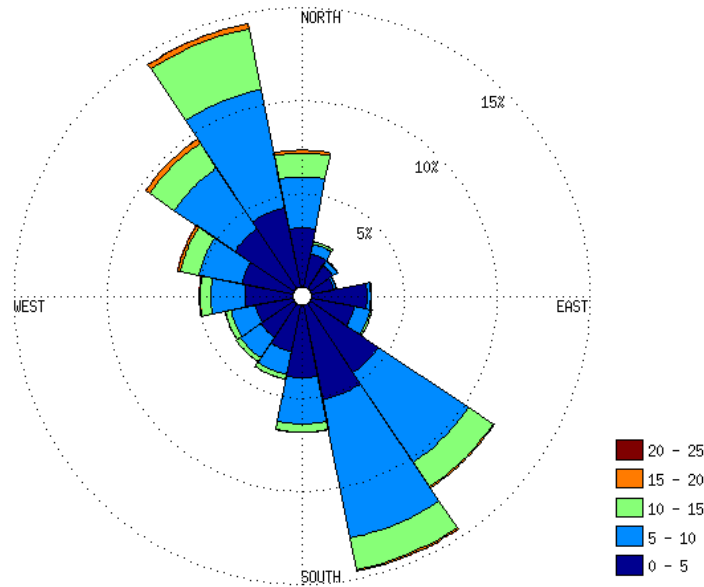


Figure 7: Wind rose of wind direction and intensities as measured on at the La Perouse Weather Buoy. Colour indicates wind speed, the spoke orientation indicates the direction the wind is blowing to, the dotted concentric circles indicate frequency of occurrence.

5.1.4 Wind Setup

Wind setup is a fluctuation in water level resulting from shear stress of wind over the water surface. Wind setup is largest where the wind blows over long stretches of shallow water. A 2D wind setup model was developed using the RiCOM hydrodynamic modelling software [11]. The model was run using the unstructured grid of Section 5.1.5. The model was forced by winds of Section 5.1.3 and run with a still water level corresponding to high tide. A quasi-static approach to modelling was used where a constant wind speed was applied to the model until a steady state response was achieved. This was repeated for each directional octant at wind speed increments of 5m/s. The steady state response of each model run was assembled into a response matrix for each shoreline transect. The time-series wind setup at each transect was then estimated by interpolating the wind setup matrix with the wind speed and direction at each time step.

As noted in Section 5.1.2, the estimate of storm surge from the Ucluelet tide gauge also includes wind setup. To avoid double counting wind setup, which is in the both the storm surge and wind-setup estimates, the wind setup estimate from the location of the Ucluelet tide gauge was subtracted from the wind setup estimate at each transect prior to inclusion in the hind-cast.

The largest wind surge occurs at the head of Ucluelet Inlet and is just a few centimetres.

5.1.5 Wave Conditions

Large waves impacting the DOU primarily originate in the Pacific Ocean and propagate into coastal waters. The exception is in the upper reaches of the Ucluelet Inlet where waves are primarily locally generated. To include waves in the coastal hind-cast a 2D computational wave model was developed using the industry

standard, SWAN wave modelling software [34]. The computational grid for this model was created using bathymetric and topographic data as described in Section 4.2 and extends from Bamfield to Tofino, and offshore as far as La Perouse Bank. The computational grid was developed in a similar manner to that described in Section 6.3.1, but without inclusion of topography beyond high water. The computational grid is shown in Figure 8. Grid resolution varies from approximately 1000m at the ocean boundary to 30 m at the western shoreline with a total of 100945 nodes.

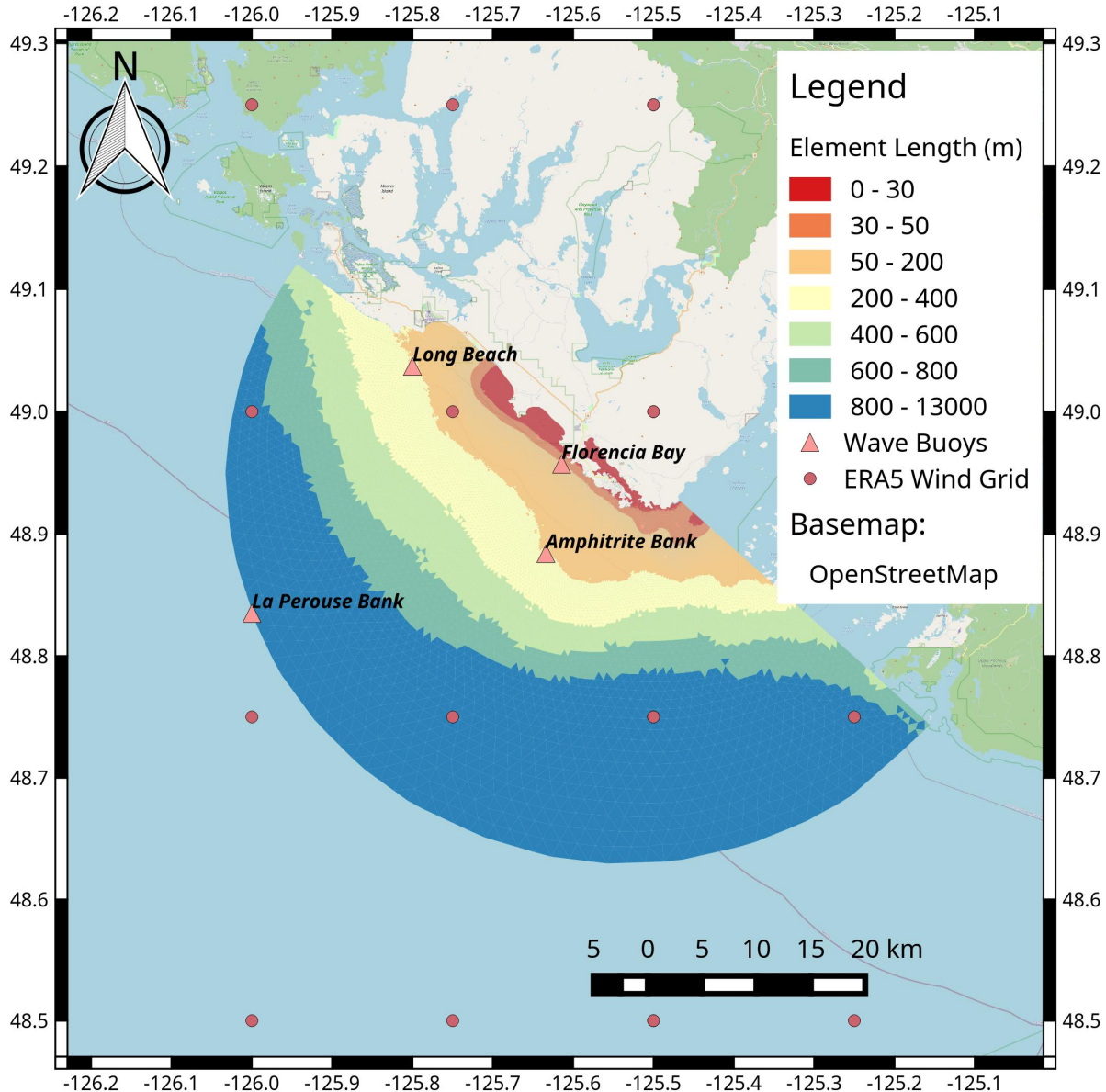


Figure 8: Average element length of the wave model grid. Triangles indicate locations of wave measurement buoys.

The SWAN wave model is forced by the local wind data-set described in Section 5.1.3. Water levels were

specified based on measurements at the Ucluelet and Tofino tide stations (Sections 5.1.1 and 5.1.2).

The SWAN wave model is forced at the outer boundary with directional wave spectra from the NCEP WavewatchIII 30-Year Wave Hindcast (1979-2009) and Production Hindcast (2010-2018) [32, 35]. The location of these data coincides with the location of the La Perouse weather buoy (c46206) (see Figure 8). The WavewatchIII wave data were calibrated to significant wave height (H_{m0}) using wave measurements from the buoy. Consequently, spectral densities were scaled using the factor of eq (3):

$$S_{fac} = \sqrt{1.1 - 0.3/H_{m0}} \quad (3)$$

Evaluation statistics mean value (\bar{X}), bias (B), RMS difference (E_{RMS}), scatter index (SI), and correlation coefficient (R) for the calibrated significant wave height and peak wave period (T_p) are provided in Table 2. The scatter of measured and modelled significant wave height is plotted in Figure 9.

Table 2: Evaluation statistics comparing SWAN wave model estimates to observations at the La Perouse weather buoy (c4606)

	Records	\bar{X}	B	E_{RMS}	SI	R
H_{m0}	67035	2.23m	0.02m	0.41m	19%	0.94
T_p	65232	10.8sec	0.9sec	3.0sec	28%	0.52

The model was evaluated by comparison to long term wave measurements deployed at Amphitrite Bank, Long Beach and Florencia Bay (see Appendix D). The evaluation indicates that the hind-cast model has very good skill in reproducing the observed integrated wave parameters, significant wave height (H_{m0}) and peak wave period (T_p).

The wave model was run on a 3-hourly time-step for the 40 year hind-cast period (1979-2018). Results were output and saved offshore of each shoreline transect. The largest waves occur on the exposed west shore of the Ucluelet Peninsula where waves can be as large as 12 m in H_{m0} . In the sheltered areas of the Inlet, waves rarely exceed 0.5 m in H_{m0} .

5.1.6 Wave Effect

Wave runup is the upwash of water on the shoreline due to wave forcing. Wave setup is an increase in water level shoreward of the wave breaking zone due to momentum transfer from breaking waves. In practical applications such as this one, wave runup and wave setup are often lumped together and assessed as a single quantity referred to simply as wave runup.

At any wave exposed beach the water level oscillates constantly as each wave breaks and washes up. Even over a short period of 20 minutes, the extent of each wave upwash may vary considerably. The 'wave effect' must quantify this variable water level over a short period with a single representative metric. In this assessment, the metric used is the the wave runup elevation exceeded by only 2% of waves ($R_{2\%}$). The $R_{2\%}$ metric is suggested in the BC Provincial Guidelines [5, 6, 7] for this application and is used by most available empirical wave runup models [36].

At each transect, wave runup was estimated at time-step throughout the hind-cast. The runup estimated at each transect is representative of the runup along the entire reach. However variability in incident wave conditions and shore slope conditions along the reach will result in variability in wave runup that is not captured by the estimate at the reach-representative transect. This is particularly true on Ucluelet's exposed western shore, where the rocky shoreline is extremely irregular.

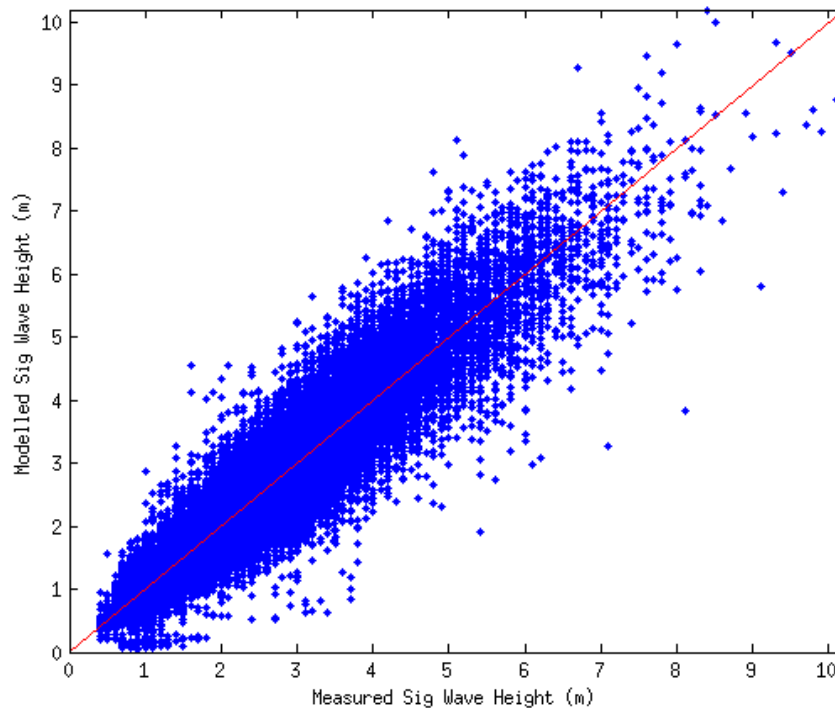


Figure 9: Scatter of measured and modelled (WavewatchIII) significant wave height at the La Perouse weather buoy.

Two approaches were used for calculating wave runup; one for lower sloped shores and one for larger slopes and both based on wave conditions from intermediate depth. The first is Parametric Direct Integration Method (DIM) [37]. This method is applicable for natural beaches with slopes lower than about 1:8 and captures the infra-gravity contribution that is important with long period waves typical to the Pacific. The DIM produces similar estimates to the Stockdon equations [36]. The second method used is the equations of Van der Meer and Stam [38]. This method is applicable to shore and barrier slopes from about 1:8 to 1:1 and provide similar estimates to the TAW and EurOtop equations [36].

Inputs to the wave runup calculation are significant wave height, peak period and spectral narrowness factor as well as the average beach slope. Wave parameters were sourced from the wave model outside the breaking zone. The effective beach slope was estimated at each transect and each time step based on the location of wave breaking and the estimated $R_{2\%}$ extent, so that the effective slope may change with each time-step.

The largest wave runup occurs where large waves break on a steep slope. At several transects on the exposed west coast of Ucluelet, estimated runup alone can exceed 10m.

5.1.7 Total Wave Runup Elevation

The total wave runup elevation sums the influence of RSLR, tide, storm surge, wind setup and waves to estimate the total vertical extent of the 2% wave runup relative to geodetic datum. The FCRP is similar, but

refers specifically to the total wave runup elevation associated with a design event.

The total wave runup elevation has been calculated at 15 minute time steps throughout the hind-cast period. The storm surge (at 1 hour time-step) and the wave conditions (at 3 hour time-step) were interpolated to achieve this temporal resolution. The hind-cast was run with RSLR = 0.5, 1.0 and 2.0 m to estimate total runup elevation over the same period but with increasing levels of RSLR.

5.2 Hind-cast Evaluation

The hind-cast was evaluated by comparison to shoreline indicators of storm activity. The largest storm in the hind-cast occurred January 18, 2018. Somewhat surprisingly, a site visit conducted in December of 2019 showed few signs of the 2018 storm remaining. Luckily DOU staff were able to provide photos of the storm event, along with location and elevation estimates (Figure 10, for example). A tabulation of the observed and estimated runup elevation for several transects is provided in Table 3. In general the model agrees reasonably well with the observations.

A comprehensive evaluation for all transects was conducted using ortho-photos and LIDAR data to establish an elevation for the storm evidence. See Appendix E for details on this analysis. Based on this evaluation, the runup elevation hind-cast is judged appropriate for the purposes of this work.



Figure 10: Wave impacting the Amphitrite Lighthouse. Estimated observed elevation is 9.3 m, modelled runup elevation is 10.3 m. Photo credit: John Towgood.

Table 3: Comparison of the observed and modelled runup elevation during the Jan 18, 2018 storm.

Trans #	Name	Observed Elevation (m)	Modelled Elevation (m)
39	Pass of Melfort	9.6	7.8
40	Amphitrite Point Lighthouse	9.3	10.3
42	Terrace Beach	4.5	5.5
44	Little Beach	4.2	5.3
46	Big Beach	5.4	6.1

5.3 Extreme Value Analysis

Extreme value analysis was applied to the total runup elevation at each transect to estimate frequency-response curves. A peak-over-threshold approach was used with the threshold specified as the 99.95 percentile of occurrences and a minimum separation criteria of 3 days. For most transects this resulted in about 1-2 events identified in each year. The WAFO toolbox [39] was used to fit a Generalized Pareto Distribution to each storm set. The fitted distribution and its confidence intervals was then used to generate the lower (5%), maximum likelihood and upper (95%) estimates of total wave runup elevation associated with the 6.67%, 2%, 1%, 0.5% and 0.2% AEP events (15, 50, 100, 200 and 500 year return period). Results for RSLR = 0 m, 0.5% and 0.2% AEP are provided in Table 4. Results for all RSLR levels and return periods are available in Appendix F. It is noted that the hind-cast period is relatively short and consequently the confidence interval on the 200 and 500 year return period estimates are very wide in some cases. This arises of the relatively short length of the hind-cast and because of scatter in the runup event set that is used to fit the extreme value distribution.

Table 4: Estimated FCRP (m) for 1 m RSLR associated with the 0.5% and 0.2% AEP events. L, M and U indicate lower (5%), maximum likelihood and upper (95%) confidence estimates.

Trans #	Max in Hind-cast	99.95 %tile	# Events	0.5% AEP			0.2% AEP		
				L	M	U	L	M	U
1	5.7	4.2	59	4.7	5.6	8.4	4.7	5.9	9.7
2	5.7	4.2	55	4.7	5.6	8.3	4.7	5.8	9.5
3	3.7	3.0	64	3.3	3.8	4.8	3.3	3.8	5.0
4	4.3	3.6	62	3.9	4.3	5.5	3.9	4.4	5.7
5	4.0	3.4	62	3.7	4.1	4.8	3.7	4.1	4.9
6	4.0	3.2	70	3.6	4.0	4.5	3.6	4.0	4.6
7	3.0	2.4	86	2.7	3.1	4.5	2.7	3.2	4.9
8	2.7	2.2	77	2.4	2.8	3.6	2.4	2.8	3.8
9	3.5	2.7	76	3.1	3.5	4.2	3.1	3.5	4.4
10	2.8	2.2	77	2.5	2.8	3.6	2.5	2.9	3.8
11	2.7	2.1	75	2.4	2.7	3.3	2.4	2.7	3.4
12	3.0	2.3	81	2.7	3.0	3.9	2.7	3.1	4.2
13	2.7	2.2	83	2.4	2.8	4.0	2.4	2.9	4.4
14	2.9	2.2	81	2.5	2.9	4.0	2.5	2.9	4.3
16	2.9	2.3	83	2.6	3.0	3.8	2.6	3.0	4.1
18	2.7	2.1	72	2.4	2.7	3.7	2.4	2.8	3.9
19	2.7	2.1	80	2.4	2.7	3.3	2.4	2.7	3.5
20	3.1	2.4	78	2.8	3.1	3.7	2.8	3.2	3.9
22	2.8	2.2	78	2.5	2.8	3.5	2.5	2.9	3.6
24	2.6	2.1	78	2.3	2.7	3.6	2.3	2.7	3.8
25	3.0	2.3	76	2.7	3.0	3.6	2.7	3.0	3.7
26	3.0	2.3	87	2.6	3.0	3.8	2.6	3.0	4.1
27	2.7	2.1	78	2.4	2.8	4.2	2.4	2.9	4.7
28	3.1	2.4	84	2.7	3.1	3.8	2.8	3.1	3.9
29	2.7	2.2	77	2.4	2.7	3.4	2.4	2.8	3.6
30	3.1	2.5	84	2.8	3.2	4.0	2.8	3.2	4.3
31	2.7	2.2	81	2.5	2.8	3.8	2.5	2.9	4.0
32	3.3	2.4	78	2.8	3.5	5.7	2.8	3.7	6.7
33	5.2	3.8	62	4.3	5.2	8.1	4.3	5.5	9.7
34	3.2	2.4	75	2.8	3.3	4.2	2.8	3.3	4.4
35	2.8	2.3	71	2.5	2.9	3.8	2.5	2.9	4.0
36	3.8	3.1	70	3.4	3.9	5.0	3.4	4.0	5.4
37	4.8	3.7	63	4.1	4.9	7.5	4.1	5.1	8.8
38	7.6	5.3	50	5.9	7.5	13.5	6.0	8.0	17.3
39	7.7	5.3	44	6.3	7.6	10.9	6.3	7.9	12.1
40	10.4	7.6	65	8.8	10.5	14.7	8.8	10.8	16.2
41	9.6	6.4	40	7.0	10.1	30.2	7.1	11.3	48.9
42	5.8	4.2	80	4.8	6.1	10.1	4.9	6.4	12.3
43	6.7	4.9	74	5.8	6.6	8.0	5.9	6.7	8.3
44	5.3	3.7	80	4.4	5.6	9.2	4.4	5.8	10.7
45	5.0	3.7	62	4.2	4.9	6.8	4.2	5.1	7.7
46	6.1	4.3	51	4.8	6.1	10.4	4.9	6.5	12.9
47	8.3	5.7	43	6.6	8.1	12.3	6.6	8.5	14.4
48	12.2	8.4	35	9.6	12.2	20.6	9.6	12.7	24.2
49	6.2	4.4	55	5.0	6.0	8.9	5.1	6.3	10.3
50	11.2	8.2	39	9.0	11.9	27.2	9.0	12.8	39.4
51	4.8	3.9	66	4.3	4.8	5.6	4.3	4.8	5.9
52	8.8	6.7	45	7.5	8.9	13.6	7.5	9.3	16.0

6 Tsunami Hazard Assessment

This section describes the work conducted to assess the coastal flooding hazard due to tsunami events.

Some definitions are required in order to understand the quantities discussed in the analysis. There are numerous ways to define the water surface elevation associated with tsunami. Wave height is a term used in wave theory and is defined as the vertical distance between successive crests and troughs of a wave. This is not a useful measure for tsunami because the waves are very asymmetric and the quantity of interest is the maximum water elevation. Alternatively, wave crest elevation is defined as the maximum value for water level with respect to some fixed reference such as mean sea level or a land reference. However, this quantity includes tides and other sea level variations so must be corrected for site comparisons. Here, tsunami amplitude is defined as the maximum elevation of the wave crest with respect to the ambient or prevailing water levels. Thus tsunami observations must be corrected for tide and other variations to derive this quantity. For the most part, amplitude is the quantity of interest in this report and can be combined with tides, storm surges, or other variations to find maximum water elevation.

The British Columbia Coastline is exposed to tsunami hazard from multiple sources - near (or local), intermediate (or regional) and far field (or remote) sources. For this area, the greatest hazard in most cases comes from near and intermediate sources. The BC Flood Hazard Land Use Guidelines suggest that at minimum the hazard due to the 1964 Alaska megathrust event and a possible Cascadia subduction zone (CSZ) event should be assessed [3].

6.1 1964 Alaska Earthquake

The 1964 Alaska earthquake generated a tsunami which impacted much of British Columbia. At most locations little damage was incurred. However at some locations the local geography amplified the wave, creating a much larger hazard. One of the hardest hit BC towns was Port Alberni where the tsunami excited a resonance in the Alberni Inlet which amplified the wave to over 4 m in amplitude. The response at Tofino tide gauge was a more moderate 1 m amplitude [17]. There are no water level measurements available in Ucluelet during the 1964 tsunami event. However, Barb Gudbranson of the Ucluelet Historical Society kindly provided oral accounts from several community members, including a remembered account from her Grandfather and Father.

My grandparents lived on Imperial Lane and I remember my Grandpa saying the water in the harbour raised three feet. When I asked my Dad about it he said that he was standing with my mother on the dock at Imperial Oil and they listened to the roaring of the water in the darkness and the water in the harbour raised four feet. The Imperial Oil dock doesn't exist anymore but it was larger than the Main Street Dock (Whiskey Dock). All the trollers were out in the middle of the harbour waiting for the tsunami to arrive. The rapidly rising and falling tide caused by the tsunami caused the log booms and bundles to move at the head of the bay. The booms and bundles became battering rams which knocked out pilings and dolphins and the logs scattered.

This account of a three to four foot tsunami is in-line with measurements made at Tofino and modelling conducted for Barkley Sound and Port Alberni by Seaconsult [17]. The tsunami arrived at about midnight during a neap high tide of about 0.6 m. The result of the combined tide and tsunami height was likely less than 2 m, or similar in magnitude to storm tides routinely experienced during the winter at Ucluelet. That the tsunami wave was not larger suggest that it did not excite a resonance in the Inlet, however this potential is still of considerable importance.

The potential for resonance in Ucluelet Inlet was investigated as part of this work (see Appendix A). The

main resonant mode of the Inlet appears to occur for wave periods between 66 to 75 minutes. This is well short of the 112 minute period of the 1964 tsunami in Barkley Sound and suggest a non-resonant condition in Ucluelet Inlet. However, the possibility that Ucluelet Inlet could be excited into resonance by a tsunami cannot be excluded.

6.2 Cascadia Subduction Zone Earthquake

The 1700 Cascadia event occurred before the advent of written history in the region. The impacts of the earthquake and tsunami have been studied extensively through fieldwork, the oral history of BC First Nations and written history from Japan (which was impacted by the tsunami) [18]. However, based on these studies it can be difficult to assess the hazard from this event at specific locations. Hence, simulation using a computational model is most often used to study tsunami hazard in more detail.

Cherniawsky et al. published the results of a series of numerical simulations approximating the Cascadia 1700 megathrust event [19]. These simulations were based on a high resolution, non-planar rupture model of Wang [20] (hereafter W2003). This rupture model is based on a set of simplified assumptions, which were necessitated by the state of the science at time. Therefore, the W2003 rupture model is referred to as a *traditional* model. The Cherniawsky et al. study focused on the tsunami response at Ucluelet, Esquimalt and Victoria. The results at Ucluelet indicate a tsunami amplitude up to 7 m on the exposed outer shores of the DOU, and about 4 m within Ucluelet Inlet.

In 2013 the Capital Regional District commissioned AECOM to study tsunami hazard and risk in the region with a hypothetical modern faulting of the Cascadia Subduction Zone [21]. This study used rupture models of the US National Seismic Hazard Maps. The rupture selected for tsunami simulation was a 9.0 M_W shallow dipping subduction zone fault, which was modelled by 550 planar faults. Though focused on the Capital Regional District, simulation results from that work indicate a tsunami amplitude of greater than 5 m offshore of Ucluelet.

In 2019, Cascadia Coast Research and Ebbwater Consulting executed a coastal flood hazard assessment for the District of Tofino [22]. As part of this work Cascadia simulated tsunami propagation and runup at Tofino based on the W2003 rupture model. Though focused on Tofino, this work indicated tsunami amplitude exceeding 6 m offshore of Ucluelet.

Takabatake et al. recently published a numerical modelling study focused on tsunami impacts at several communities on the West Coast of Vancouver Island, including Ucluelet [23]. The study uses a relatively coarse representation of the CSZ fault geometry that is available within the ComMIT/MOST tsunami modelling software [24]. The rupture model consists of approximately ten 50 x 100 km planar tiles. Several different fault scenarios ranging from M_W 8.7-9.3 were generated by specifying different values of spatially constant slip along the fault. Maximum wave amplitude on the outer coast of Ucluelet are shown as approximately 13.5 and 6.5 m for the 9.3 and 9.0 M_W scenarios respectively. Inside Ucluelet Inlet, for the 9.3 M_W scenario, tsunami amplitude appears to be about 3.5 m south of Lyche Island and less than 1 m north of Lyche Island. These values are surprisingly small given the amplitude of the wave of the outer coast.

Gao et al. recently published a new set for megathrust tsunami rupture scenarios for the northernmost CSZ [25], hereafter referred to as G2018. The authors use a three-dimensional dislocation model (an update on that of [20]) to construct rupture models for three different types of fault rupture scenarios for the CSZ: buried rupture, trench-breaching, and splay. Additionally, they include the potential for simultaneous faulting of the Explorer Plate, north of the CSZ. While the buried rupture is similar in form to that of W2003 and that used by AECOM [21], the trench-breaching and splay faults are considerably different. Low resolution tsunami modelling executed as part of the study estimated that the splay faults generated tsunami amplitudes 50-100% larger than the buried rupture scenario.

In this Section we seek a detailed estimation of the flooding hazard at Ucluelet associated with a rupture of the Cascadia Subduction Zone. We focus on simulating tsunami associated with the rupture models of G2018, as these are the most detailed, and scientifically corroborated sources available for the northern CSZ. We also simulate the W2003 rupture model to facilitate comparison to past tsunami modelling studies.

6.3 Tsunami Simulation

Modeling tsunami dynamics requires a series of steps: First generating a computational grid with land and seabed topography, then specifying the initial condition of sea level from the various sources, and finally calculating wave propagation and runup using a numerical model.

6.3.1 Grid generation

The computational grid was constructed using the TQGG grid generation software⁷ (see [26] for a description of an older program). A triangular unstructured computational grid is used to allow flexibility in the representation of complex coastlines and allow variability in the grid resolution. Bathymetric and topographic data were sourced from the DEM (Section 4.2). The model domain was developed from this data-set as follows:

The model domain is composed of open boundaries which are set in the open ocean away from the influence of the source displacements, shoreline boundaries where there are no topographic data, and land boundaries at the 18m contour where there are topographic data. First the open boundaries were defined. Then shoreline boundaries were sampled with spacing related to the location with respect to the study site. The land boundary away for Ucluelet were defined as the current high water contour as available from the Canadian Hydrographic Service (see Section 4.2). Within Ucluelet Inlet and the immediately surrounding area, the land boundary was created by first gridding over all land areas. Grid nodes with elevation greater than 18m were then eliminated from the mesh and the mesh was updated accordingly. Including land topography allows the tsunami wave to run-up in a natural manner without interface boundaries. In general, node spacing on the outer edge of the model domain was specified in such a way as to maintain accuracy while minimizing the number of nodes. An 'advancing front' generation algorithm was used to create the grid. The grid resolution varies from 5000 m at the ocean boundary to 5 m over the DOU and contains 710744 nodes.

⁷<https://github.com/rusk/TQGG>

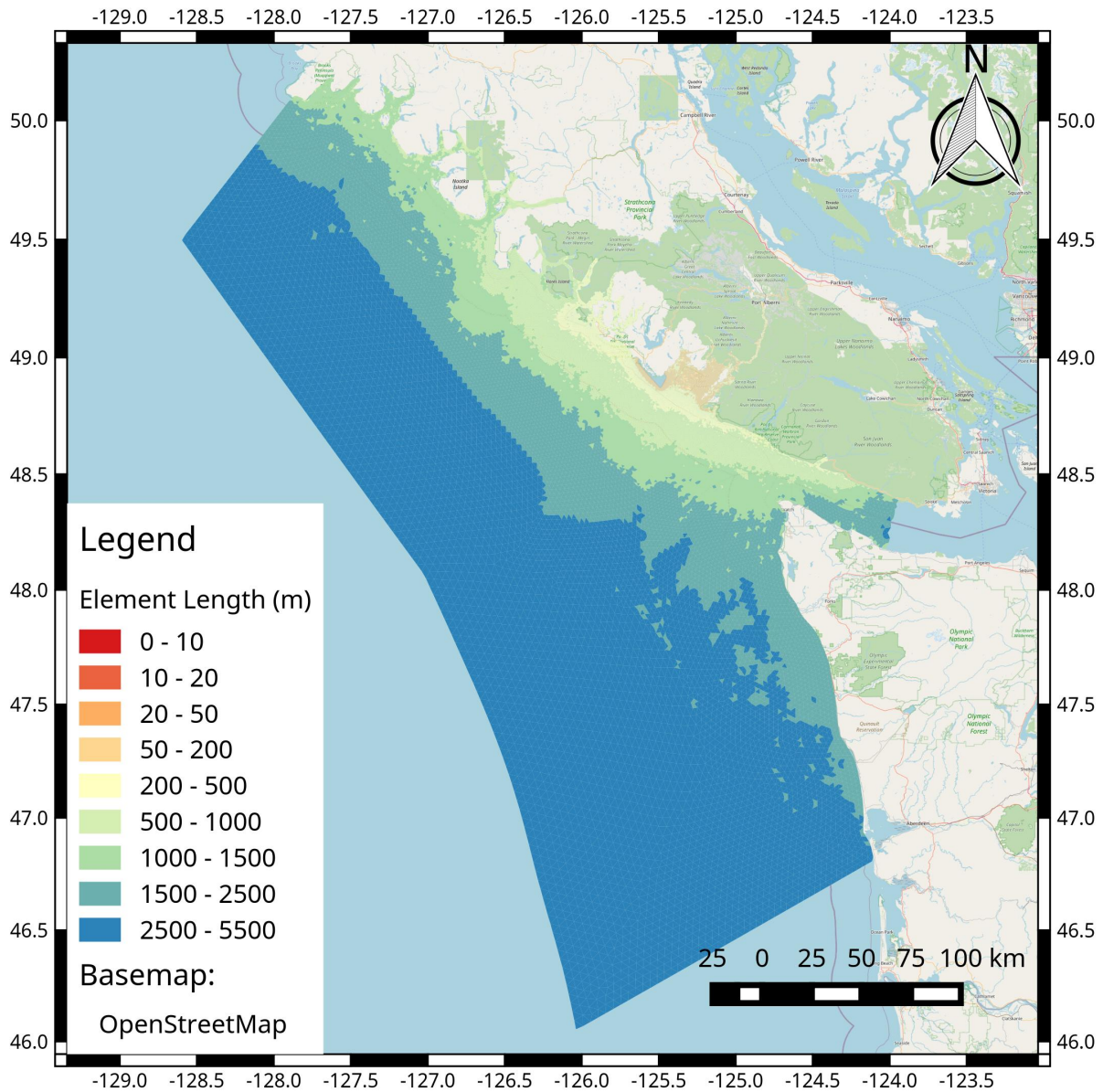


Figure 11: Average element length of the Tsunami model grid.

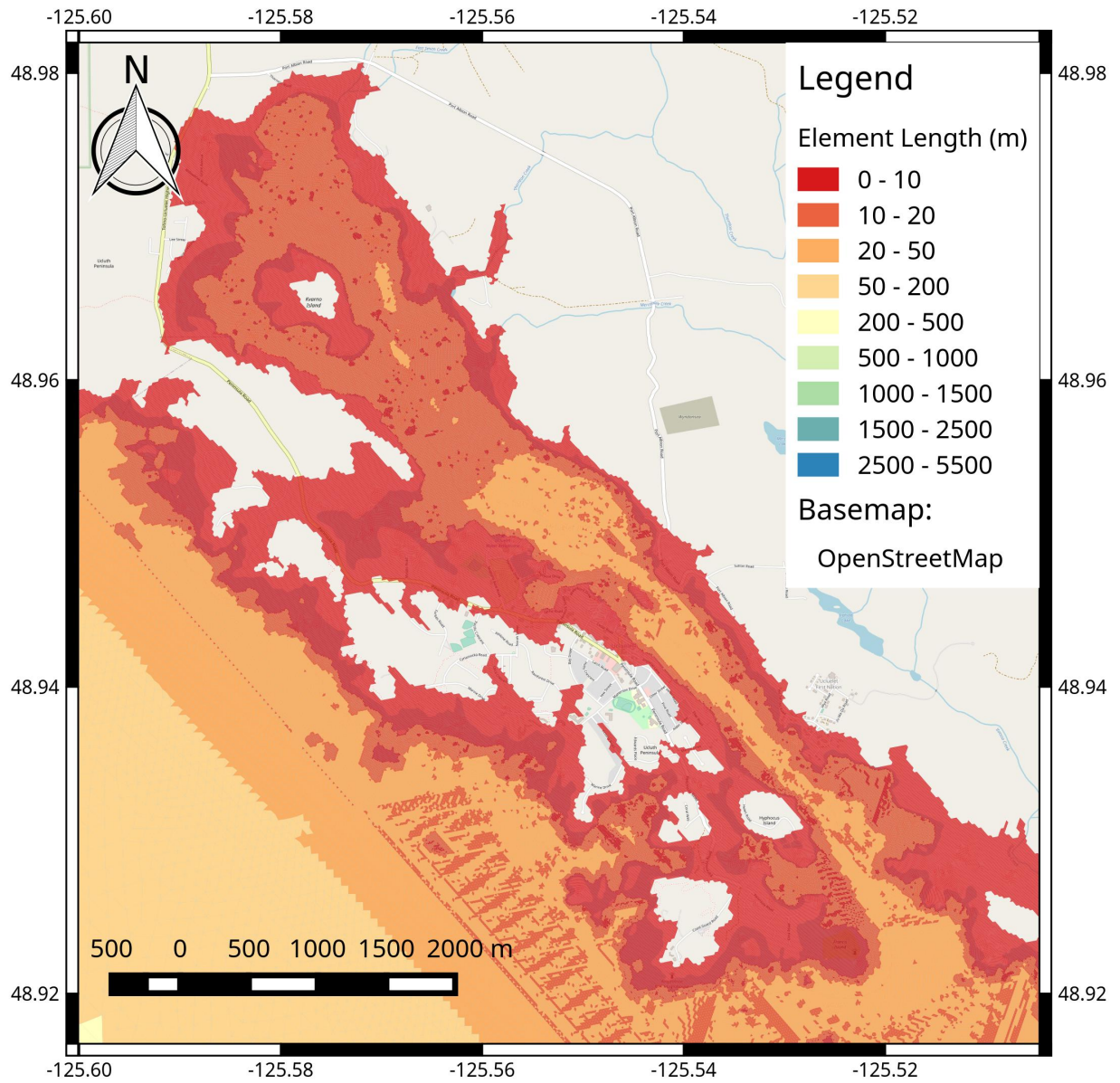


Figure 12: Average element length of the Tsunami model grid, detail of the DOU.

6.3.2 Initial and boundary conditions

The fault rupture model is used to specify the initial conditions on the water surface and seabed. In this work we consider the rupture model of W2003, and several rupture models from G2018. From G2018 we consider only those faults which include a rupture of the whole CSZ and the Explorer Plate. A description of each rupture model is provided in Table 5.

Table 5: Fault models used for tsunami simulation.

Name	Description	Source
G2018-B	Buried rupture	G2018
G2018-S-A	Splay-faulting rupture A	G2018
G2018-S-B	Splay-faulting rupture B	G2018
G2018-T-50	Trench-breaching 50% of peak slip	G2018
G2018-T-100	Trench-breaching 100% of peak slip	G2018
W2003	<i>Traditional Model</i>	W2003

The horizontal and vertical extent of the rupture varies considerably between the rupture scenarios. However, in the DOU, all of the rupture models cause the land to subside by about 2 m. A fundamental assumption is that the fault rupture occurs in a short time compared to wave propagation timescales. Hence, the rupture occurs instantaneously and the rupture model is used as an initial condition so that both the seabed and water surface elevation are deformed accordingly. Figure 13 provides an image of the G2018-S-A rupture model. Figures for all rupture models are provided in Appendix B.

The 1700 CSZ event occurred after approximately 500 years of locking and stress accumulation, whereas currently only 320 years of locking have occurred since the last CSZ event. All of these fault model represent 500 years of stress accumulation. A present day fault of the CSZ would likely result in a smaller subsidence and tsunami than the 1700 event. However, defining the hazard based on the 1700 event provides a degree of conservatism when considering a small set of event scenarios in the hazard analysis.

For boundary conditions, radiation conditions are specified at all open boundaries so that the tsunami is free to propagate out of the source area without spurious reflections. At land boundaries there is no flow normal to the boundary so only reflections are allowed. Where land topography is included, the wave will inundate the land until it reaches the run-up limit or reaches the boundary of the grid. For this study, land topography up to 18 m elevation is included throughout the region of the DOU so the wave will propagate over land according to the model algorithm described in Appendix G. This method is fully nonlinear and mass conservative.

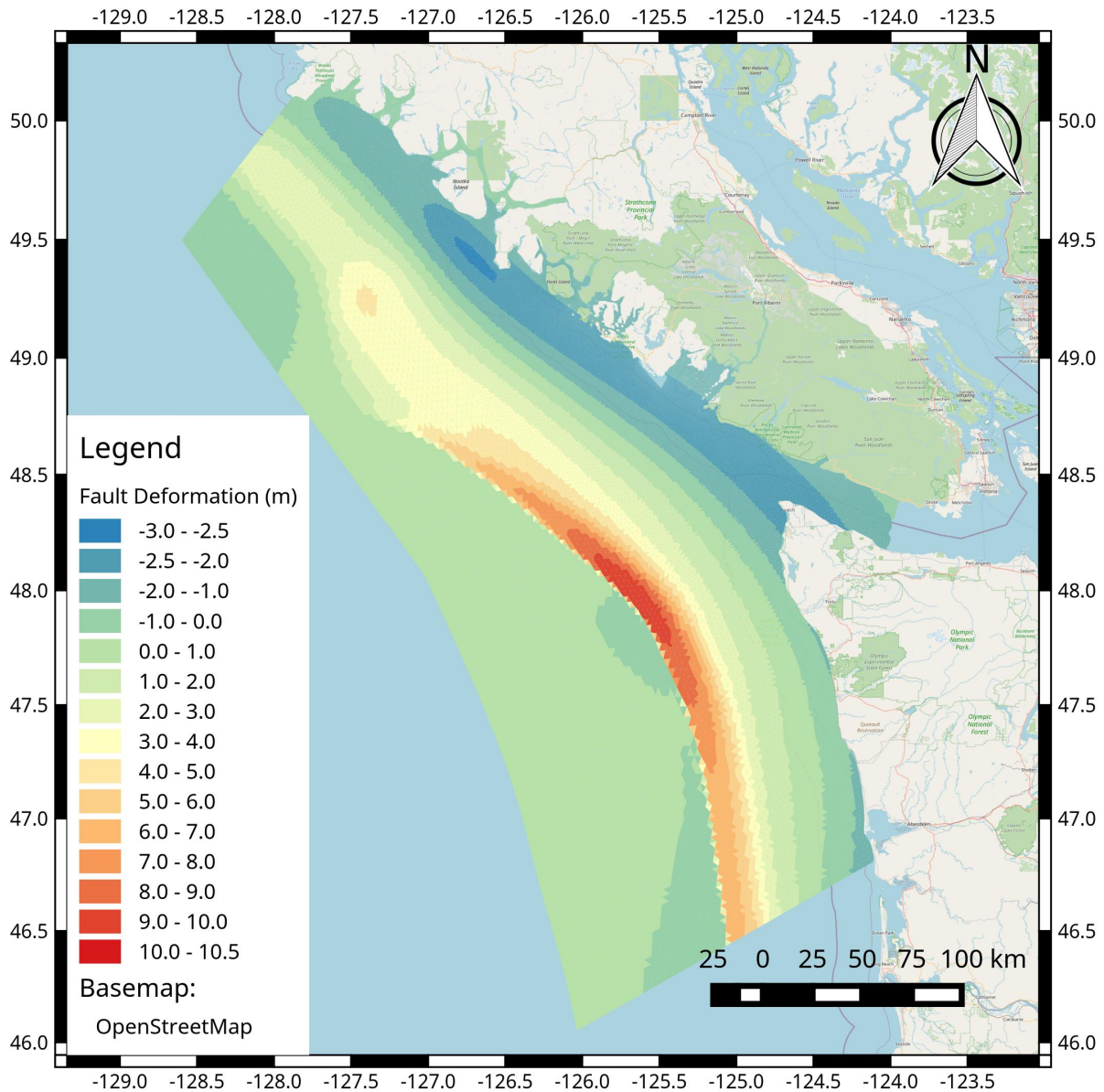


Figure 13: The G2018-S-A fault deformation model, interpolated onto the tsunami model grid.

6.3.3 Numerical model

The numerical model used here is RiCOM (River and Coastal Ocean Model), which is based on the Reynolds-averaged Navier-Stokes equations and continuity equation. For the simulations in this study, a 2-dimensional (horizontal) hydrostatic version is used [27]. This approximation is suitable for long-wave (tsunami) propagation. For these simulations, the bottom drag coefficient defined in equation 9 of Appendix G is $C_D = 0.0025$, a commonly accepted value. For water depth greater than 50 m or so, bottom friction is negligible. The time step was 0.06 seconds. The methods are second order in time so this is a very

accurate range.

Details about the model are contained in Appendix G. Reference to earlier studies using this model can be found in [28] (fault rupture), [29] (submarine landslide), and [30] (a variety of scenarios).

6.4 Tsunami Results

Four tsunami simulations were executed, each with a still water level equal to the sum of high tide (2.0 m) and RSLR of 0, 0.5, 1.0 and 2.0 m.

From a dynamical point of view, the initial surface displacement from the fault rupture can be considered as two waves travelling in opposite directions such that the water velocity vanishes everywhere. One wave will then propagate offshore westward towards Japan, and the other will propagate onshore toward the North American coastline. A good summary of the wave dynamics is contained in plots of maximum tsunami amplitude, which is tabulated during the total period of simulated time (see Figure 14). In deep and intermediate water the difference in amplitude between the scenarios is negligible as would be expected.

The DOU lies approximately 75 km north-east of the fault. Most of the tsunami energy is directed westward in the offshore direction, and eastward toward the Pacific coast of North America. The initial water displacement due to the fault rupture ranges from 4 to 12 m depending on the fault rupture scenario. As the eastward wave propagates towards shore the amplitude decreases to about half the initial amplitude. However as the waves pass the 50 m bathymetric contour, the amplitude increases to nearly its initial amplitude due to shoaling.

From the perspective of a fixed structure or point near the shoreline on one of the exposed beaches, the fault rupture causes a subsidence of about 2 m. The water will recede for about 5 minutes into the subsidence trough that was created slightly offshore. Following this, the water will flood over a period of 25 minutes and reach a height relative to the land surface of the sum of the subsidence, plus the ambient water level before the earthquake, plus the tsunami amplitude calculated here.

The tsunami wave peak arrives at the DOU approximately 30 minutes after the rupture. The amplitude at shore depends only somewhat on the RSLR scenario considered. The G2018-S-A produces the largest tsunami wave of the considered fault rupture scenarios, almost twice as large as W2003. The time series of water elevation (relative to mean sea level) for the RSLR = 0 m scenarios are provided for some reaches in Figure 15. Plots of maximum tsunami amplitude and speed are given in Figures 17 and 18. The maximum tsunami amplitude reaches eight to twelve metres on the DOU's western shore. The wave overtops Ucluelet Peninsula in several places: transect 49, transect 44 (Little Beach), and transect 42 (Terrace Beach). The overland current speed reach 10 m/s. It is interesting to note that at transect 53, the third wave is much larger than the first. This appears to be due to constructive interference between reflected wave, and appears to varying degrees in all of the tsunami simulation scenarios.

The tsunami wave is delayed somewhat as it enters Ucluelet Inlet. The tsunami amplitude in Ucluelet south of Lyche Island is similar to that at the entrance of the inlet, about 6 m. The flow associated with the tsunami is constricted by Lyche Island, accelerating the flow to up to 6 m/s, and heavily damping basin-scale oscillations. The lowest tsunami amplitudes in the Inlet occur between Lyche Island and Kvarno Island and are around 4 m. At the head of the Inlet, tsunami amplitude again increases to about 6m.

Results from each tsunami simulations were tabulated at each transect, and the results for the RSLR = 0 m scenario are provided in Table 6. Tsunami amplitude is relative to the still water level (in this case 2 m). FRCP is referenced to CGVD28 and includes the effect of tide, tsunami amplitude and subsidence. Subsidence (ΔZ) is treated as an apparent increase to the maximum tsunami elevation and is relatively uniform throughout the DOU. Tidal elevation is set equal to higher high water large tide (2.0 m). Figures and tabulated results for all tsunami scenarios can be found in Appendix C.

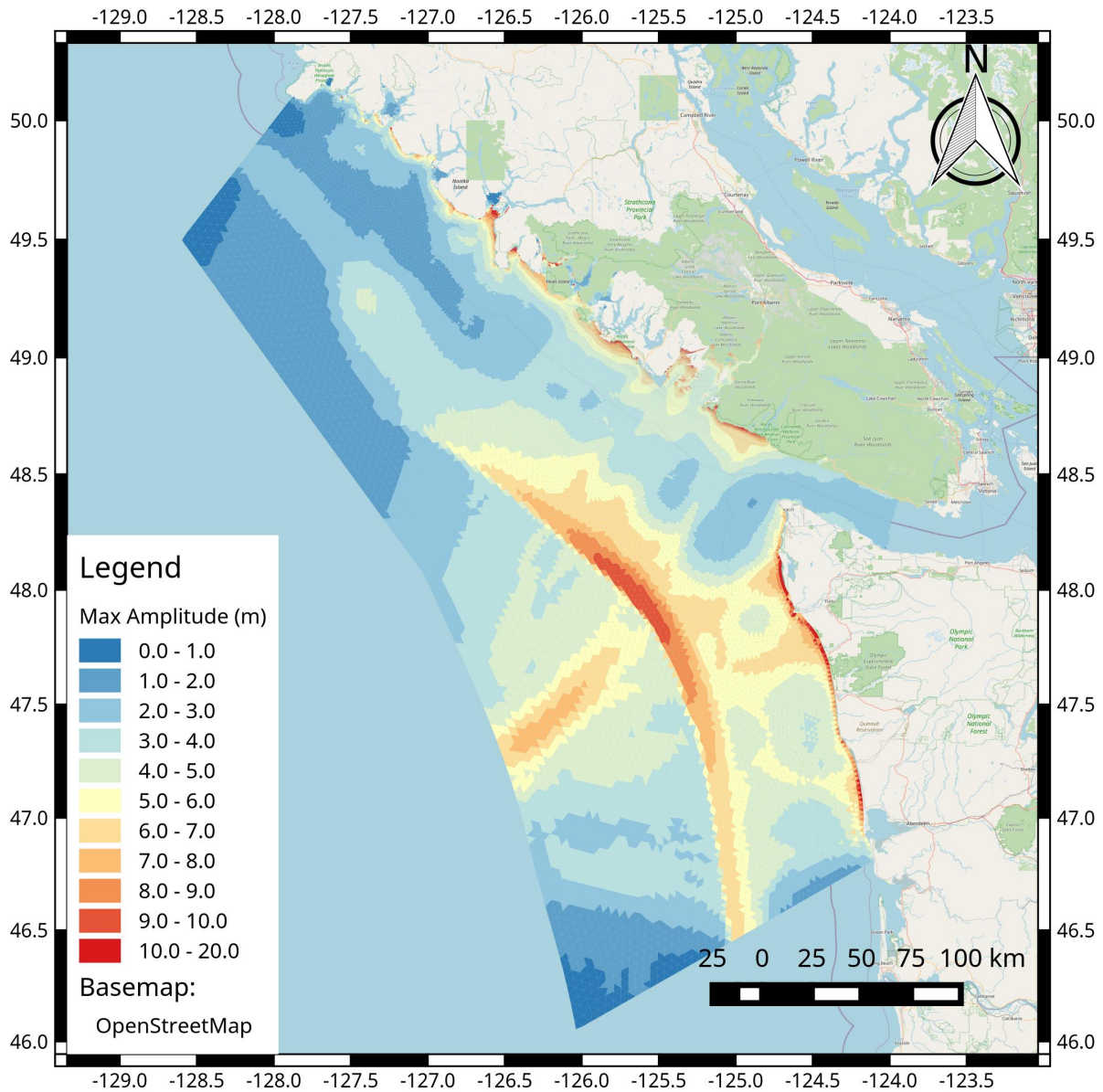


Figure 14: Maximum tsunami amplitude for the G2018-S-A fault rupture model.

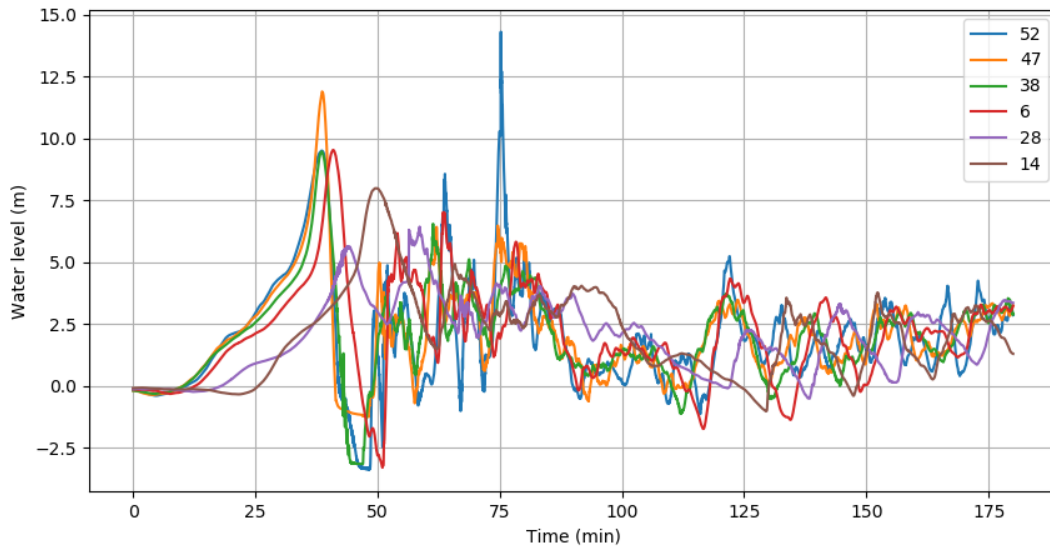


Figure 15: Time series of tsunami water elevation for the G2018-S-A rupture (relative to mean sea level). Transect numbers indicated in legend.

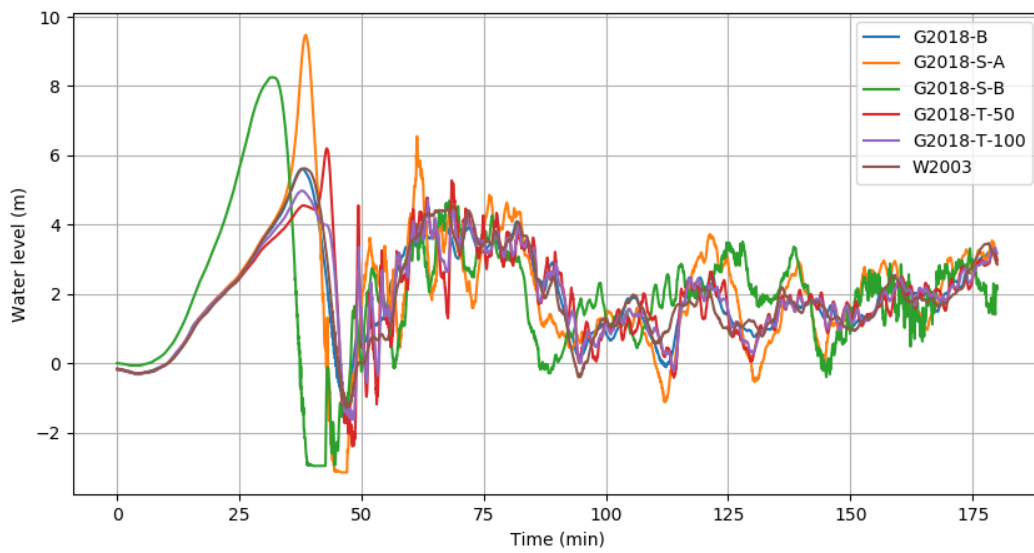


Figure 16: Time series of tsunami water elevation for all simulated ruptures, at transect 38 (relative to mean sea level).

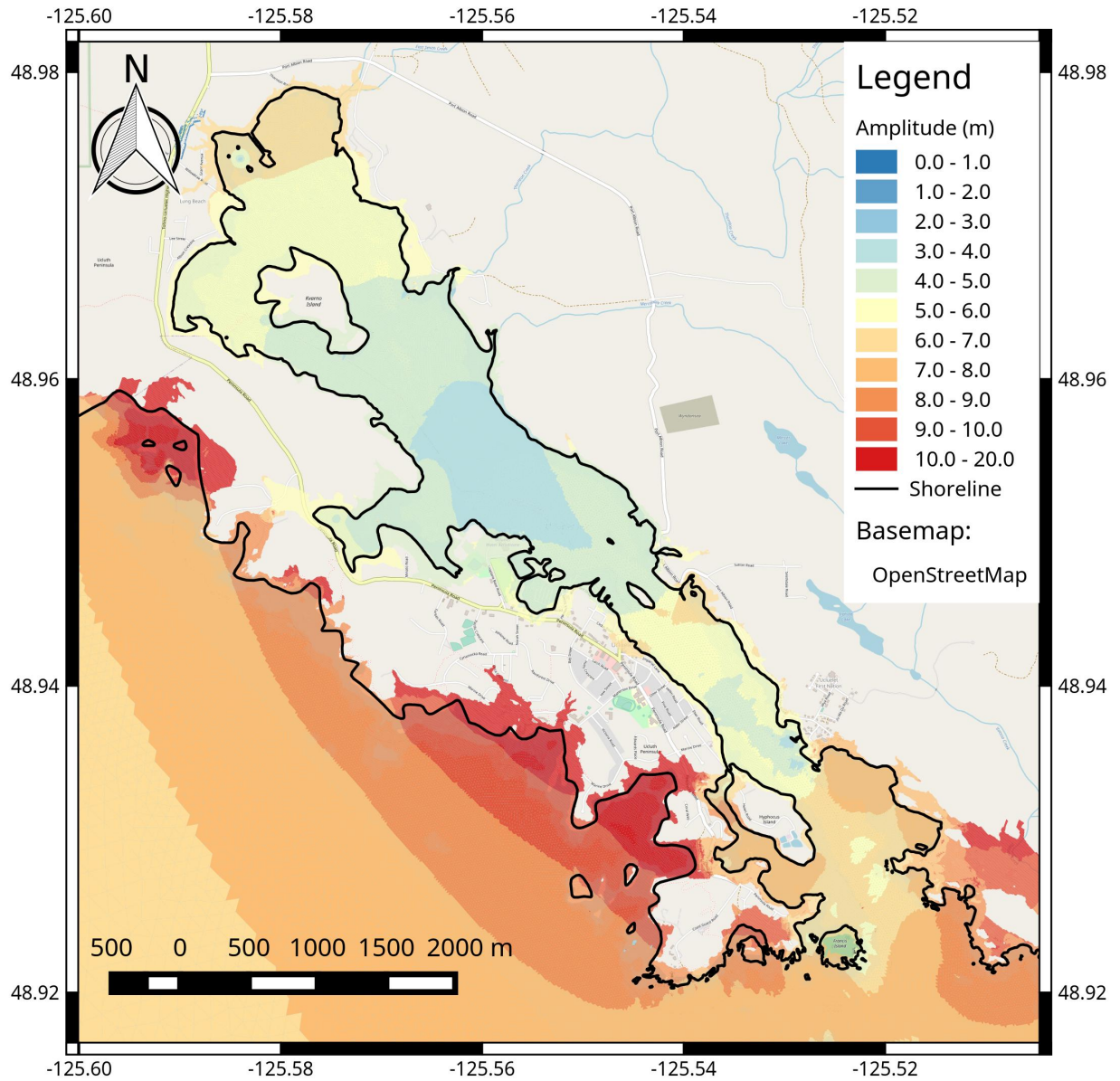


Figure 17: Maximum tsunami amplitude for G2018-S-A rupture, detail of the DOU. Ambient water level = 2 m (2 m tide + 0 m RSLR).

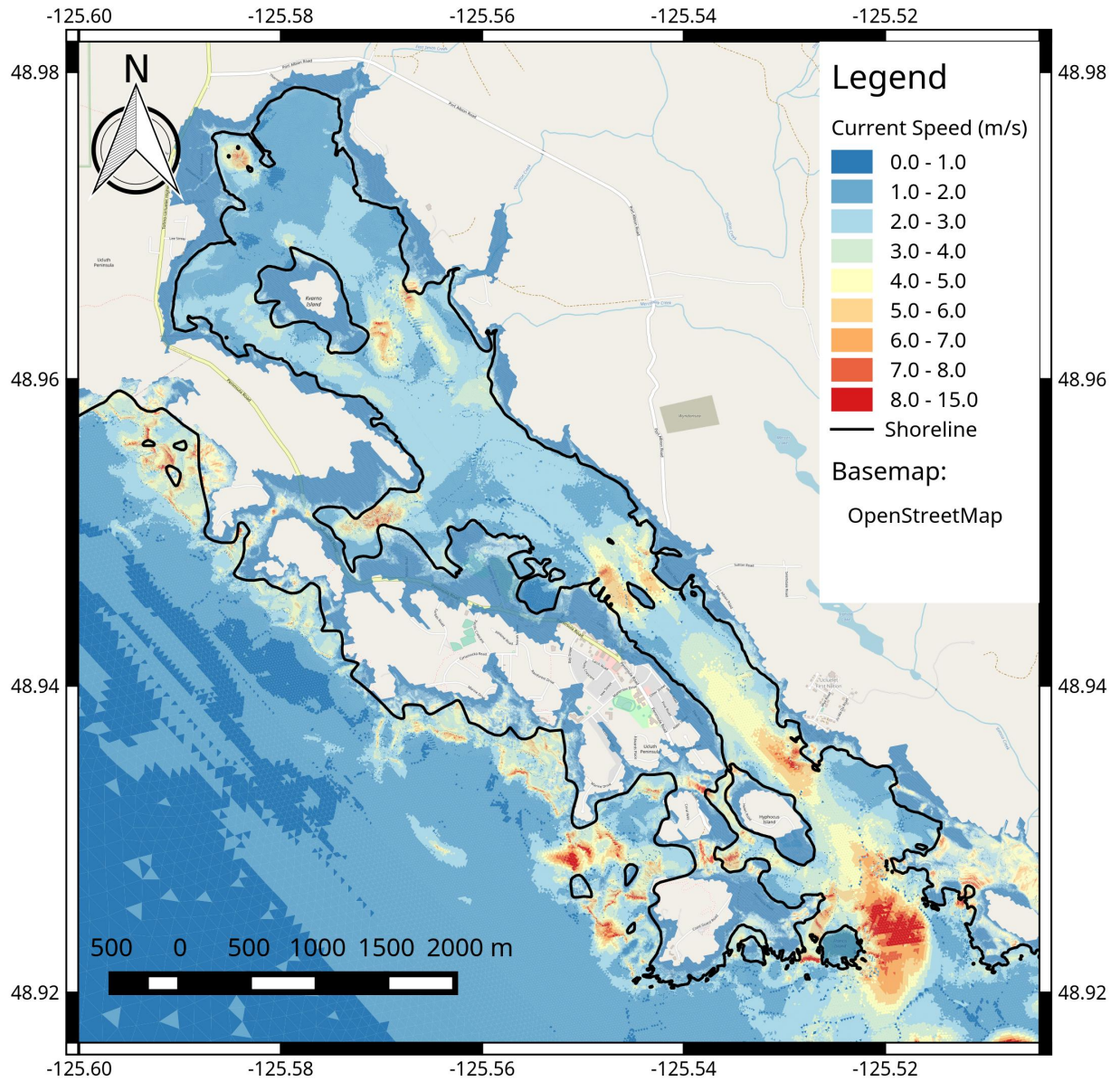


Figure 18: Maximum tsunami current speed for G2018-S-A rupture, detail of DOU. Ambient water level = 2 m (2 m tide + 0 m RSLR).

Table 6: Tsunami results for all simulated ruptures, at transects for the RSLR = 0 m scenario.

TS#	G2018-B		G2018-S-A		G2018-S-B		G2018-T-100		G2018-T-50		W2003	
	Amp (m)	FCRP (m)	Amp (m)	FCRP (m)	Amp (m)	FCRP (m)	Amp (m)	FCRP (m)	Amp (m)	FCRP (m)	Amp (m)	FCRP (m)
1	3.8	7.9	8.1	12.3	6.6	10.5	4.4	8.6	3.1	7.3	3.8	7.9
2	3.7	7.8	7.9	12.1	6.5	10.5	4.3	8.5	3.0	7.2	3.7	7.8
3	3.4	7.5	7.6	11.7	5.9	9.8	4.1	8.2	2.7	6.9	3.4	7.5
4	3.3	7.4	7.2	11.4	5.8	9.8	3.7	7.8	2.7	6.8	3.4	7.4
5	3.5	7.6	7.6	11.8	6.1	10.1	4.0	8.1	2.9	7.0	3.5	7.6
6	3.5	7.6	7.5	11.7	6.1	10.1	4.0	8.1	2.9	7.0	3.5	7.6
7	2.8	6.9	5.3	9.5	4.8	8.7	3.2	7.3	2.4	6.5	2.9	7.0
8	2.8	6.9	5.8	9.9	4.5	8.4	3.2	7.3	2.3	6.5	2.8	6.9
9	2.1	6.2	4.8	8.9	2.9	6.8	2.7	6.8	2.0	6.1	2.2	6.3
10	2.4	6.5	4.4	8.5	3.3	7.2	2.9	7.0	2.2	6.3	2.5	6.6
11	2.8	6.9	4.3	8.4	4.3	8.2	3.3	7.4	2.8	6.8	2.9	7.0
12	3.8	7.8	5.8	9.8	5.2	9.1	3.6	7.7	3.4	7.5	3.9	7.9
13	4.0	8.0	6.3	10.3	5.4	9.3	4.0	8.1	3.5	7.6	4.0	8.1
14	3.9	8.0	6.0	10.1	5.4	9.3	4.0	8.1	3.5	7.6	4.0	8.1
16	2.9	7.0	4.4	8.5	4.4	8.3	3.4	7.5	2.9	7.0	3.0	7.1
18	3.7	7.9	5.5	9.7	5.4	9.3	4.0	8.1	3.3	7.5	3.8	7.9
19	3.2	7.3	4.4	8.5	4.8	8.7	3.5	7.6	3.0	7.1	3.3	7.4
20	2.7	6.8	4.1	8.3	3.7	7.7	3.1	7.2	2.4	6.5	2.7	6.8
22	2.7	6.9	4.2	8.3	3.9	7.8	3.1	7.2	2.4	6.6	2.8	6.9
24	2.7	6.8	4.2	8.4	3.8	7.7	3.1	7.2	2.4	6.5	2.8	6.9
25	2.6	6.7	4.0	8.2	3.6	7.6	3.0	7.1	2.3	6.5	2.7	6.8
26	2.4	6.6	4.0	8.2	3.3	7.2	2.9	7.1	2.2	6.3	2.5	6.6
27	2.4	6.5	4.7	8.9	3.1	7.1	3.1	7.2	2.2	6.3	2.4	6.5
28	2.3	6.4	4.4	8.6	3.0	6.9	2.7	6.8	2.1	6.2	2.3	6.4
29	2.8	6.9	5.8	10.0	4.3	8.2	3.3	7.4	2.4	6.5	2.8	6.9
30	2.8	6.9	5.7	9.9	4.4	8.3	3.2	7.3	2.4	6.5	2.8	6.9
31	2.6	6.7	5.2	9.4	4.3	8.3	3.1	7.2	2.2	6.4	2.7	6.8
32	2.6	6.7	5.8	9.9	4.5	8.5	3.1	7.3	2.1	6.3	2.6	6.7
33	3.4	7.5	7.4	11.6	6.1	10.1	3.3	7.5	2.8	6.9	3.4	7.6
34	3.5	7.6	7.9	12.1	6.0	10.0	3.8	7.9	2.8	7.0	3.5	7.6
35	3.5	7.7	7.7	11.9	6.1	10.0	3.6	7.8	2.9	7.1	3.5	7.7
36	3.4	7.5	7.6	11.8	6.0	10.0	3.4	7.5	2.8	6.9	3.4	7.6
37	3.2	7.3	6.2	10.4	6.0	10.0	3.6	7.7	2.6	6.8	3.3	7.4
38	3.6	7.8	7.5	11.7	6.3	10.3	4.2	8.4	3.0	7.2	3.6	7.8
39	3.9	8.0	8.4	12.6	6.6	10.6	4.8	9.0	3.2	7.4	3.9	8.0
40	3.8	8.0	7.8	12.0	6.5	10.5	4.4	8.6	3.1	7.3	3.8	8.0
41	4.2	8.4	9.2	13.4	7.0	11.0	5.2	9.4	3.6	7.8	4.3	8.4
42	4.8	9.0	10.3	14.5	7.2	11.2	5.7	9.9	3.8	8.0	4.7	8.8
43	4.9	9.1	11.0	15.2	7.2	11.2	5.8	9.9	4.0	8.2	4.8	9.0
44	5.1	9.2	11.5	15.7	7.2	11.2	6.7	10.8	4.1	8.3	5.0	9.2
45	4.8	9.0	10.6	14.8	7.2	11.2	5.2	9.4	3.9	8.1	4.7	8.9
46	4.4	8.6	9.6	13.8	7.1	11.1	4.8	9.0	3.6	7.8	4.4	8.5
47	4.4	8.6	9.9	14.1	7.2	11.2	4.8	9.0	3.6	7.8	4.4	8.6
48	4.3	8.5	8.5	12.7	7.3	11.3	3.9	8.1	3.6	7.8	4.4	8.5
49	5.0	9.2	8.5	12.6	7.4	11.3	4.6	8.8	4.6	8.8	5.0	9.2
50	4.4	8.6	7.8	11.9	7.4	11.4	4.7	8.9	4.6	8.8	4.5	8.7
51	5.8	10.0	9.9	14.1	7.6	11.5	6.0	10.1	4.9	9.1	6.0	10.2
52	6.8	10.9	12.7	16.9	9.2	13.1	5.9	10.1	6.0	10.2	7.0	11.2

7 Results and Discussion

7.1 Flood Construction Reference Plane

In the DOU the estimated tsunami flood hazard is much larger than the storm flood hazard. Here we specify the tsunami FCRP as the largest FCRP of all the simulations at each transect. Table 7 provides the tsunami FCRPs and 0.2% AEP storm FCRPs at each transect for each RSLR scenario.

Table 7: Comparison of FCRP estimates based on tsunami and 0.2% AEP storm flooding hazard at each transect.

RSLR (m): Source: AEP (%)	0.0		0.5		1.0		2.0	
	Tsunami NA	Storm 0.2	Tsunami NA	Storm 0.2	Tsunami NA	Storm 0.2	Tsunami NA	Storm 0.2
TS#	FCRP (m)	FCRP (m)						
1	12.3	5.9	12.7	6.8	13.2	7.7	14.2	9.5
2	12.1	5.8	12.5	8.0	13.0	9.3	14.0	10.8
3	11.7	3.8	12.2	4.2	12.7	4.7	14.1	5.5
4	11.4	4.4	11.9	4.9	12.5	5.4	13.9	6.4
5	11.8	4.1	12.3	4.6	12.8	5.5	14.0	6.6
6	11.7	4.0	12.2	5.2	12.8	5.6	13.8	6.2
7	9.5	3.2	9.9	3.2	10.5	4.3	11.5	5.9
8	9.9	2.8	10.6	3.3	11.2	3.7	12.4	4.7
9	8.9	3.5	9.5	4.0	10.0	4.4	11.1	5.4
10	8.5	2.9	8.9	3.4	9.6	3.9	10.8	4.8
11	8.4	2.7	9.0	3.2	9.7	3.7	10.9	4.9
12	9.8	3.1	10.5	3.6	11.2	3.8	12.5	4.6
13	10.3	2.9	11.0	3.3	11.7	3.8	13.0	4.8
14	10.1	2.9	10.8	3.4	11.5	3.7	12.8	5.4
16	8.5	3.0	9.1	3.5	9.8	4.3	11.1	5.3
18	9.7	2.8	10.3	3.2	11.0	3.7	12.4	4.8
19	8.7	2.7	9.4	3.2	10.1	3.7	11.4	5.6
20	8.3	3.2	8.9	3.6	9.6	3.8	10.9	4.8
22	8.3	2.9	8.9	3.4	9.6	3.7	10.9	4.7
24	8.4	2.7	9.0	3.2	9.6	3.7	10.8	4.7
25	8.2	3.0	8.8	3.5	9.5	4.0	10.7	5.0
26	8.2	3.0	8.8	3.1	9.5	3.6	10.7	4.7
27	8.9	2.9	9.4	3.4	9.9	3.6	11.1	4.7
28	8.6	3.1	9.3	3.3	9.7	3.7	10.6	4.8
29	10.0	2.8	10.5	3.3	11.1	3.7	12.2	4.7
30	9.9	3.2	10.4	4.1	11.1	4.4	12.3	5.4
31	9.4	2.9	10.0	3.8	10.6	4.3	11.7	5.4
32	9.9	3.7	10.5	4.0	11.1	4.5	12.4	5.6
33	11.6	5.5	12.0	5.9	12.5	6.9	13.5	9.3
34	12.1	3.3	12.6	3.8	13.2	4.3	14.2	5.3
35	11.9	2.9	12.4	3.6	13.0	4.1	13.9	5.1
36	11.8	4.0	12.2	5.1	12.8	5.4	13.7	6.6
37	10.4	5.1	10.8	5.8	11.3	6.4	12.4	7.8
38	11.7	8.0	12.1	8.6	12.6	9.3	13.5	10.4
39	12.6	7.9	13.0	9.0	13.5	9.3	14.5	11.2
40	12.0	10.8	12.5	11.3	13.0	11.9	13.9	12.9
41	13.4	11.3	13.8	11.4	14.3	12.3	15.2	13.5
42	14.5	6.4	14.8	7.8	15.2	8.4	16.0	12.0
43	15.2	6.7	15.6	7.7	16.0	7.9	16.7	10.8
44	15.7	5.8	16.0	6.4	16.4	7.1	17.1	9.4
45	14.8	5.1	15.2	5.9	15.6	6.4	16.4	7.4
46	13.8	6.5	14.2	6.9	14.7	7.4	15.7	8.2
47	14.1	8.5	14.5	9.2	14.9	10.1	15.8	11.7
48	12.7	12.7	13.2	13.7	13.6	14.5	14.6	15.5
49	12.6	6.3	13.1	6.9	13.6	7.4	14.6	8.5
50	11.9	12.8	12.4	13.3	12.9	13.8	13.9	14.8
51	14.1	4.8	14.0	5.4	14.7	5.9	15.0	7.0
52	16.9	9.3	16.0	9.8	15.8	10.3	16.1	11.3

7.2 Uncertainties and Freeboard Recommendations

The accuracy of the storm flood estimates rely on the accuracy of the coastal hind-cast. The water level estimates (tide + surge) are based on measurements, but are assumed spatially constant throughout the District, introducing a small amount of uncertainty. Despite evaluation of the spectral wave model to long term measurements off-shore and near-shore, uncertainty persists in these estimates. Although the shoreline is sub-divided into 48 reaches, variation in shoreline type, slope, and orientation still exist within each reach. These variations may result in both higher and lower wave runup within each reach. As a consequence of these factors, the wave runup portion of the coastal hind-cast will have a larger uncertainty compared to the tide and surge contributions. This is particularly true on the exposed west coast of the DOU, where runup can exceed 10 m and the shore is extremely irregular.

The use of the hind-cast to estimate probability of future storm flooding assumes that the future climate at the DOU will be similar to the historic climate. For example, that the DOU will experience a similar number of storms each year with similar intensity to that which have been experienced historically. Climate change will cause the future climate to deviate from the existing one and these changes will be different from region to region. The available literature suggests only minor changes to the DOU ocean climate over the next century, however future research may suggest otherwise.

Flood Construction Level defines the elevation of the underside of a wooden floor system or top of concrete slab for habitable buildings and is calculated as the FCRP plus an appropriate freeboard allowance. The freeboard allowance is intended to account for uncertainties in the hazard analysis. For the storm flooding analysis approach used in this work a freeboard of 0.6 m is generally used [3]. However, given the very large wave runup contributions along the exposed coast, the DOU may consider a larger freeboard along these reaches.

The accuracy of the tsunami flood estimates rely on the accuracy of the tsunami modelling including the deformation model, bathymetry and assumptions about the tidal level. Furthermore, only a small set of deterministic events were modelled. The modelled events are based on a CSZ megathrust event with 500 years of accumulated stress. The fault rupture models are an estimate based on the available evidence at the time of development [20, 25]. While all of these fault ruptures are plausible based on the evidence, the authors have not provided relative probabilities. It is likely that a present day CSZ event would result in smaller deformation than the ones modelled, but that is not certain. Even for an event with smaller or similar deformation, the characteristics of the deformation may result in a larger response in the DOU. This is illustrated with the significant differences in the magnitude of the tsunami generated by the G2018-S-A and G2018-B events. Finally, a tidal level of higher high water large tide (2.0 m) was assumed to coincide with each tsunami event.

Given similar uncertainties associated with the tsunami flood estimates in the Capital Regional District (CRD) [21], AECOM applied a 50% *factor for public safety* when defining tsunami hazard elevations. A similar factor for public safety may be applied at the DOU, however, it is acknowledged that this may not be practical to do so, given the very large estimated inundation levels. At minimum, when defining the tsunami hazard line, the DOU should consider all available data concerning potential tsunami inundation, including all simulations from this work, and from the work of others, such as [23].

Notwithstanding the uncertainties discussed here, the results of this work provides a detailed assessment of tsunami and coastal storm flooding hazard in the DOU and will be useful for short and long term planning as well as future risk assessment and mitigation activities.

8 References

- [1] L. J. Leonard, G. C. Rogers, and S. Mazzotti, “Tsunami hazard assessment of Canada,” *Natural Hazards*, vol. 70, pp. 237–274, Jan 2014.
- [2] B. D. Bornhold and R. E. Thomson, *Climate Trends and Projections for the Pacific Large Aquatic Basin*, ch. TRENDS IN SEA LEVEL, p. 27. Fisheries and Oceans Canada, 2013.
- [3] Ministry of Water, Land and Air Protection, “Flood Hazard Area Land Use Management Guidelines,” tech. rep., Province of British Columbia, 2017.
- [4] IPCC, *Climate Change 2013: The Physical Science Basis. Contribution of Working Group I to the Fifth Assessment Report of the Intergovernmental Panel on Climate Change*. Cambridge, United Kingdom and New York, NY, USA: Cambridge University Press, 2013.
- [5] Ausenco Sandwell, “Climate change adaption guidelines for sea dikes and coastal flood hazard land use - guidelines for management of coastal flood hazard land use,” tech. rep., BC Ministry of Environment, 2011.
- [6] Ausenco Sandwell, “Climate change adaption guidelines for sea dikes and coastal flood hazard land use - sea dike guidelines,” tech. rep., BC Ministry of Environment, 2011.
- [7] Ausenco Sandwell, “Climate change adaption guidelines for sea dikes and coastal flood hazard land use - draft policy discussion paper,” tech. rep., BC Ministry of Environment, 2011.
- [8] APEGBC, “APEGBC Professional Practice Guidelines - Flood Mapping in BC,” tech. rep., The Association of Professional Engineers and Geoscientists of BC, 2017.
- [9] A. J. Garner, J. L. Weiss, A. Parris, R. E. Kopp, R. M. Horton, J. T. Overpeck, and B. P. Horton, “Evolution of 21st century sea level rise projections,” *Earth’s Future*, vol. 6, no. 11, pp. 1603–1615, 2018.
- [10] S. Mazzotti, C. Jones, and R. E. Thomson, “Relative and absolute sea level rise in western Canada and northwestern United States from a combined tide gauge-GPS analysis,” *Journal of Geophysical Research: Oceans*, vol. 113, no. C11, pp. n/a–n/a, 2008. C11019.
- [11] R. A. Walters, “A coastal ocean model with subgrid approximation,” *Ocean Modelling*, vol. 102, pp. 45–54, 2016.
- [12] L. Erikson, C. Hegermiller, P. Barnard, P. Ruggiero, and M. van Ormondt, “Projected wave conditions in the Eastern North Pacific under the influence of two CMIP5 climate scenarios,” *Ocean Modelling*, pp. –, 2015.
- [13] M. A. Hemer, Y. Fan, N. Mori, A. Semedo, and X. L. Wang, “Projected changes in wave climate from a multi-model ensemble,” *Nature Clim. Change*, vol. 3, pp. 471–476, May 2013.
- [14] X. L. Wang, Y. Feng, and V. R. Swail, “Changes in global ocean wave heights as projected using multimodel CMIP5 simulations,” *Geophys. Res. Lett.*, vol. 41, pp. 1026–1034, Feb. 2014.
- [15] FEMA, “Guidelines and Specifications for Flood Hazard Mapping Partners. Appendix D: Guidance for Coastal Flooding Analyses and Mapping,” tech. rep., Federal Emergency Management Agency, 2003.
- [16] D. H. Douglas and T. K. Peucker, “Algorithms for the reduction of the number of points required to represent a digitized line or its caricature,” *Cartographica: The International Journal for Geographic Information and Geovisualization*, vol. 10, no. 2, pp. 112–122, 1973.

- [17] Seaconsult Marine Research, "Evaluation of tsunami levels along the British Columbia coast," tech. rep., Department of Fisheries and Oceans, 1988.
- [18] B. Atwater, S. Musumi-Rokkaku, K. Satake, Y. Tsuji, K. Ueda, and D. Yamaguchi, *The orphan tsunami of 1700 - Japanese clues to a parent earthquake in North America, 2nd ed.* University of Washington Press, 2015.
- [19] J. Y. Cherniawsky, V. V. Titov, K. Wang, and J.-Y. Li, "Numerical simulations of tsunami waves and currents for Southern Vancouver Island from a Cascadia megathrust earthquake," *Pure and Applied Geophysics*, vol. 164, pp. 465–492, Mar 2007.
- [20] K. Wang, R. Wells, S. Mazzotti, R. D. Hyndman, and T. Sagiya, "A revised dislocation model of inter-seismic deformation of the Cascadia subduction zone," *Journal of Geophysical Research: Solid Earth*, vol. 108, no. B1, 2003.
- [21] AECOM, "Modelling of potential tsunami inundation limits and run-up," tech. rep., Capital Regional District, 2013.
- [22] C. Hiles and R. Walters, "Coastal Flood Hazard Analysis: The District of Tofino, BC.," tech. rep., Cascadia Coast Research Ltd., 2019.
- [23] T. Takabatake, I. Nistor, and P. St-Germain, "Tsunami evacuation simulation for the district of tofino, vancouver island, canada," *International Journal of Disaster Risk Reduction*, vol. 48, p. 101573, 2020.
- [24] National Oceanic and Atmospheric Administration, "Manual of Splitting Tsunami (MOST) Software Manual," tech. rep., National Oceanic and Atmospheric Administration, 2006.
- [25] D. Gao, K. Wang, T. L. Insua, M. Sypus, M. Riedel, and T. Sun, "Defining megathrust tsunami source scenarios for northernmost Cascadia," *Natural Hazards*, vol. 94, pp. 445–469, Oct 2018.
- [26] R. F. Henry and R. A. Walters, "Geometrically based, automatic generator for irregular triangular networks," *Communications in Numerical Methods in Engineering*, vol. 9, no. 7, pp. 555–566, 1993. I have printed and read this paper.
- [27] R. Walters and V. Casulli, "A robust, finite element model for hydrostatic surface water flows," *Communications in Numerical Methods in Engineering*, vol. 14, pp. 931–40, Oct. 1998.
- [28] R. A. Walters, P. Barnes, and J. R. Goff, "Locally generated tsunami along the Kaikoura coastal margin: Part 1. fault ruptures," *New Zealand Journal of Marine and Freshwater Research*, vol. 40, no. 1, pp. 1–16, 2006.
- [29] R. Walters, P. Barnes, K. Lewis, J. R. Goff, and J. Fleming, "Locally generated tsunami along the Kaikoura coastal margin: Part 2. submarine landslides," *New Zealand Journal of Marine and Freshwater Research*, vol. 40, no. 1, pp. 17–28, 2006.
- [30] R. A. Walters, J. Goff, and K. Wang, "Tsunamigenic sources in the Bay of Plenty, New Zealand," *Science of Tsunami Hazards*, vol. 25, pp. 339–357, 2006.
- [31] Copernicus Climate Change Service (C3S), "ERA5: Fifth generation of ECMWF atmospheric reanalyses of the global climate." Copernicus Climate Change Service Climate Data Store (CDS), 2017.
- [32] A. Chawla, D. Spindler, and H. Tolman, "30 Year Wave Hindcasts using WAVEWATCH III with CFSR winds," tech. rep., National Oceanic and Atmospheric Administration, 2012.
- [33] R. Pawlowicz, B. Beardsley, and S. Lentz, "Classical tidal harmonic analysis including error estimates in MATLAB using T-TIDE," *Computers and Geosciences*, vol. 28, pp. 929–37, Oct. 2002.

- [34] N. Booij, R. Ris, and L. Holthuijsen, "A third-generation wave model for coastal regions. 1. model description and validation," *Journal of Geophysical Research*, vol. 104, pp. 7649–66, Apr. 1999.
- [35] NCEP, "WAVEWATCH III Production Hindcast, Multigrid: Feb 2005 to September 2018." http://polar.ncep.noaa.gov/waves/hindcasts/prod-multi_1.php, 2018.
- [36] J. A. Melby, "Wave runup prediction for flood hazard assessment," tech. rep., Army Corps of Engineers, 2012.
- [37] Northwest Hydraulic Consultants, "Coastal flood hazard analysis and mapping for the Pacific Coast of the United States," tech. rep., FEMA, 2004.
- [38] J. W. van der Meer and C. M. Stam, "Wave runup on smooth and rock slopes of coastal structures," *Journal of Waterway, Port, Coastal, and Ocean Engineering*, vol. 118, pp. 534–550, Sept. 1992.
- [39] WAFO-group, *WAFO - A Matlab Toolbox for Analysis of Random Waves and Loads - A Tutorial*. Math. Stat., Center for Math. Sci., Lund Univ., Lund, Sweden, 2000.
- [40] I. V. Fine, J. Y. Cherniawsky, A. B. Rabinovich, and F. Stephenson, "Numerical modeling and observations of tsunami waves in alberni inlet and barkley sound, british columbia," *Pure and Applied Geophysics*, vol. 165, pp. 2019–2044, Dec 2008.
- [41] R. A. Walters, E. Lane, and R. Henry, "Semi-lagrangian methods for a finite element coastal ocean model," *Ocean Modelling*, vol. 19, no. 3, pp. 112 – 124, 2007.
- [42] R. A. Walters, E. M. Lane, and E. Hanert, "Useful time-stepping methods for the coriolis term in a shallow water model," *Ocean Modelling*, vol. 28, no. 1-3, pp. 66–74, 2009.
- [43] R. Walters, E. Hanert, J. Pietrzak, and D. Le Roux, "Comparison of unstructured, staggered grid methods for the shallow water equations," *Ocean Modelling*, vol. 28, no. 1-3, pp. 106–117, 2009.
- [44] V. Casulli, "A high-resolution wetting and drying algorithm for free-surface hydrodynamics," *International Journal for Numerical Methods in Fluids*, vol. 60, no. 4, pp. 391–408, 2008.

Appendices

A Inlet Resonance Analysis

Inlet resonance has the potential to amplify tsunami response and increase the resulting hazard, as was the case for the 1964 tsunami impact at Port Alberni. In that case the tsunami wave entered the Alberni Inlet with an amplitude of about two metres. Due to inlet narrowing and resonant response, the tsunami amplitude at Port Alberni increased from the first to the third wave. By the third wave, the amplitude had grown to over four metres. Studies have since shown that the Alberni Inlet has a resonant mode at about 112 minute period, which is very close to the period of the wave forcing from the 1964 tsunami [40].

The tsunami simulations performed as part of this project were analyzed to investigate the potential for resonance. Qualitatively, the tsunami amplitude at the head of the Ucluelet Inlet was, for each fault rupture scenario, of similar magnitude to that at the entrance of the Inlet. Further quantitative analysis was performed on the results of each simulation by calculating the amplitude spectrum of water levels at the entrance and head of Ucluelet Inlet; the amplification factor was calculated as the ratio of later to the former, and is plotted in Figure 19. Because of the short (3 hour) duration of the tsunami simulations, the frequency resolution in the band of interest (0-6 cycles per hour [cph]), is rather low, however there appears to be possible resonant modes at approximately 0.7, 3.0, and 4.0 cph. A longer time-series is needed to increase the frequency resolution. The tsunami forcing lasts only a few hours at most, so another approach is required to investigate inlet resonance in more detail.

The potential for resonance was further investigated in a manner similar to Fine [40]. A constant amplitude spectrum was developed, covering the 0.5 to 6.0 cph, with a bin-width of 0.0175 cph, and an amplitude of 0.64 mm. Unlike the tsunami forcing, this small amplitude spectral forcing should generate a near linear response in the inlet. The spectrum was converted to a time-series 32 hours long. The tsunami model was driven at the open ocean with the synthesized water level time series. It was "spun up" for a period 3 hours, then run for an additional 29 hours, during which time-series data were saved at locations in and around Ucluelet and Alberni Inlets.

The amplification factors were calculated for both the Alberni and Ucluelet Inlets. At the Alberni Inlet, the amplification spectrum is similar to that calculated in [40], with modes at 0.65 cph, 1.55 cph, and 2.60 cph. At Ucluelet there is a large mode at 0.76 to 0.91 cph, and additional smaller modes at 3 cph and 5 cph (see Figure 20). The location of largest mode appears to correlate well with the spectral results derived directly from the tsunami simulations, however, its magnitude is much smaller in the tsunami simulations. This difference likely due to damping in the inlet system. The mode at 3 cph also roughly correlates with the tsunami simulation results and is of similar magnitude. The apparent mode at 5 cph in Figure 20 does not appear in 19, but is perhaps damped from the system.

The main frequency of the 1965 Alaska tsunami in Barkley Sound was between 0.5 and 0.59 cph [40]. The amplification spectra produced here would suggest that the 1964 tsunami would not have excited a significant resonance in Ucluelet Inlet. However, the largest resonant mode estimated for Ucluelet Inlet is between 0.76 and 0.91 cph, which is in the range of potential tsunami frequencies. So it appears possible that Ucluelet Inlet could be excited by a tsunami into resonance in a similar way that happened with Port Alberni during the 1964 tsunami.

It should be cautioned that this is a preliminary analysis, which was not within the main scope of the project. It could be improved by using a more realistic driving spectrum, and simulating a longer period as in [40].

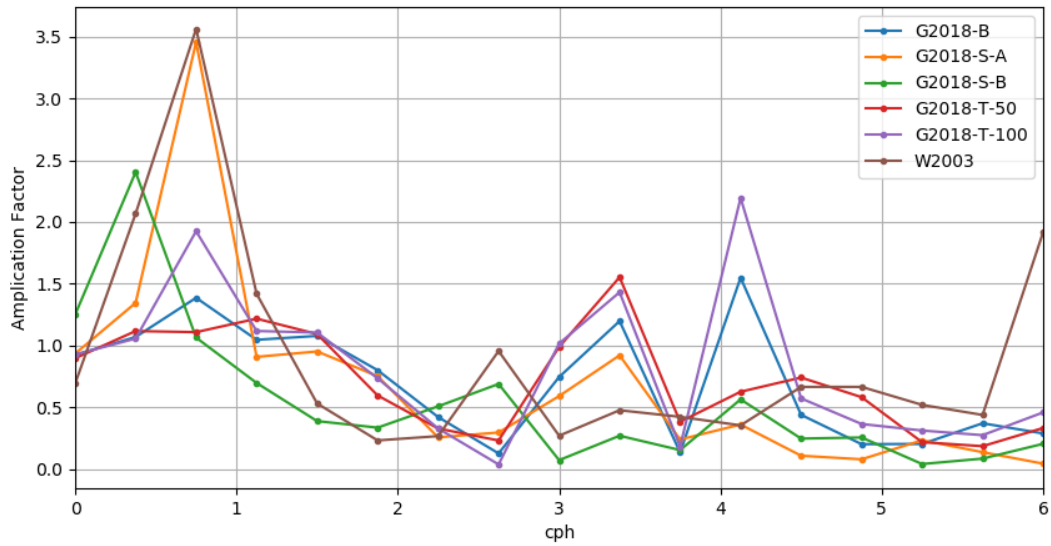


Figure 19: Inlet amplification factor at Ucluelet for each of the simulated tsunami.

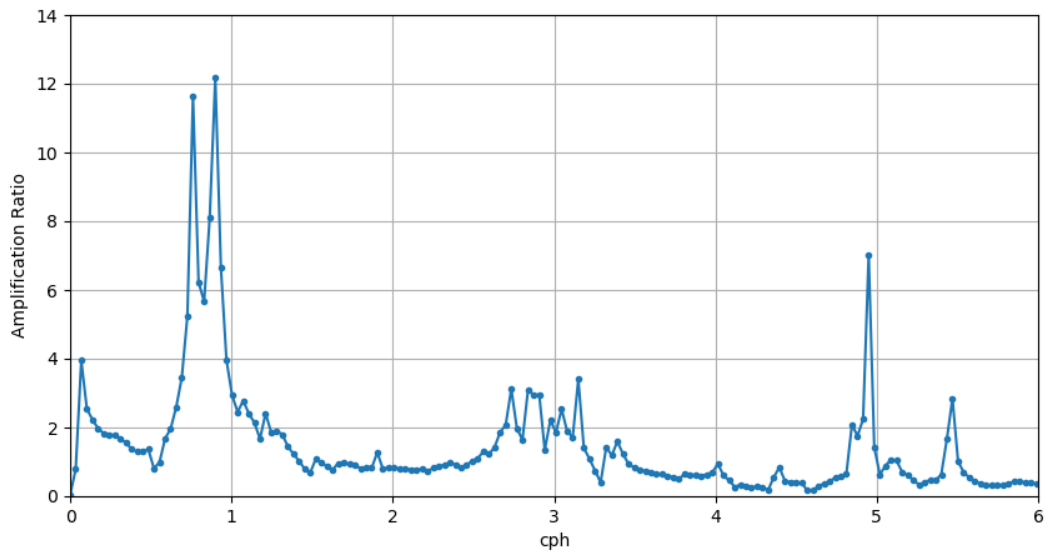


Figure 20: Inlet amplification factor at Ucluelet based on synthesized spectral forcing.

B Cascadia Subduction Zone Fault Rupture Models

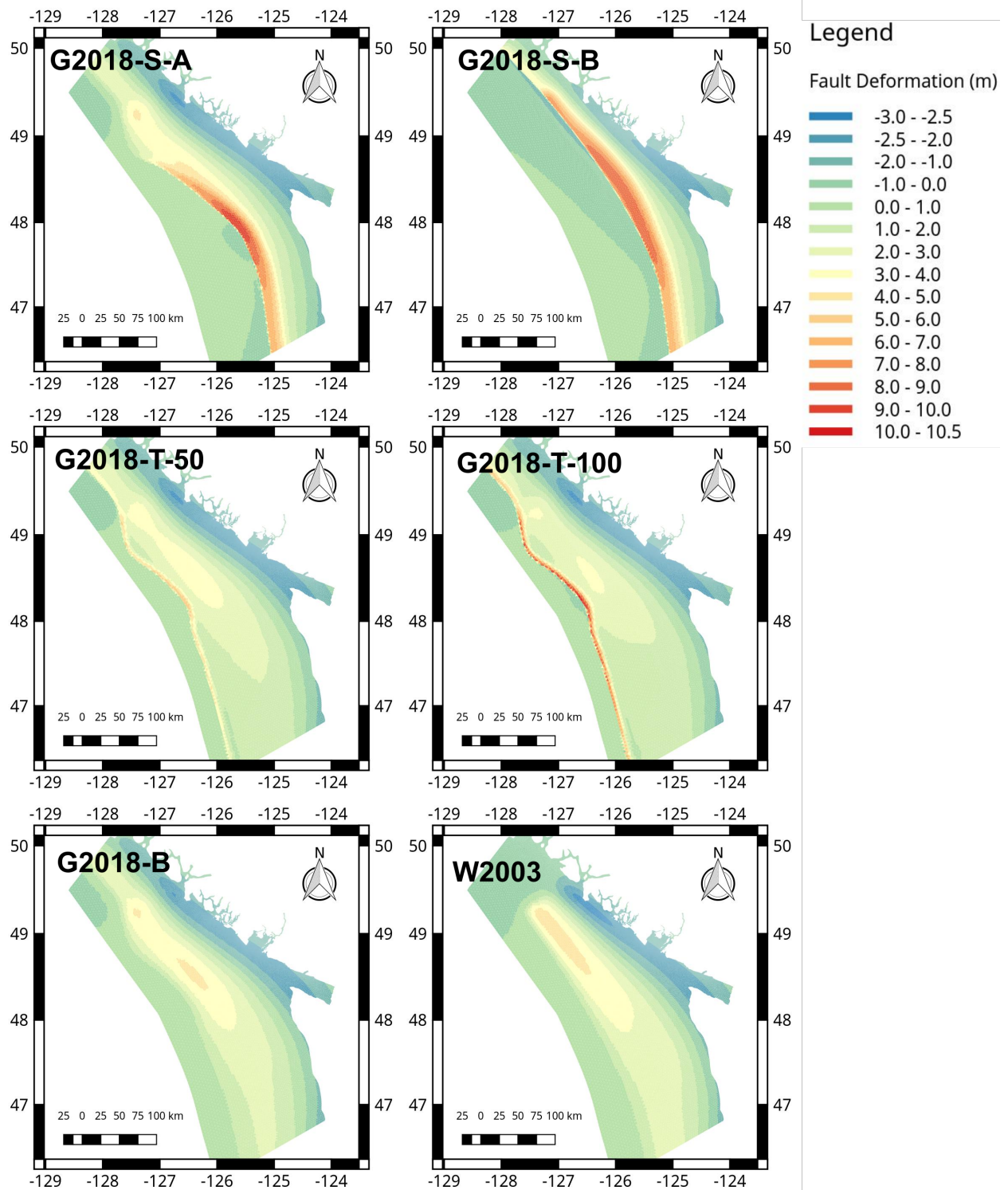


Figure 21: Fault rupture models used in tsunami modelling. Only vertical component of rupture is considered.

C Tsunami Hazard Results

C.1 G2018-B

Table 8: Tsunami results for G2018-B rupture, at transects, for each RSLR scenario. ΔZ is the local subsidence, *Amp* is the tsunami amplitude.

RSLR (m):		0.0		0.5		1.0		2.0	
Tide (m):		2.0		2.0		2.0		2.0	
TS#	ΔZ	Amp (m)	FCRP (m)						
1	-2.1	3.8	7.9	3.7	8.4	3.7	8.9	3.7	9.8
2	-2.1	3.7	7.8	3.6	8.3	3.6	8.8	3.6	9.8
3	-2.1	3.4	7.5	3.4	8.0	3.4	8.5	3.5	9.6
4	-2.1	3.3	7.4	3.3	7.9	3.3	8.4	3.4	9.5
5	-2.1	3.5	7.6	3.5	8.1	3.5	8.6	3.6	9.7
6	-2.1	3.5	7.6	3.5	8.1	3.5	8.6	3.6	9.7
7	-2.1	2.8	6.9	2.9	7.5	3.0	8.1	2.8	8.9
8	-2.1	2.8	6.9	2.9	7.5	2.9	8.0	3.1	9.2
9	-2.1	2.1	6.2	2.3	6.9	2.4	7.5	2.6	8.7
10	-2.1	2.4	6.5	2.5	7.1	2.6	7.7	2.8	8.9
11	-2.1	2.8	6.9	2.9	7.5	3.0	8.1	3.2	9.3
12	-2.1	3.8	7.8	3.9	8.5	4.0	9.0	4.1	10.2
13	-2.1	4.0	8.0	4.1	8.6	4.2	9.2	4.3	10.3
14	-2.1	3.9	8.0	4.0	8.6	4.1	9.2	4.2	10.3
16	-2.1	2.9	7.0	3.6	8.2	3.1	8.2	3.3	9.5
18	-2.1	3.7	7.9	3.8	8.5	4.0	9.1	4.2	10.3
19	-2.1	3.2	7.3	3.3	7.9	3.5	8.6	3.7	9.8
20	-2.1	2.7	6.8	2.8	7.4	2.8	8.0	3.0	9.1
22	-2.1	2.7	6.9	2.8	7.5	2.9	8.1	3.1	9.2
24	-2.1	2.7	6.8	2.8	7.4	2.9	8.0	3.0	9.2
25	-2.1	2.6	6.7	2.7	7.3	2.8	7.9	2.9	9.0
26	-2.1	2.4	6.6	2.5	7.2	2.6	7.7	2.7	8.8
27	-2.1	2.4	6.5	2.5	7.1	2.6	7.7	2.7	8.8
28	-2.1	2.3	6.4	2.4	7.0	2.5	7.6	2.6	8.7
29	-2.1	2.8	6.9	2.8	7.4	2.9	8.0	3.0	9.1
30	-2.1	2.8	6.9	2.8	7.5	2.9	8.0	3.0	9.1
31	-2.1	2.6	6.7	2.7	7.3	2.7	7.9	2.8	8.9
32	-2.1	2.6	6.7	2.6	7.2	2.6	7.8	2.8	9.0
33	-2.1	3.4	7.5	3.4	8.0	3.4	8.5	3.5	9.6
34	-2.2	3.5	7.6	3.4	8.1	3.4	8.6	3.3	9.5
35	-2.2	3.5	7.7	3.5	8.2	3.5	8.7	3.4	9.6
36	-2.2	3.4	7.5	3.4	8.0	3.3	8.5	3.4	9.6
37	-2.2	3.2	7.3	3.2	7.8	3.2	8.3	3.2	9.3
38	-2.2	3.6	7.8	3.6	8.3	3.6	8.7	3.5	9.7
39	-2.2	3.9	8.0	3.9	8.5	3.8	9.0	3.8	10.0
40	-2.2	3.8	8.0	3.8	8.5	3.8	9.0	3.7	9.9
41	-2.2	4.2	8.4	4.3	9.0	4.4	9.6	4.3	10.5
42	-2.2	4.8	9.0	4.8	9.5	4.8	10.0	4.7	10.9
43	-2.2	4.9	9.1	4.9	9.6	4.9	10.0	4.8	11.0
44	-2.2	5.1	9.2	5.0	9.7	5.0	10.1	4.9	11.1
45	-2.2	4.8	9.0	4.8	9.5	4.8	10.0	4.7	10.9
46	-2.2	4.4	8.6	4.4	9.1	4.4	9.6	4.4	10.6
47	-2.2	4.4	8.6	4.4	9.1	4.4	9.6	4.4	10.5
48	-2.2	4.3	8.5	4.3	9.0	4.3	9.5	4.2	10.4
49	-2.2	5.0	9.2	4.9	9.6	4.8	10.0	4.9	11.0
50	-2.2	4.4	8.6	4.4	9.1	4.4	9.5	4.3	10.5
51	-2.2	5.8	10.0	5.8	10.4	5.7	10.8	5.8	11.9
52	-2.2	6.8	10.9	6.6	11.3	6.6	11.8	6.5	12.6

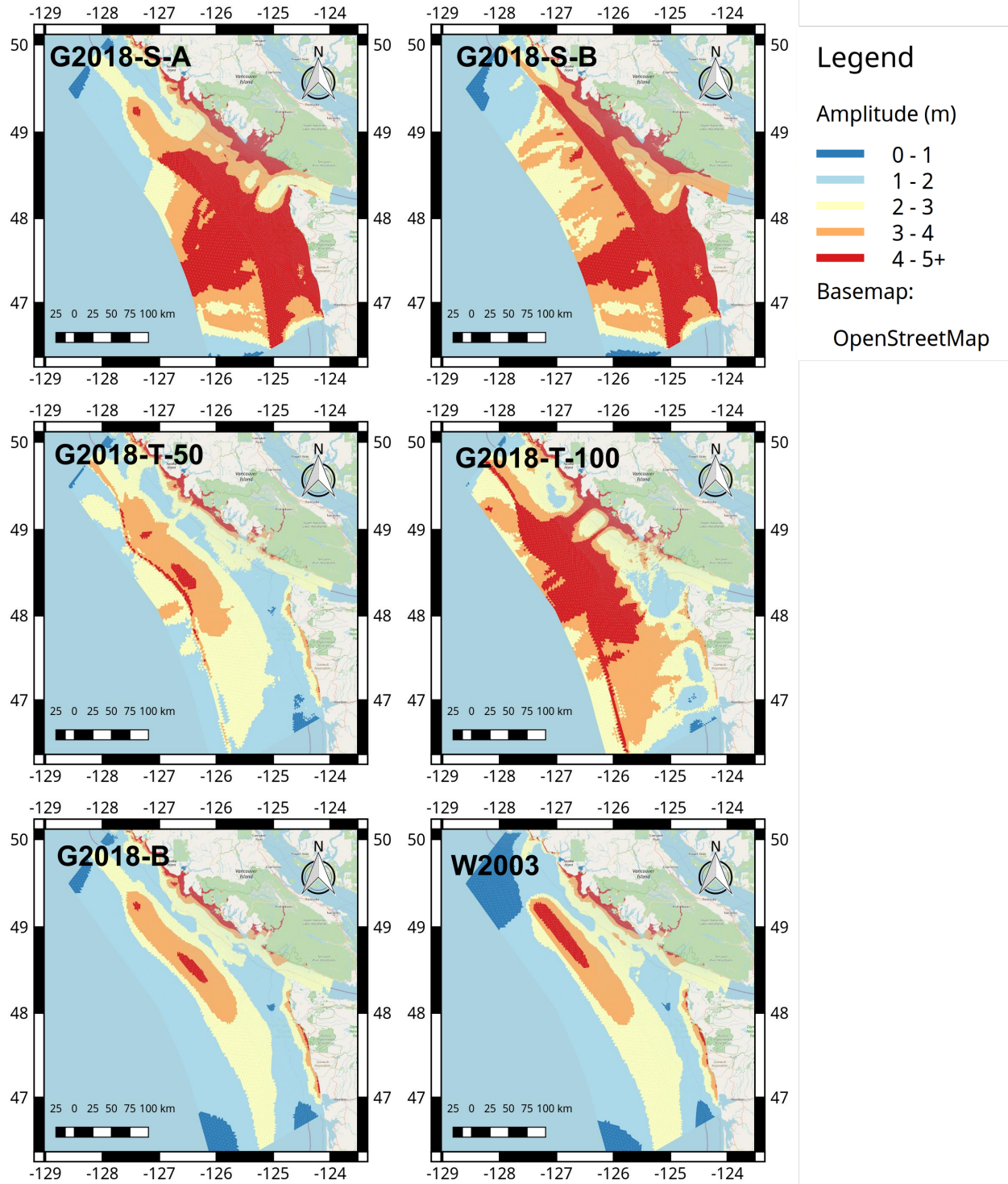


Figure 22: Maximum tsunami amplitude during for each fault rupture scenario. Ambient water level = 2 m (2 m tide + 0 m RSLR).

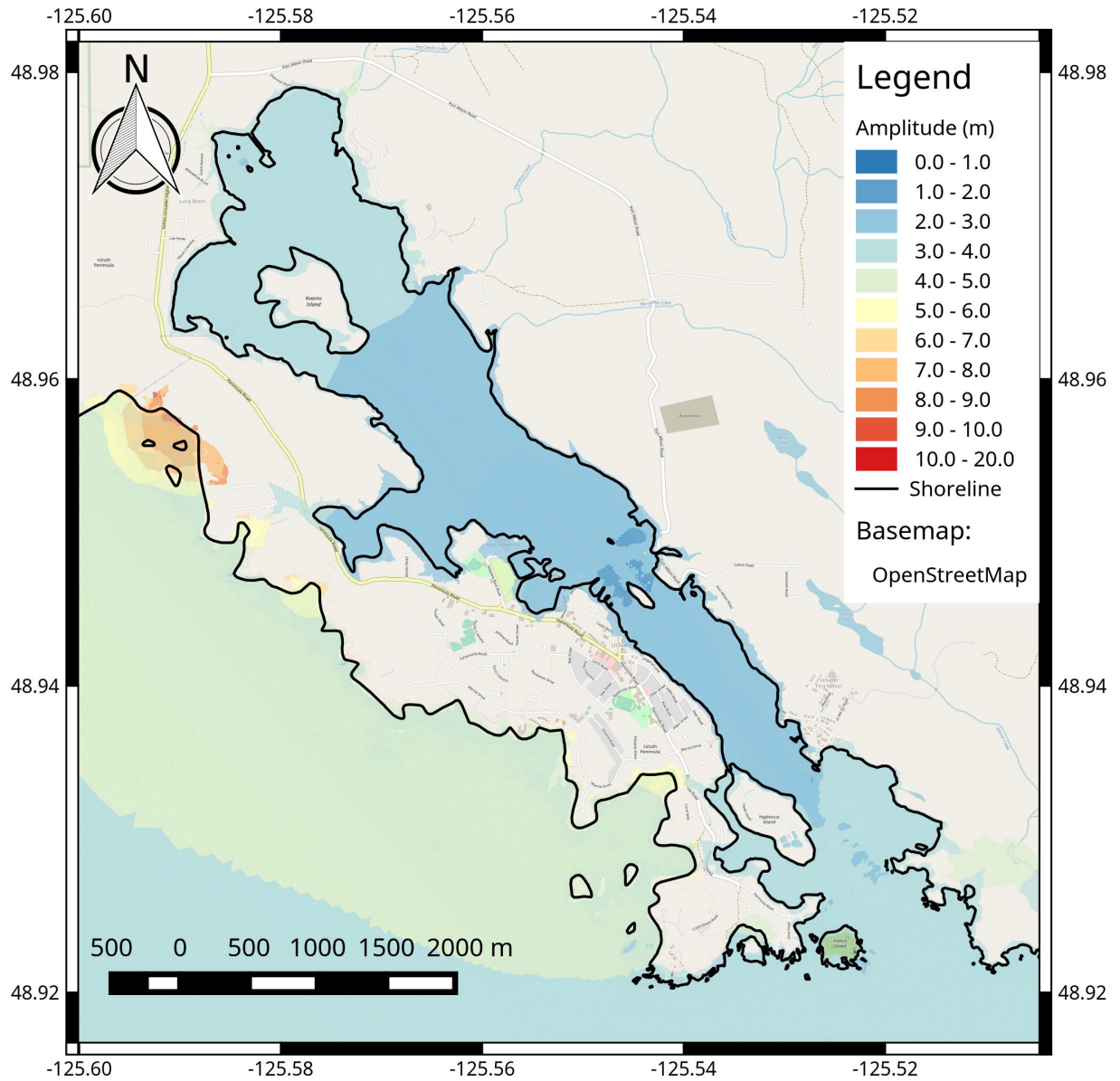


Figure 23: Maximum tsunami amplitude for rupture G2018-B, relative to ambient water level. Ambient water level = 2 m (2 m tide + 0 m RSLR).

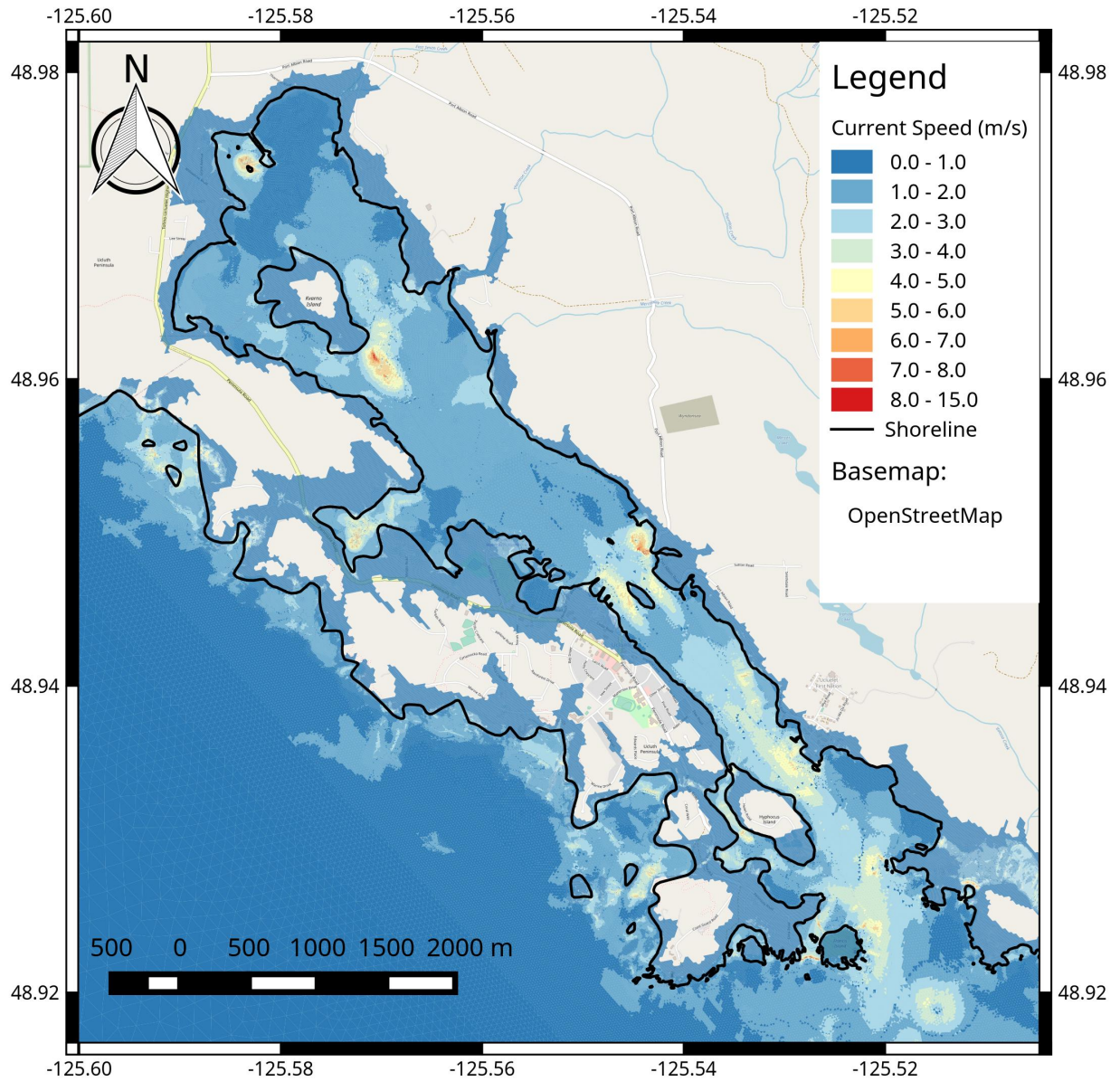


Figure 24: Maximum tsunami current speed for rupture G2018-B. Ambient water level = 2 m (2 m tide + 0 m RSLR).

C.2 G2018-S-A

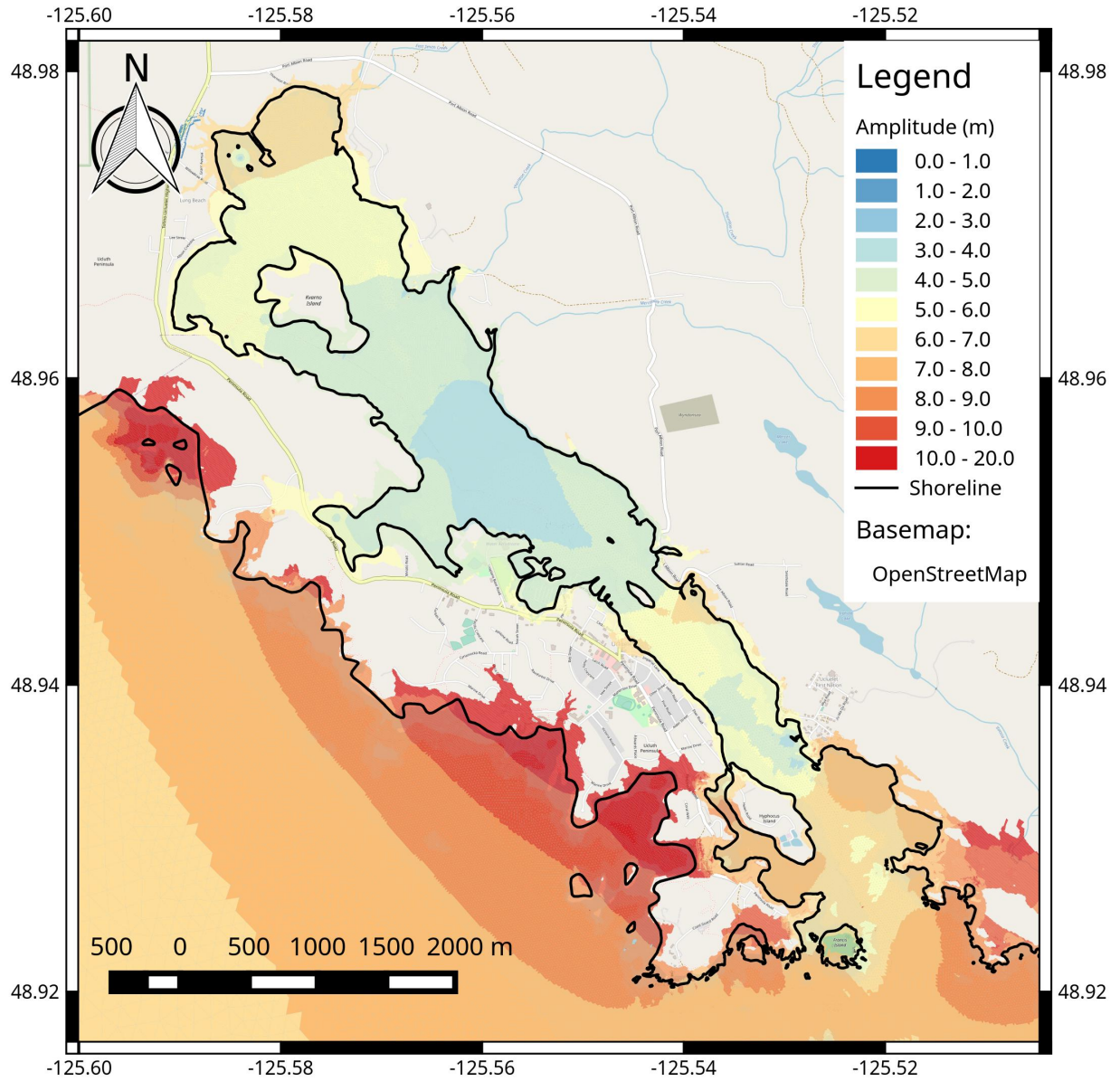


Figure 25: Maximum tsunami amplitude for rupture G2018-S-A, relative to ambient water level. Ambient water level = 2 m (2 m tide + 0 m RSLR).

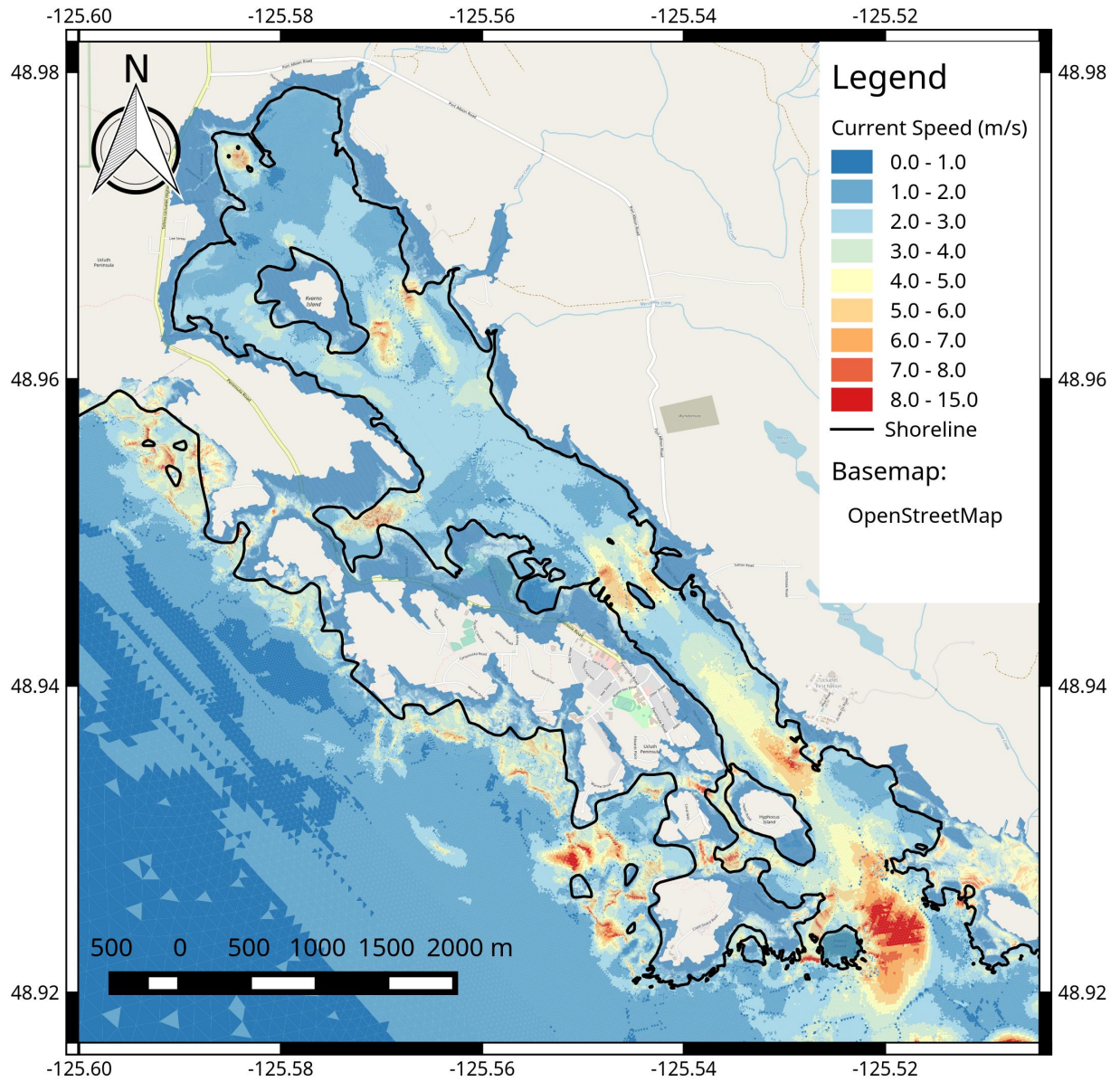


Figure 26: Maximum tsunami current speed for rupture G2018-S-A. Ambient water level = 2 m (2 m tide + 0 m RSLR).

Table 9: Tsunami results for G2018-S-A rupture, at transects, for each RSLR scenario. ΔZ is the local subsidence, *Amp* is the tsunami amplitude.

RSLR (m):		0.0		0.5		1.0		2.0	
Tide (m):		2.0		2.0		2.0		2.0	
TS#	ΔZ	Amp (m)	FCRP (m)						
1	-2.2	8.1	12.3	8.0	12.7	8.0	13.2	8.0	14.2
2	-2.2	7.9	12.1	7.9	12.5	7.8	13.0	7.8	14.0
3	-2.1	7.6	11.7	7.6	12.2	7.5	12.7	7.9	14.1
4	-2.1	7.2	11.4	7.3	11.9	7.4	12.5	7.7	13.9
5	-2.1	7.6	11.8	7.7	12.3	7.7	12.8	7.8	14.0
6	-2.1	7.5	11.7	7.6	12.2	7.7	12.8	7.7	13.8
7	-2.1	5.3	9.5	5.3	9.9	5.3	10.5	5.4	11.5
8	-2.1	5.8	9.9	5.9	10.6	6.1	11.2	6.3	12.4
9	-2.1	4.8	8.9	4.9	9.5	4.9	10.0	4.9	11.1
10	-2.1	4.4	8.5	4.3	8.9	4.5	9.6	4.7	10.8
11	-2.1	4.3	8.4	4.4	9.0	4.6	9.7	4.8	10.9
12	-2.1	5.8	9.8	5.9	10.5	6.1	11.2	6.4	12.5
13	-2.1	6.3	10.3	6.5	11.0	6.6	11.7	7.0	13.0
14	-2.1	6.0	10.1	6.2	10.8	6.4	11.5	6.7	12.8
16	-2.1	4.4	8.5	4.5	9.1	4.7	9.8	4.9	11.0
18	-2.1	5.5	9.7	5.7	10.3	5.9	11.0	6.3	12.4
19	-2.1	4.4	8.5	4.6	9.2	4.8	9.9	5.2	11.3
20	-2.1	4.1	8.3	4.3	8.9	4.5	9.6	4.7	10.9
22	-2.1	4.2	8.3	4.3	8.9	4.5	9.6	4.8	10.9
24	-2.1	4.2	8.4	4.3	9.0	4.5	9.6	4.7	10.8
25	-2.1	4.0	8.2	4.1	8.8	4.3	9.5	4.5	10.7
26	-2.1	4.0	8.2	4.2	8.8	4.3	9.5	4.6	10.7
27	-2.1	4.7	8.9	4.8	9.4	4.8	9.9	4.9	11.1
28	-2.1	4.4	8.6	4.7	9.3	4.6	9.7	4.5	10.6
29	-2.1	5.8	10.0	5.9	10.5	6.0	11.1	6.1	12.2
30	-2.1	5.7	9.9	5.8	10.4	6.0	11.1	6.1	12.3
31	-2.1	5.2	9.4	5.3	10.0	5.5	10.6	5.6	11.7
32	-2.2	5.8	9.9	5.9	10.5	5.9	11.1	6.2	12.4
33	-2.2	7.4	11.6	7.3	12.0	7.3	12.5	7.4	13.5
34	-2.2	7.9	12.1	8.0	12.6	8.0	13.2	8.0	14.2
35	-2.2	7.7	11.9	7.7	12.4	7.8	13.0	7.7	13.9
36	-2.2	7.6	11.8	7.6	12.2	7.6	12.8	7.6	13.7
37	-2.2	6.2	10.4	6.1	10.8	6.2	11.3	6.3	12.4
38	-2.2	7.5	11.7	7.4	12.1	7.4	12.6	7.4	13.5
39	-2.2	8.4	12.6	8.4	13.0	8.3	13.5	8.3	14.5
40	-2.2	7.8	12.0	7.8	12.5	7.8	13.0	7.7	13.9
41	-2.2	9.2	13.4	9.1	13.8	9.1	14.3	9.0	15.2
42	-2.2	10.3	14.5	10.2	14.8	10.0	15.2	9.8	16.0
43	-2.2	11.0	15.2	10.9	15.6	10.8	16.0	10.5	16.7
44	-2.2	11.5	15.7	11.3	16.0	11.2	16.4	11.0	17.1
45	-2.2	10.6	14.8	10.5	15.2	10.4	15.6	10.2	16.4
46	-2.2	9.6	13.8	9.5	14.2	9.5	14.7	9.5	15.7
47	-2.2	9.9	14.1	9.8	14.5	9.7	14.9	9.6	15.8
48	-2.2	8.5	12.7	8.5	13.2	8.4	13.6	8.4	14.6
49	-2.2	8.5	12.6	8.5	13.1	8.4	13.6	8.4	14.6
50	-2.2	7.8	11.9	7.7	12.4	7.7	12.9	7.7	13.9
51	-2.2	9.9	14.1	9.3	14.0	9.5	14.7	8.9	15.0
52	-2.2	12.7	16.9	11.3	16.0	10.6	15.8	10.0	16.1

C.3 G2018-S-B

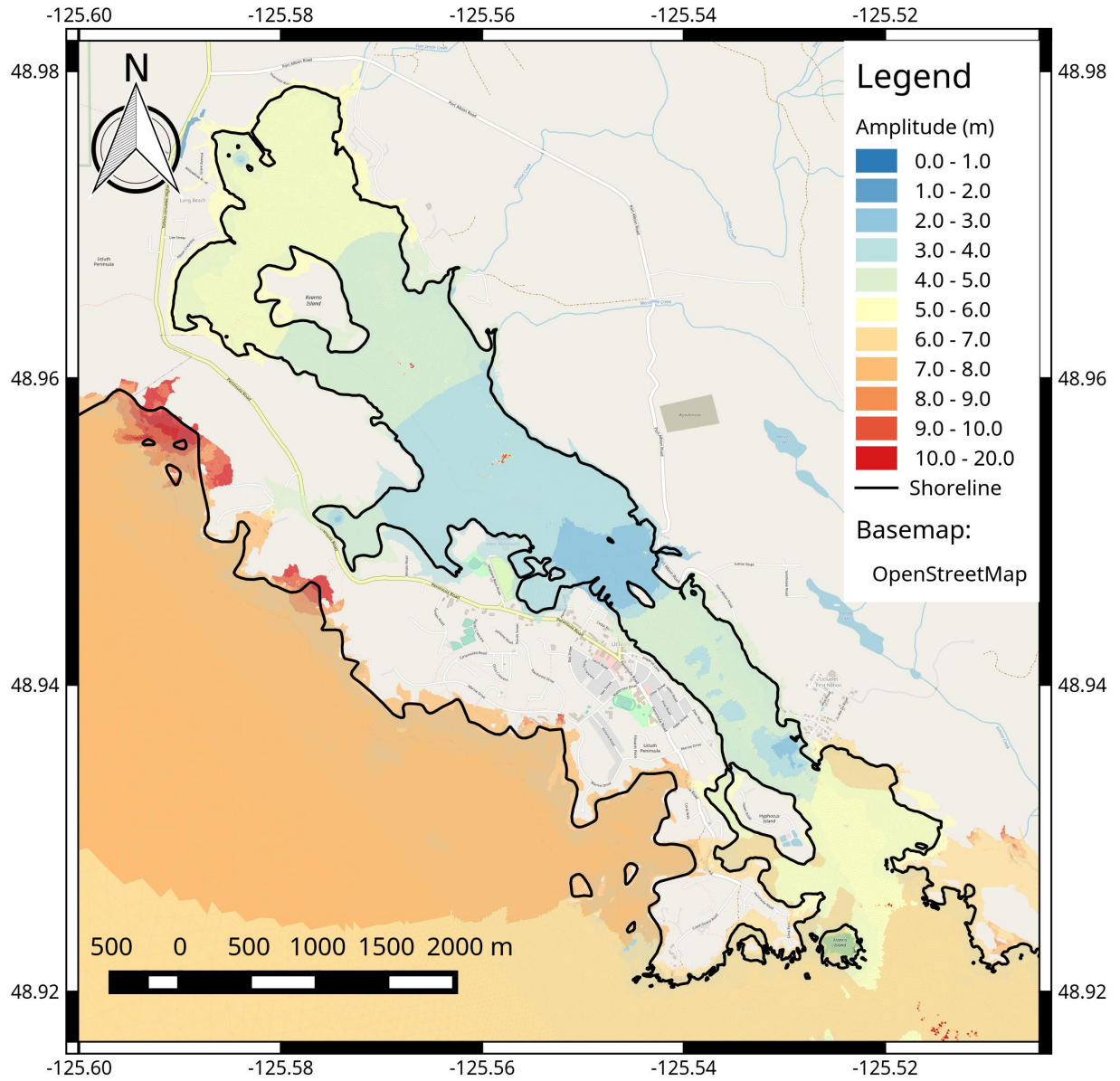


Figure 27: Maximum tsunami amplitude for rupture G2018-S-B, relative to ambient water level. Ambient water level = 2 m (2 m tide + 0 m RSLR).

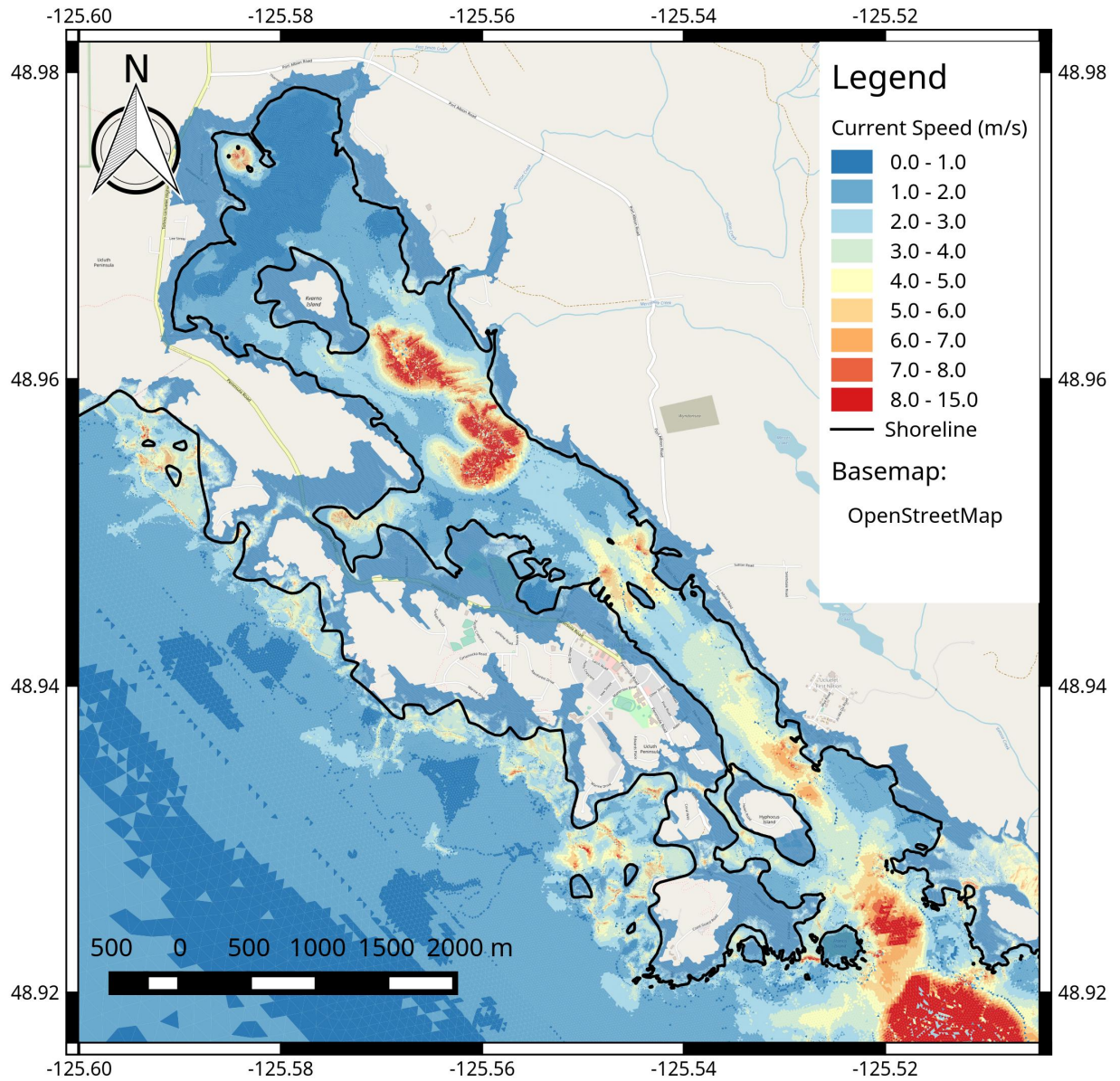


Figure 28: Maximum tsunami current speed for rupture G2018-S-B. Ambient water level = 2 m (2 m tide + 0 m RSLR).

Table 10: Tsunami results for G2018-S-B rupture, at transects, for each RSLR scenario. ΔZ is the local subsidence, *Amp* is the tsunami amplitude.

RSLR (m):		0.0		0.5		1.0		2.0	
Tide (m):		2.0		2.0		2.0		2.0	
TS#	ΔZ	Amp (m)	FCRP (m)						
1	-2.0	6.6	10.5	6.6	11.1	6.6	11.6	6.5	12.5
2	-2.0	6.5	10.5	6.5	11.0	6.5	11.5	6.5	12.5
3	-2.0	5.9	9.8	5.9	10.4	6.0	10.9	6.0	11.9
4	-1.9	5.8	9.8	5.9	10.3	5.9	10.8	5.9	11.9
5	-1.9	6.1	10.1	6.1	10.6	6.1	11.1	6.1	12.0
6	-1.9	6.1	10.1	6.1	10.5	6.1	11.0	6.0	11.9
7	-1.9	4.8	8.7	4.8	9.2	4.8	9.7	4.2	10.1
8	-1.9	4.5	8.4	4.6	9.0	4.6	9.5	4.6	10.5
9	-1.9	2.9	6.8	3.0	7.4	3.2	8.2	3.6	9.6
10	-1.9	3.3	7.2	3.4	7.8	3.6	8.5	3.9	9.8
11	-1.9	4.3	8.2	4.4	8.8	4.6	9.4	4.9	10.8
12	-1.9	5.2	9.1	5.3	9.7	5.4	10.3	5.7	11.6
13	-1.9	5.4	9.3	5.5	9.9	5.7	10.5	6.0	11.8
14	-1.9	5.4	9.3	5.5	9.9	5.6	10.5	6.0	11.8
16	-1.9	4.4	8.3	4.6	9.0	4.8	9.7	5.1	11.1
18	-1.9	5.4	9.3	5.5	10.0	5.7	10.6	6.0	11.9
19	-1.9	4.8	8.7	5.0	9.4	5.2	10.1	5.5	11.4
20	-1.9	3.7	7.7	3.9	8.3	4.0	9.0	4.3	10.2
22	-1.9	3.9	7.8	3.9	8.4	4.0	9.0	4.4	10.3
24	-1.9	3.8	7.7	3.9	8.3	4.0	9.0	4.3	10.2
25	-1.9	3.6	7.6	3.7	8.2	3.9	8.8	4.1	10.0
26	-1.9	3.3	7.2	3.4	7.8	3.5	8.5	3.8	9.7
27	-1.9	3.1	7.1	3.3	7.7	3.4	8.3	3.6	9.5
28	-1.9	3.0	6.9	3.1	7.5	3.2	8.2	3.4	9.4
29	-1.9	4.3	8.2	4.3	8.7	4.3	9.3	4.4	10.3
30	-2.0	4.4	8.3	4.4	8.8	4.4	9.4	4.5	10.4
31	-2.0	4.3	8.3	4.3	8.8	4.3	9.3	4.4	10.3
32	-2.0	4.5	8.5	4.5	9.0	4.6	9.5	4.6	10.6
33	-2.0	6.1	10.1	6.1	10.5	6.1	11.0	6.0	12.0
34	-2.0	6.0	10.0	6.0	10.4	5.9	10.9	5.8	11.8
35	-2.0	6.1	10.0	6.1	10.6	6.1	11.0	6.0	12.0
36	-2.0	6.0	10.0	6.0	10.5	6.0	11.0	6.0	12.0
37	-2.0	6.0	10.0	6.0	10.5	5.9	10.9	5.9	11.9
38	-2.0	6.3	10.3	6.3	10.8	6.3	11.3	6.3	12.3
39	-2.0	6.6	10.6	6.6	11.1	6.6	11.6	6.6	12.6
40	-2.0	6.5	10.5	6.4	11.0	6.4	11.5	6.4	12.4
41	-2.0	7.0	11.0	7.0	11.5	7.0	12.0	6.9	12.9
42	-2.0	7.2	11.2	7.2	11.7	8.7	13.7	7.1	13.1
43	-2.0	7.2	11.2	7.2	11.7	7.2	12.2	7.2	13.1
44	-2.0	7.2	11.2	7.2	11.7	7.2	12.2	7.1	13.1
45	-2.0	7.2	11.2	7.2	11.7	7.2	12.2	7.1	13.1
46	-2.0	7.1	11.1	7.2	11.6	7.1	12.1	7.1	13.1
47	-2.0	7.2	11.2	7.1	11.6	7.2	12.1	7.1	13.1
48	-2.0	7.3	11.3	7.3	11.7	7.2	12.2	7.2	13.2
49	-2.0	7.4	11.3	7.5	12.0	7.5	12.5	7.6	13.6
50	-2.0	7.4	11.4	7.4	11.9	7.4	12.4	7.4	13.3
51	-2.0	7.6	11.5	7.6	12.0	7.5	12.5	7.5	13.5
52	-2.0	9.2	13.1	8.5	13.0	8.1	13.0	7.6	13.6

C.4 G2018-T-50

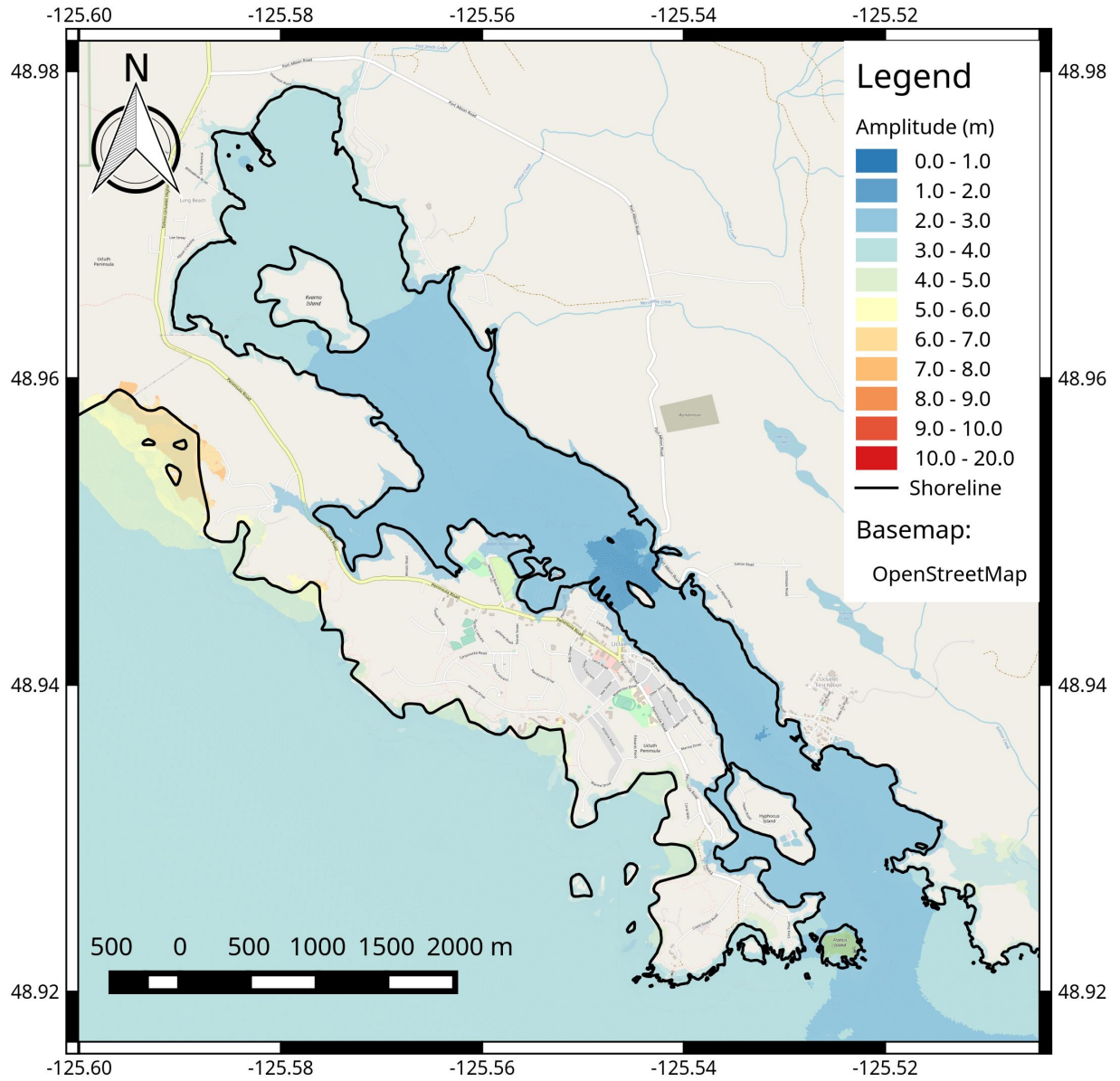


Figure 29: Maximum tsunami amplitude for rupture G2018-T-50, relative to ambient water level. Ambient water level = 2 m (2 m tide + 0 m RSLR).

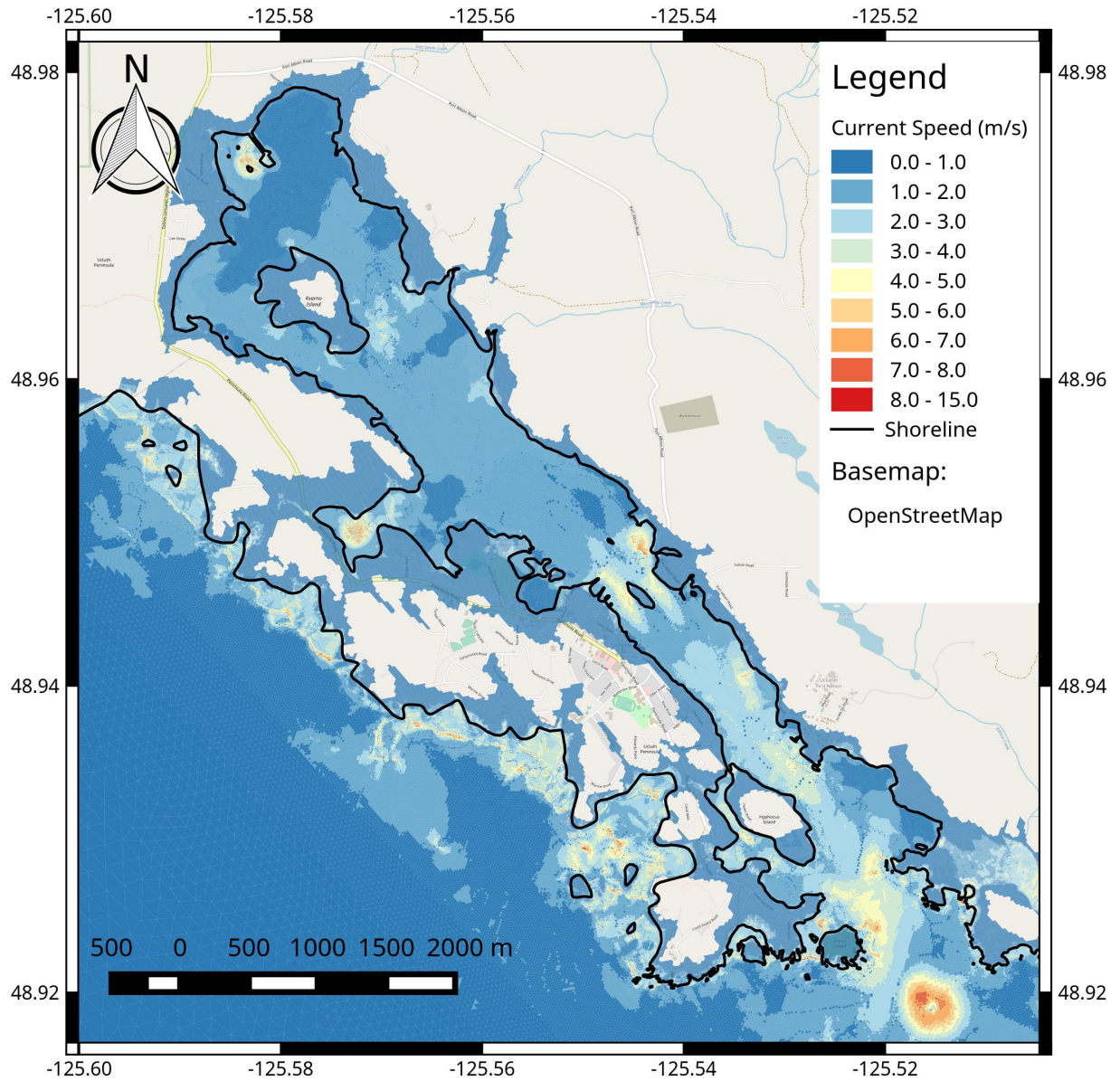


Figure 30: Maximum tsunami current speed for rupture G2018-T-50. Ambient water level = 2 m (2 m tide + 0 m RSLR).

Table 11: Tsunami results for G2018-T-50 rupture, at transects, for each RSLR scenario. ΔZ is the local subsidence, *Amp* is the tsunami amplitude.

RSLR (m):		0.0		0.5		1.0		2.0	
Tide (m):		2.0		2.0		2.0		2.0	
TS#	ΔZ	Amp (m)	FCRP (m)						
1	-2.1	3.1	7.3	3.1	7.7	3.0	8.2	3.0	9.2
2	-2.1	3.0	7.2	3.0	7.6	3.0	8.1	3.0	9.1
3	-2.1	2.7	6.9	2.8	7.5	2.9	8.0	3.1	9.2
4	-2.1	2.7	6.8	2.7	7.3	2.7	7.8	2.7	8.9
5	-2.1	2.9	7.0	2.9	7.5	2.8	8.0	2.9	9.0
6	-2.1	2.9	7.0	2.8	7.5	2.9	8.0	2.9	9.1
7	-2.1	2.4	6.5	2.4	7.1	2.5	7.6	2.3	8.4
8	-2.1	2.3	6.5	2.4	7.0	2.5	7.6	2.6	8.7
9	-2.1	2.0	6.1	2.1	6.7	2.2	7.3	2.3	8.4
10	-2.1	2.2	6.3	2.3	6.9	2.4	7.5	2.5	8.5
11	-2.1	2.8	6.8	2.9	7.5	3.0	8.1	3.2	9.2
12	-2.1	3.4	7.5	3.5	8.0	3.6	8.6	3.6	9.7
13	-2.0	3.5	7.6	3.6	8.2	3.7	8.7	3.8	9.8
14	-2.1	3.5	7.6	3.6	8.2	3.7	8.7	3.8	9.8
16	-2.1	2.9	7.0	3.0	7.6	3.1	8.2	3.2	9.3
18	-2.1	3.3	7.5	3.4	8.1	3.6	8.7	3.8	9.9
19	-2.1	3.0	7.1	3.2	7.8	3.3	8.4	3.4	9.5
20	-2.1	2.4	6.5	2.5	7.1	2.6	7.7	2.8	8.9
22	-2.1	2.4	6.6	2.5	7.2	2.6	7.8	2.8	8.9
24	-2.1	2.4	6.5	2.5	7.1	2.6	7.7	2.7	8.9
25	-2.1	2.3	6.5	2.4	7.1	2.5	7.6	2.7	8.8
26	-2.1	2.2	6.3	2.3	6.9	2.4	7.5	2.5	8.6
27	-2.1	2.2	6.3	2.2	6.9	2.3	7.4	2.4	8.5
28	-2.1	2.1	6.2	2.2	6.8	2.2	7.3	2.3	8.5
29	-2.1	2.4	6.5	2.4	7.0	2.5	7.6	2.6	8.7
30	-2.1	2.4	6.5	2.4	7.0	2.4	7.6	2.5	8.7
31	-2.1	2.2	6.4	2.3	6.9	2.3	7.5	2.4	8.5
32	-2.1	2.1	6.3	2.2	6.8	2.2	7.4	2.3	8.5
33	-2.2	2.8	6.9	2.8	7.4	2.8	7.9	2.8	9.0
34	-2.2	2.8	7.0	2.8	7.5	2.8	8.0	2.8	8.9
35	-2.2	2.9	7.1	2.9	7.5	2.8	8.0	2.8	9.0
36	-2.2	2.8	6.9	2.7	7.4	2.7	7.9	2.8	9.0
37	-2.2	2.6	6.8	2.6	7.3	2.6	7.8	2.6	8.8
38	-2.2	3.0	7.2	3.0	7.7	2.9	8.1	2.9	9.1
39	-2.2	3.2	7.4	3.2	7.9	3.2	8.4	3.1	9.3
40	-2.2	3.1	7.3	3.1	7.8	3.1	8.3	3.1	9.3
41	-2.2	3.6	7.8	3.8	8.5	3.4	8.6	3.7	9.9
42	-2.2	3.8	8.0	3.9	8.5	3.9	9.1	3.8	10.0
43	-2.2	4.0	8.2	4.0	8.7	4.0	9.1	3.9	10.1
44	-2.2	4.1	8.3	4.2	8.9	4.5	9.6	4.0	10.1
45	-2.2	3.9	8.1	3.9	8.6	3.9	9.1	3.8	10.0
46	-2.2	3.6	7.8	3.6	8.3	3.6	8.8	3.6	9.8
47	-2.2	3.6	7.8	3.6	8.3	3.6	8.8	3.6	9.8
48	-2.2	3.6	7.8	3.6	8.3	3.6	8.7	3.5	9.7
49	-2.2	4.6	8.8	4.8	9.5	4.7	9.9	4.4	10.6
50	-2.2	4.6	8.8	4.4	9.1	4.4	9.5	4.9	11.0
51	-2.2	4.9	9.1	5.1	9.8	5.1	10.2	5.1	11.2
52	-2.2	6.0	10.2	6.1	10.8	6.0	11.2	5.8	12.0

C.5 G2018-T-100

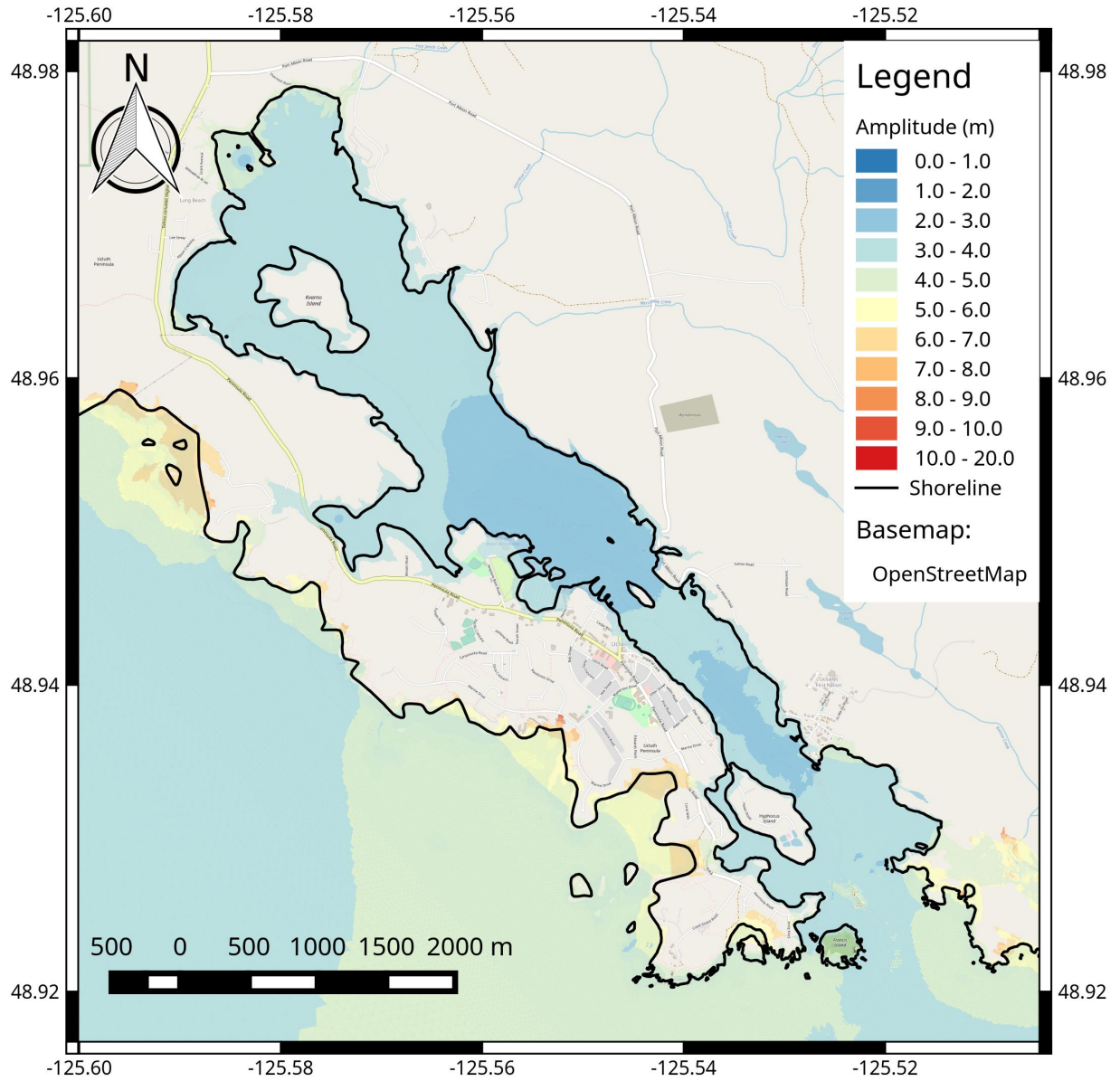


Figure 31: Maximum tsunami amplitude for rupture G2018-T-100, relative to ambient water level. Ambient water level = 2 m (2 m tide + 0 m RSLR).

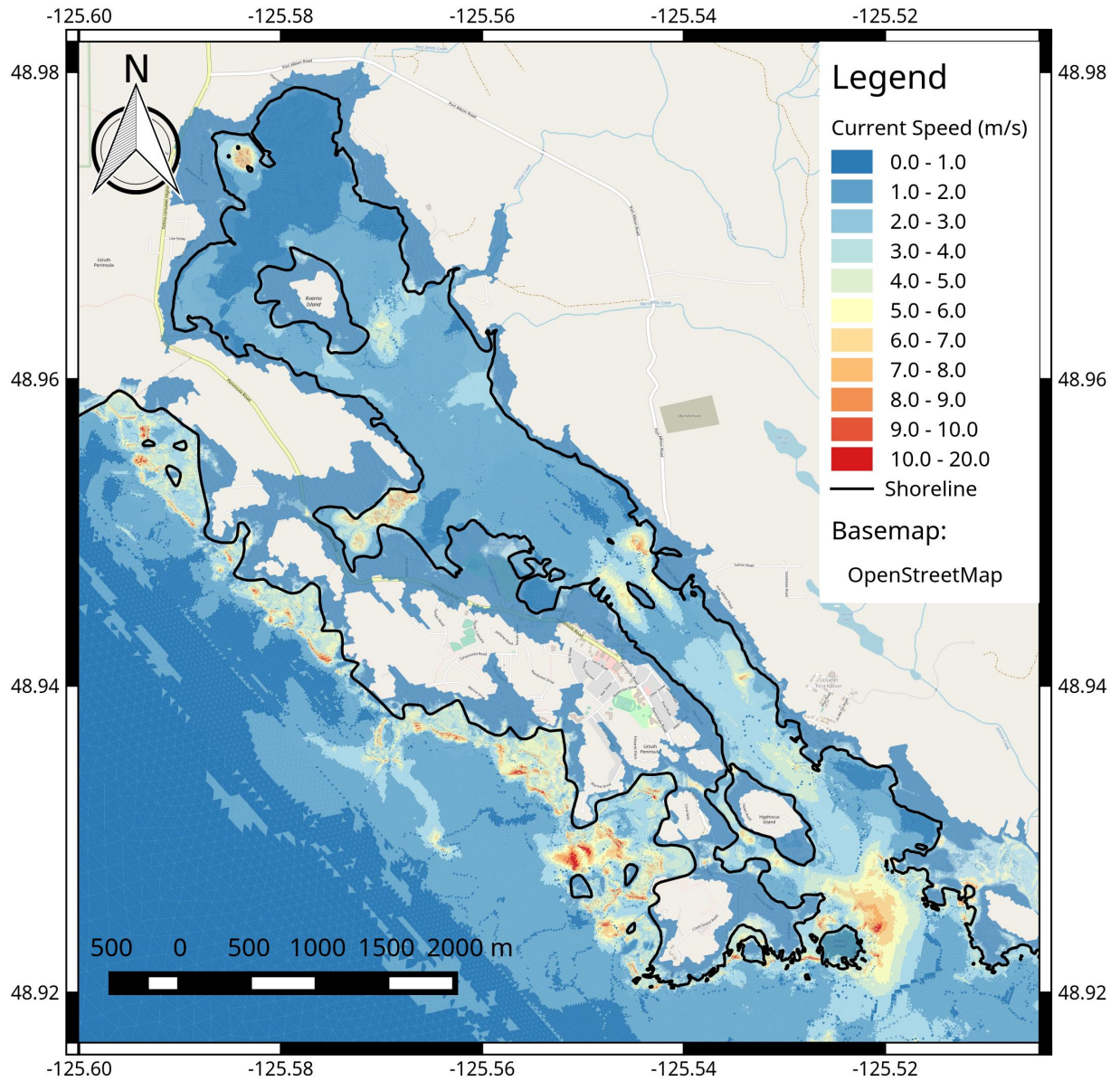


Figure 32: Maximum tsunami current speed for rupture G2018-T-100. Ambient water level = 2 m (2 m tide + 0 m RSLR).

Table 12: Tsunami results for G2018-T-100 rupture, at transects, for each RSLR scenario. ΔZ is the local subsidence, *Amp* is the tsunami amplitude.

RSLR (m):		0.0		0.5		1.0		2.0	
Tide (m):		2.0		2.0		2.0		2.0	
TS#	ΔZ	Amp (m)	FCRP (m)						
1	-2.1	4.4	8.6	4.4	9.1	4.5	9.6	4.5	10.7
2	-2.1	4.3	8.5	4.3	9.0	4.4	9.5	4.4	10.6
3	-2.1	4.1	8.2	4.1	8.7	4.1	9.3	4.1	10.3
4	-2.1	3.7	7.8	3.8	8.4	3.9	9.0	3.9	10.0
5	-2.1	4.0	8.1	4.0	8.7	4.1	9.2	4.1	10.2
6	-2.1	4.0	8.1	4.1	8.7	4.1	9.2	4.1	10.2
7	-2.1	3.2	7.3	3.3	7.9	3.4	8.5	3.4	9.5
8	-2.1	3.2	7.3	3.3	7.9	3.3	8.4	3.6	9.7
9	-2.1	2.7	6.8	2.8	7.4	2.9	8.0	3.0	9.1
10	-2.1	2.9	7.0	3.0	7.6	3.1	8.2	3.3	9.4
11	-2.1	3.3	7.4	3.5	8.0	3.6	8.7	3.7	9.8
12	-2.0	3.6	7.7	3.7	8.2	3.8	8.8	3.9	10.0
13	-2.0	4.0	8.1	4.1	8.6	4.2	9.2	4.3	10.4
14	-2.1	4.0	8.1	4.0	8.6	4.1	9.2	4.2	10.3
16	-2.1	3.4	7.5	3.5	8.1	3.6	8.7	3.8	9.9
18	-2.1	4.0	8.1	4.1	8.7	4.1	9.2	4.1	10.3
19	-2.1	3.5	7.6	3.6	8.2	3.7	8.8	3.8	10.0
20	-2.1	3.1	7.2	3.2	7.8	3.3	8.4	3.5	9.6
22	-2.1	3.1	7.2	3.2	7.9	3.3	8.5	3.6	9.7
24	-2.1	3.1	7.2	3.2	7.9	3.3	8.5	3.6	9.7
25	-2.1	3.0	7.1	3.1	7.7	3.2	8.3	3.4	9.6
26	-2.1	2.9	7.1	3.0	7.7	3.2	8.3	3.3	9.4
27	-2.1	3.1	7.2	3.2	7.8	3.3	8.4	3.5	9.6
28	-2.1	2.7	6.8	2.8	7.4	2.9	8.0	3.1	9.2
29	-2.1	3.3	7.4	3.4	8.0	3.5	8.6	3.6	9.7
30	-2.1	3.2	7.3	3.3	7.9	3.3	8.5	3.4	9.5
31	-2.1	3.1	7.2	3.2	7.8	3.3	8.4	3.4	9.5
32	-2.1	3.1	7.3	3.2	7.9	3.3	8.5	3.5	9.7
33	-2.2	3.3	7.5	3.4	8.0	3.5	8.6	3.6	9.8
34	-2.2	3.8	7.9	3.9	8.5	4.1	9.2	4.2	10.3
35	-2.2	3.6	7.8	3.7	8.3	3.7	8.8	3.8	10.0
36	-2.2	3.4	7.5	3.5	8.1	3.6	8.7	3.8	10.0
37	-2.2	3.6	7.7	3.6	8.3	3.6	8.8	3.7	9.8
38	-2.2	4.2	8.4	4.2	8.9	4.3	9.4	4.3	10.5
39	-2.2	4.8	9.0	4.8	9.5	4.8	10.0	4.9	11.1
40	-2.2	4.4	8.6	4.4	9.1	4.4	9.6	4.4	10.6
41	-2.2	5.2	9.4	5.2	9.9	5.2	10.4	5.2	11.4
42	-2.2	5.7	9.9	5.7	10.3	5.8	11.0	5.6	11.8
43	-2.2	5.8	9.9	5.9	10.6	6.0	11.2	6.0	12.2
44	-2.2	6.7	10.8	6.7	11.4	6.7	11.9	6.7	12.9
45	-2.2	5.2	9.4	5.3	10.0	5.4	10.6	5.6	11.7
46	-2.2	4.8	9.0	4.8	9.5	4.8	10.0	4.8	11.0
47	-2.2	4.8	9.0	4.8	9.5	4.8	10.0	4.8	11.0
48	-2.2	3.9	8.1	3.9	8.6	3.9	9.1	4.0	10.1
49	-2.2	4.6	8.8	4.9	9.6	4.8	10.0	4.4	10.6
50	-2.2	4.7	8.9	5.2	9.9	5.4	10.6	5.8	12.0
51	-2.2	6.0	10.1	5.5	10.2	5.4	10.6	5.3	11.4
52	-2.2	5.9	10.1	6.3	10.9	6.2	11.3	5.7	11.9

C.6 W2003

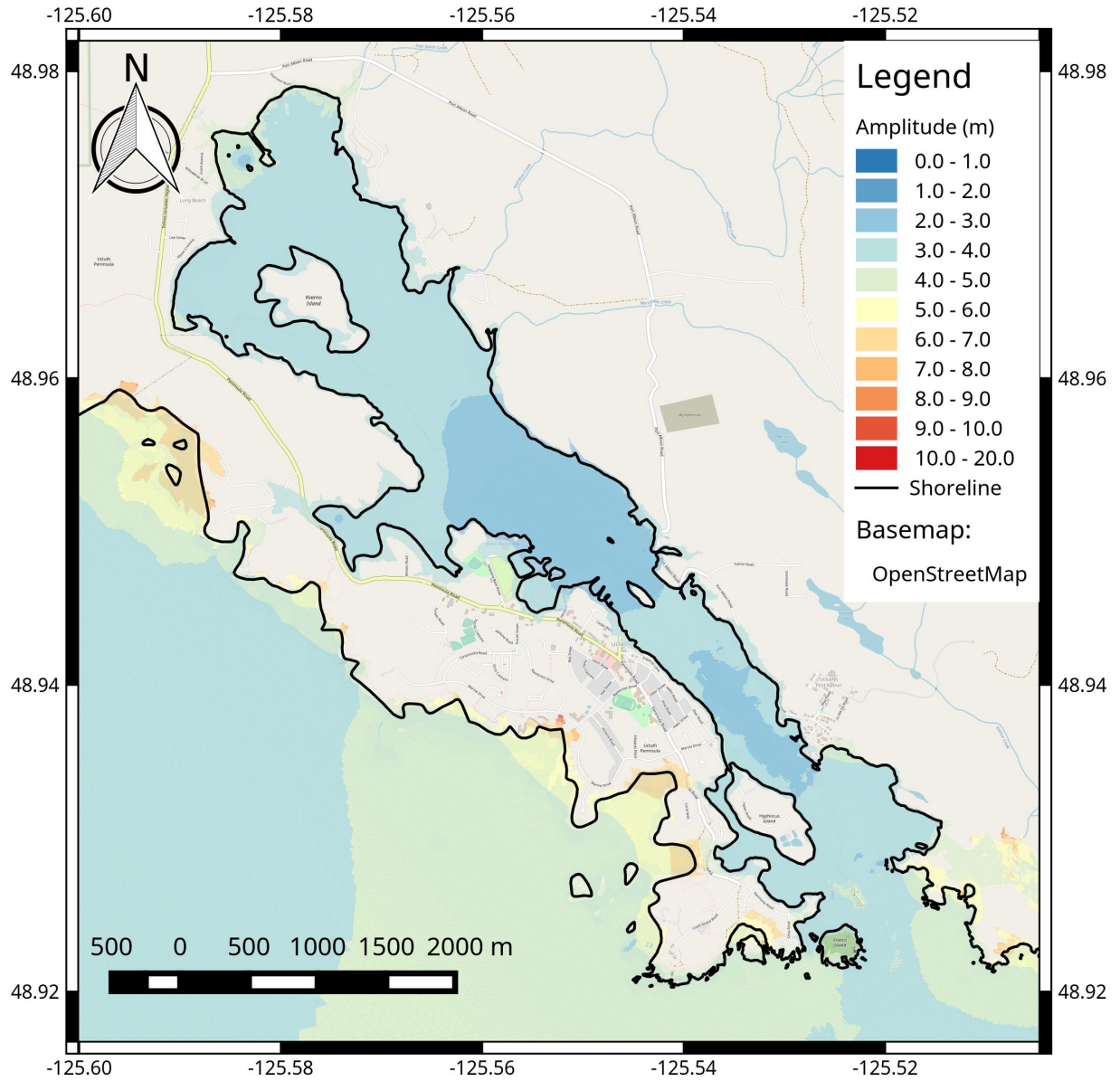


Figure 33: Maximum tsunami amplitude for rupture W2003, relative to ambient water level. Ambient water level = 2 m (2 m tide + 0 m RSLR).

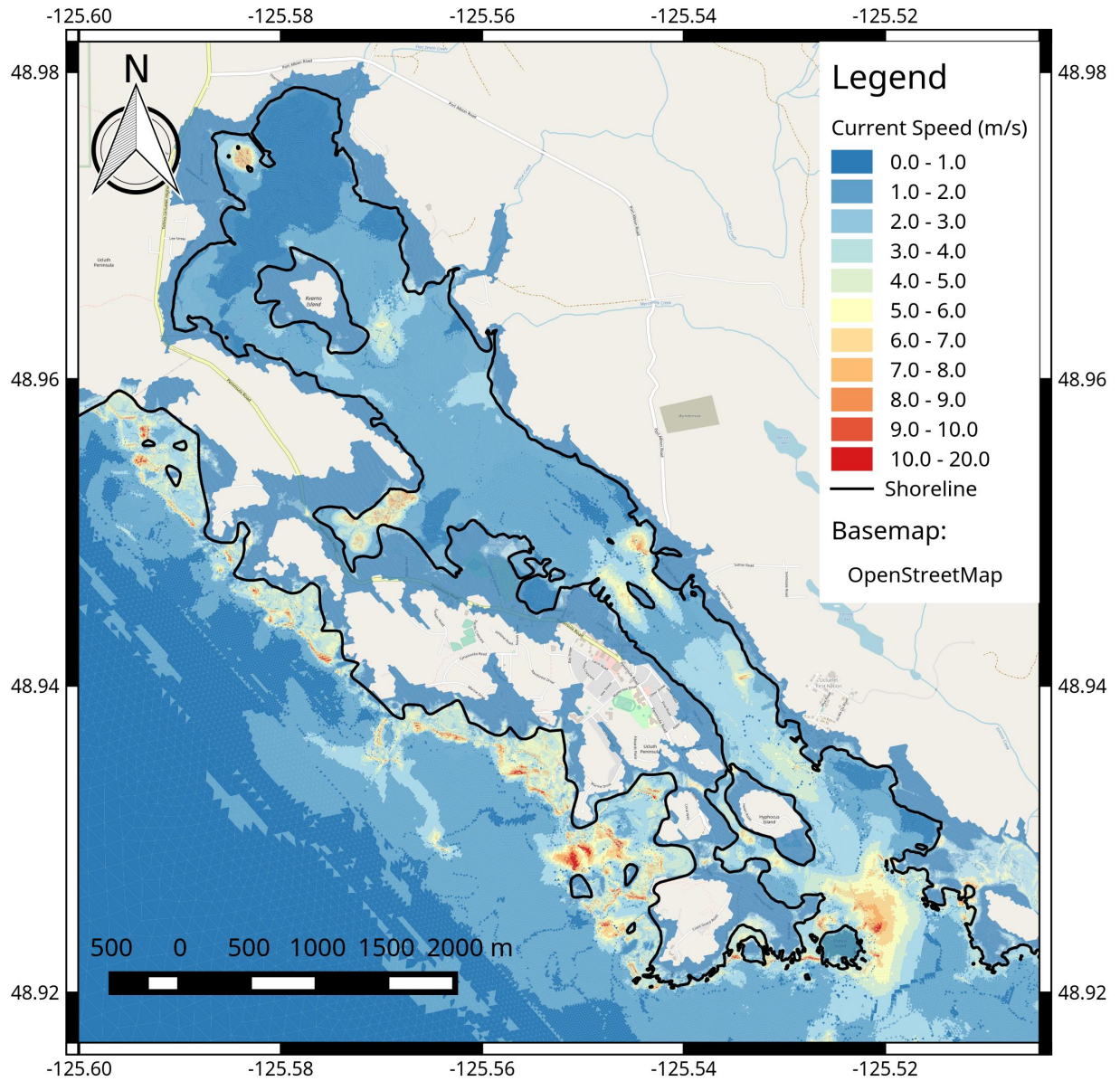


Figure 34: Maximum tsunami current speed for rupture W2003. Ambient water level = 2 m (2 m tide + 0 m RSLR).

Table 13: Tsunami results for W2003 rupture, at transects, for each RSLR scenario. ΔZ is the local subsidence, *Amp* is the tsunami amplitude.

RSLR (m):		0.0		0.5		1.0		2.0	
Tide (m):		2.0		2.0		2.0		2.0	
TS#	ΔZ	Amp (m)	FCRP (m)						
1	-2.1	3.8	7.9	3.7	8.4	3.7	8.8	3.7	9.8
2	-2.1	3.7	7.8	3.6	8.3	3.6	8.8	3.8	9.9
3	-2.1	3.4	7.5	3.4	8.0	3.4	8.5	3.5	9.6
4	-2.1	3.4	7.4	3.3	7.9	3.3	8.4	3.4	9.5
5	-2.1	3.5	7.6	3.5	8.1	3.5	8.6	3.6	9.7
6	-2.1	3.5	7.6	3.5	8.1	3.5	8.6	3.6	9.7
7	-2.1	2.9	7.0	3.0	7.6	3.0	8.1	2.8	8.9
8	-2.1	2.8	6.9	2.9	7.5	2.9	8.0	3.1	9.2
9	-2.1	2.2	6.3	2.4	6.9	2.5	7.6	2.6	8.7
10	-2.1	2.5	6.6	2.6	7.2	2.7	7.7	2.8	8.9
11	-2.1	2.9	7.0	3.0	7.6	3.1	8.2	3.3	9.4
12	-2.0	3.9	7.9	4.0	8.5	4.0	9.1	4.2	10.2
13	-2.0	4.0	8.1	4.1	8.7	4.2	9.2	4.3	10.3
14	-2.1	4.0	8.1	4.1	8.6	4.2	9.2	4.3	10.3
16	-2.1	3.0	7.1	3.1	7.7	3.3	8.4	3.5	9.6
18	-2.1	3.8	7.9	3.9	8.6	4.1	9.2	4.3	10.4
19	-2.1	3.3	7.4	3.4	8.0	3.6	8.7	3.8	9.9
20	-2.1	2.7	6.8	2.8	7.4	2.9	8.0	3.1	9.2
22	-2.1	2.8	6.9	2.9	7.5	3.0	8.1	3.1	9.3
24	-2.1	2.8	6.9	2.9	7.5	3.0	8.1	3.1	9.2
25	-2.1	2.7	6.8	2.8	7.4	2.9	8.0	3.0	9.1
26	-2.1	2.5	6.6	2.6	7.2	2.7	7.8	2.8	8.9
27	-2.1	2.4	6.5	2.5	7.1	2.5	7.7	2.7	8.8
28	-2.1	2.3	6.4	2.4	7.0	2.5	7.6	2.6	8.7
29	-2.1	2.8	6.9	2.8	7.4	2.9	8.0	3.0	9.1
30	-2.1	2.8	6.9	2.8	7.4	2.9	8.0	3.0	9.1
31	-2.1	2.7	6.8	2.7	7.4	2.8	7.9	2.8	9.0
32	-2.1	2.6	6.7	2.6	7.3	2.7	7.8	2.9	9.0
33	-2.1	3.4	7.6	3.4	8.1	3.5	8.6	3.5	9.6
34	-2.1	3.5	7.6	3.4	8.1	3.4	8.5	3.4	9.5
35	-2.1	3.5	7.7	3.5	8.2	3.5	8.6	3.4	9.6
36	-2.1	3.4	7.6	3.4	8.1	3.4	8.6	3.4	9.6
37	-2.1	3.3	7.4	3.3	7.9	3.3	8.4	3.3	9.4
38	-2.2	3.6	7.8	3.6	8.2	3.6	8.7	3.6	9.7
39	-2.2	3.9	8.0	3.8	8.5	3.8	9.0	3.8	9.9
40	-2.2	3.8	8.0	3.8	8.5	3.8	9.0	3.7	9.9
41	-2.2	4.3	8.4	4.2	8.9	4.2	9.4	4.3	10.4
42	-2.2	4.7	8.8	4.7	9.4	4.7	9.9	4.6	10.7
43	-2.1	4.8	9.0	4.8	9.4	4.7	9.9	4.7	10.8
44	-2.1	5.0	9.2	4.9	9.5	4.8	9.9	4.7	10.9
45	-2.2	4.7	8.9	4.7	9.4	4.7	9.8	4.6	10.8
46	-2.2	4.4	8.5	4.4	9.0	4.4	9.5	4.3	10.5
47	-2.2	4.4	8.6	4.4	9.1	4.4	9.5	4.3	10.5
48	-2.2	4.4	8.5	4.3	9.0	4.3	9.5	4.3	10.5
49	-2.2	5.0	9.2	4.7	9.4	4.5	9.7	4.7	10.9
50	-2.2	4.5	8.7	4.5	9.1	4.4	9.6	4.4	10.6
51	-2.2	6.0	10.2	6.3	11.0	6.2	11.3	6.0	12.1
52	-2.2	7.0	11.2	7.1	11.7	6.8	11.9	6.7	12.9

D Wave model evaluation

The wave model was evaluated by comparison to measurements made by wave measurement buoys within the model domain. Two of the buoys are operated by the the University of Victoria, the other was operated by the Department of Fisheries and Oceans Canada. The buoys used in this analysis are shown in Figure 8 and detailed in Table 14.

Table 14: Details of wave measurement buoys used in model evaluation.

ID/Name	Buoy Type	Start Date	End Date	Lat	Long	Depth
UVIC - Amphitrite Bank	Axys Watchmate Buoy	2009/12/02	2019/07/24	48.889	-125.636	45
UVIC - Florencia Bay	Axys TriAxys Buoy	2013/06/04	2018/08/26	48.957	-125.6144	30
MEDS103 - Long Beach	Datawell Waverider	1970/06/26	1998/06/17	49.037	-125.800	40

For each buoy location, a series of diagnostic plots which illustrate the skill of the model are presented (see Figures 35 to 46). These plots present time-series comparison of measured and modelled wave parameters, significant wave height and peak wave period (T_p). Comparisons of these parameters are also given in the form of scatter plots and quantile-quantile comparison plots. The time-series plots also show evaluation statistics comparing the measured and modelled values, including: the *good records* which match temporally between the data-sets, the model bias, the normalized model bias, the root-mean-square difference, the scatter index, and the correlation coefficient.

In general, the model reproduces the significant wave height (H_{m0}) well through most conditions. Comparing the measured and modelled H_{m0} probability distributions, the model estimates tend to have a very little bias. The agreement between the model and measurement for T_p is less consistent, which is typical for the T_p parameter, however the correlation is still very acceptable.

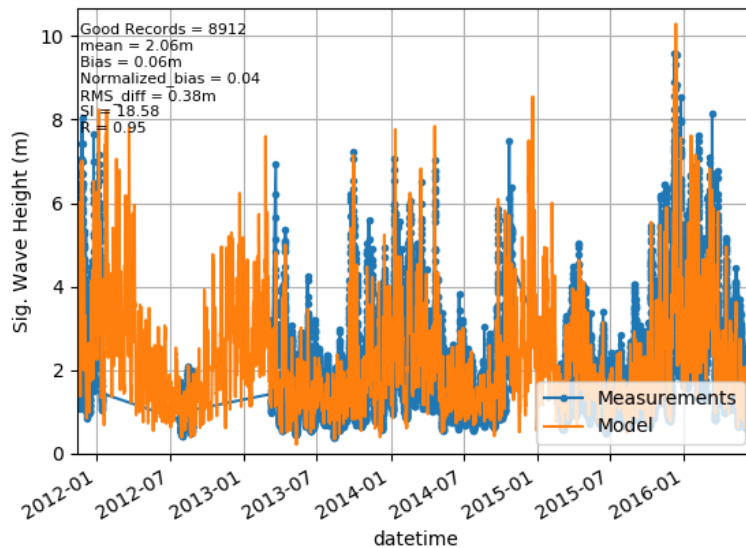


Figure 35: Modelled and measured H_{m0} time-series at Amphitrite Bank.

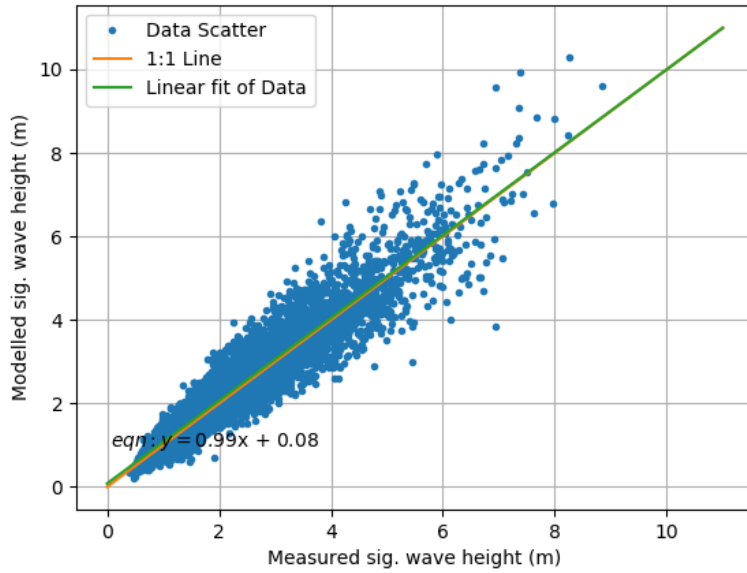


Figure 36: Modelled and measured H_{m0} scatter at med336.

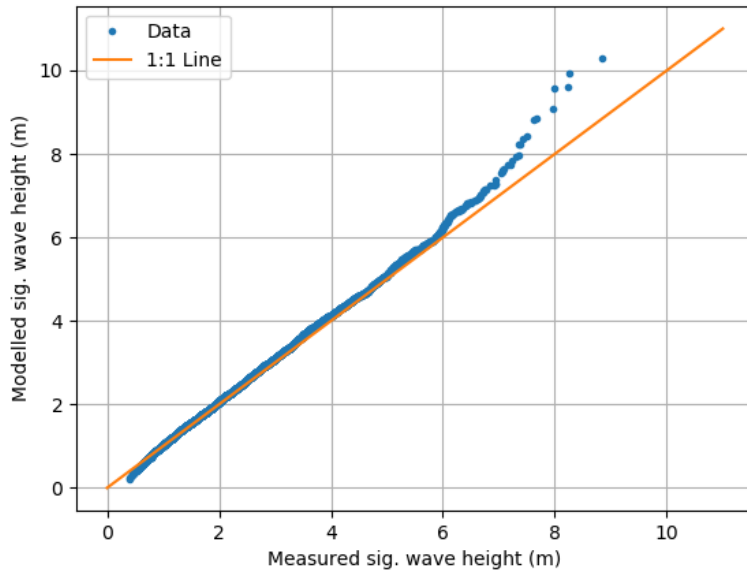


Figure 37: Modelled and measured H_{m0} quantile-quantile plot at Amphitrite Bank.

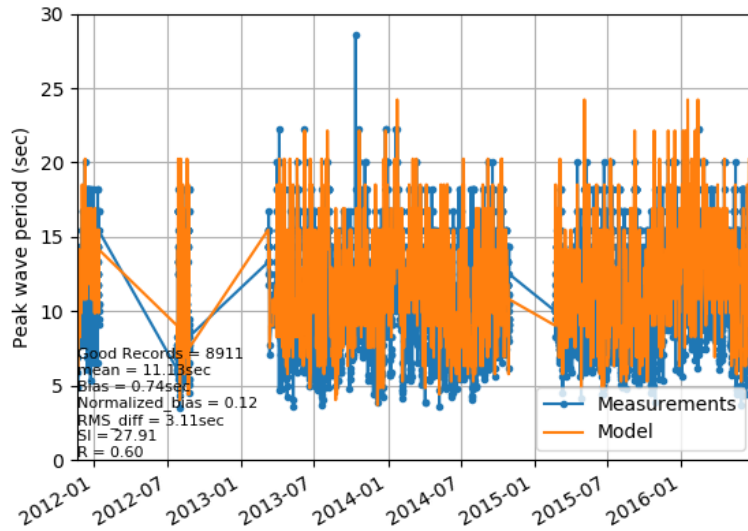


Figure 38: Modelled and measured T_p time-series at Amphitrite Bank.

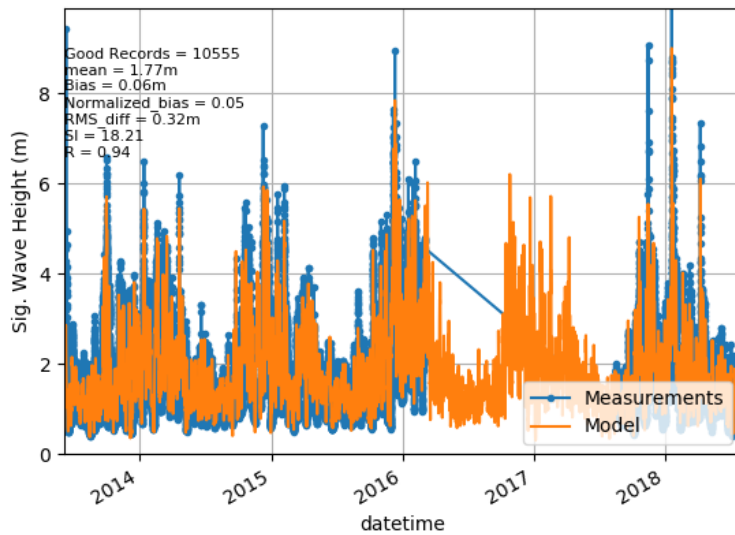


Figure 39: Modelled and measured H_{m0} time-series at Florencia Bay.

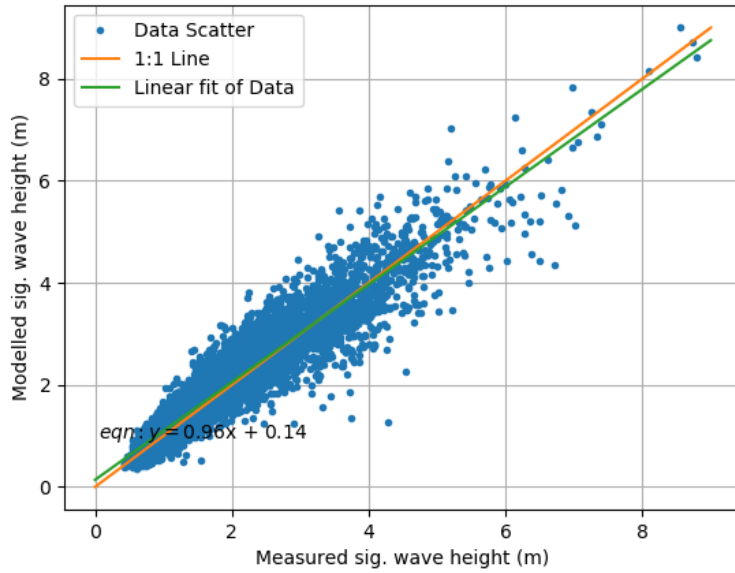


Figure 40: Modelled and measured H_{m0} scatter at Florencia Bay.

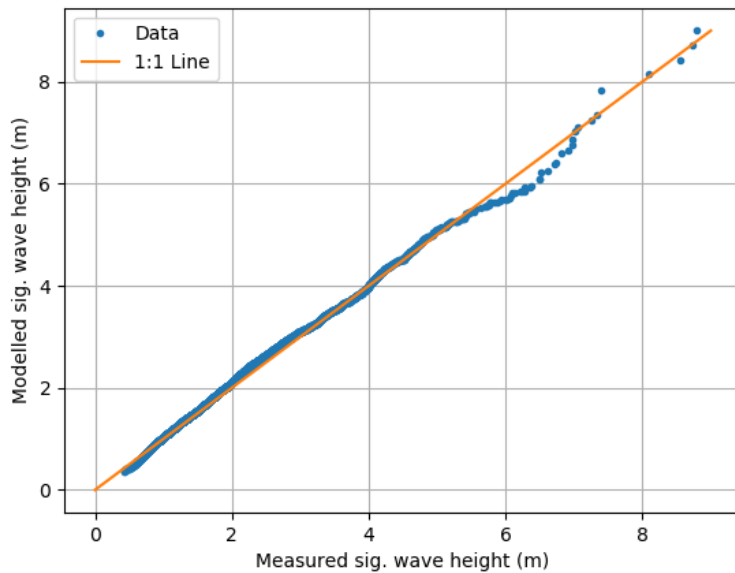


Figure 41: Modelled and measured H_{m0} quantile-quantile plot at Florencia Bay.

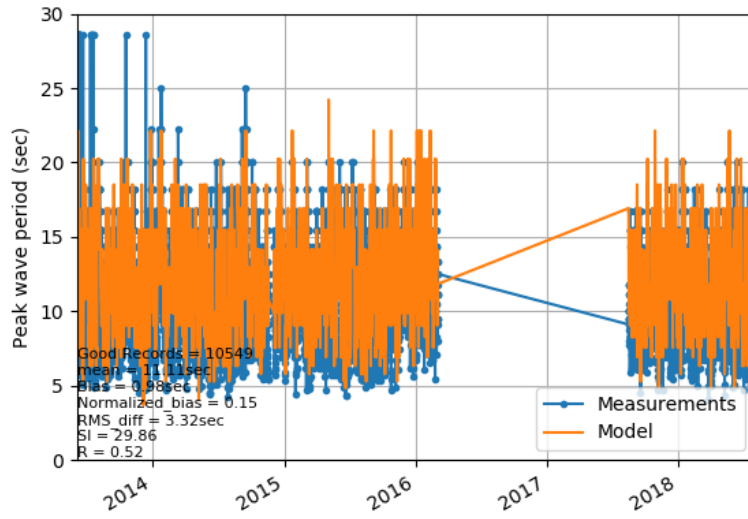


Figure 42: Modelled and measured T_p time-series at Florencia Bay.

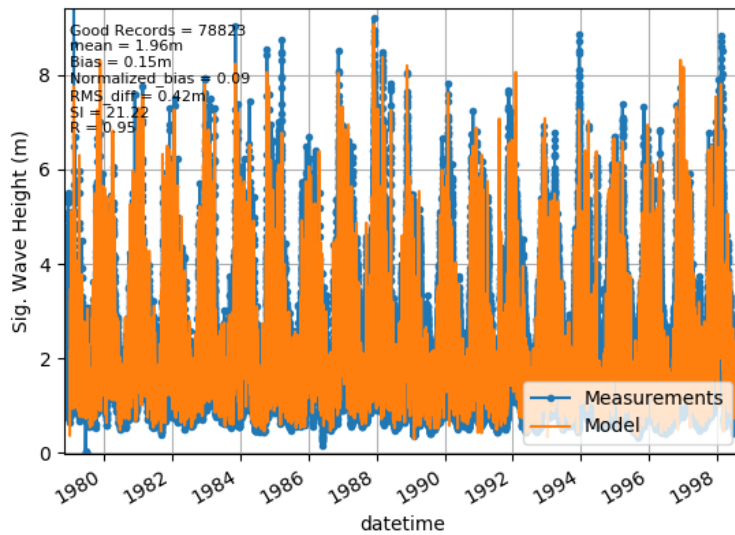


Figure 43: Modelled and measured H_{m0} time-series at Long Beach.

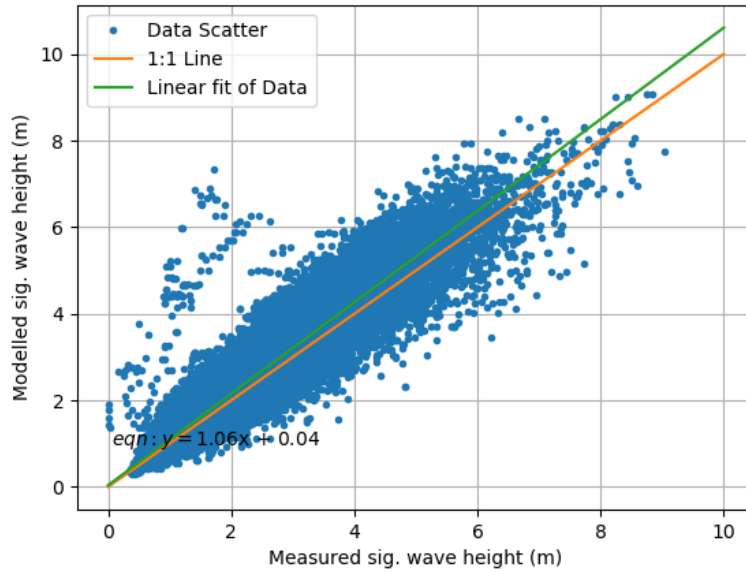


Figure 44: Modelled and measured H_{m0} scatter at Long Beach.

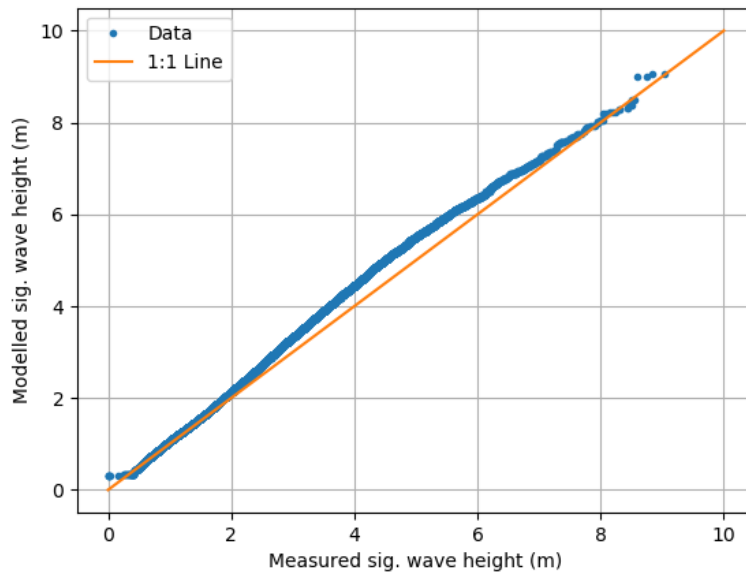


Figure 45: Modelled and measured H_{m0} quantile-quantile plot at Long Beach.

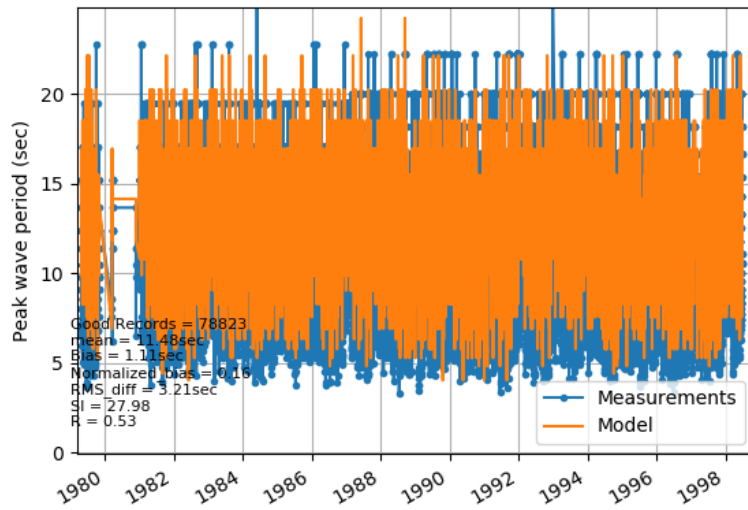


Figure 46: Modelled and measured T_p time-series at Long Beach.

E Wave Runup Hind-cast Evaluation

The hind-cast was evaluated by comparison to shoreline indicators of storm activity. The largest storm in the hind-cast occurred January 18, 2018. Somewhat surprisingly, a site visit conducted December of 2019 showed few signs of the 2018 storm remaining. Luckily DOU staff were able to provide photos of the storm event, along with location and elevation estimates. Photos of the January 2018 storm were available for transects 39, 40, 42, 44, and 46 (see Table 3). Figure 47 show the wave wash on the rocks, as viewed from a lookout up-shore of Melfort Pass. Figure 48, shows erosion of an engineered shoreline at Terrace Beach.

The remainder of the transects were evaluated by comparing evidence of storm activity to the ten largest events events in the transect hind-cast. Ortho photography and LiDAR data were used to establish the elevation of storm evidence. Figure 49 shows an example of logs on the rocky shoreline at reach 1. Note that the LiDAR contours have a spacing of 0.3 m, so this is the resolution of the observed estimates. Table 15 summarizes this evaluation exercise for each reach. Generally the storm evidence corresponds well with the hind-cast estimates of FCRP.



Figure 47: Wave wash as viewed from a lookout up-shore of Melfort Pass. Estimated observed elevation is 9.6 m, modelled runup elevation is 7.75 m. Photo credit: John Towgood.



Figure 48: Erosion of an engineered shoreline at Terrace Beach. Estimated observed elevation is 4.5 m, modelled runup elevation is 5.5 m. Photo credit: John Towgood.

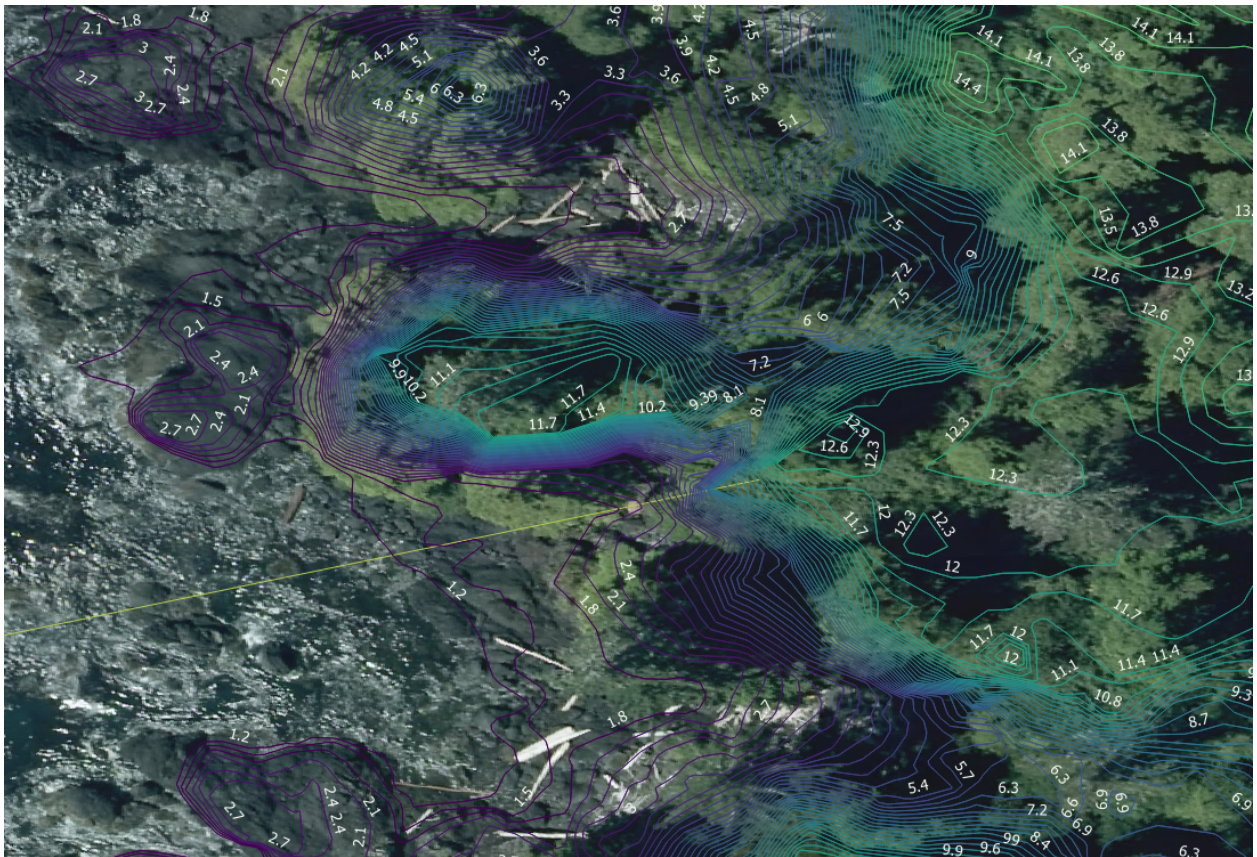


Figure 49: LiDAR contours over ortho photo showing logs on the rocky beach slope of reach 1.

Table 15: Comparison of hind-cast runup elevation for 10 largest events to observed evidence of storm activity for different shoreline reaches.

Reach Number	Hind-cast Runup Elev (m)	Observed Storm Evidence (m)	Observation Note
1	4.7-5.7	4.2	logs on beach, start of vegetation
2	4.6-5.7	3.3	logs on beach, start of vegetation
3	3.4-3.6	2.7	logs on beach, start of vegetation
4	4.0-4.3	3.3	start of vegetation
5	3.8-4.1	3.3	logs on beach, start of vegetation
6	3.7-4.0	3.3	logs on beach, start of vegetation
7	2.8-2.9	2.7	top of rip wrap, road
8	2.5-2.6	2.7	start of manicured lawns
9	3.1-3.5	2.1	start of vegetation
10	2.6-2.8	2.7	logs on beach, start of vegetation
11	2.7-2.6	1.8	logs on beach, start of vegetation
12	2.7-3.0	4.2	Parking lot elevation
13	2.5-2.7	2.1	logs on beach, start of vegetation
14	2.56-2.8	2.1	logs on beach, start of vegetation
16	2.6-2.9	2.1	logs on beach, start of vegetation
18	2.5-2.6	2.1	logs on beach, start of vegetation
19	2.5-2.8	NA	Not visible in ortho-photo
20	2.7-3.1	1.8	logs on beach, start of vegetation
22	2.6-2.8	2.1	logs on beach, start of vegetation
24	2.4-2.6	2.1	logs on beach, start of vegetation
25	2.7-2.8	NA	Not visible in ortho-photo
26	2.7-3.0	3.3	Parking lot elevation
27	2.5-2.7	2.1	logs on beach, start of vegetation
28	2.8-3.0	2.1	grass elevation
29	2.5-2.7	2.7	Parking lot elevation
30	2.8-3.1	2.1	logs on beach
31	2.5-2.7	2.4	logs on beach
32	2.9-3.2	2.7	logs on beach
33	4.2-5.2	3.3	logs on beach
34	2.8-3.2	2.1	start of vegetation
35	2.6-2.8	2.1	start of vegetation
36	3.4-3.8	2.7	logs on beach
37	3.8-4.8	3.0	start of vegetation
38	6.0-7.6	7.5	start of vegetation
39	6.0-7.8	9.6	photo from Jan 2018 storm
40	8.8-10.4	9.3	photo from Jan 2018 storm
41	7.2-9.6	8.7	start of vegetation
42	4.9-5.8	4.5	photo from Jan 2018 storm
43	5.8-6.7	4.8	logs on beach
44	4.4-5.3	4.2	photo from Jan 2018 storm
45	4.0-5.0	4.5	logs on beach
46	4.8-6.1	5.4	photo from Jan 2018 storm
47	6.3-8.3	8.1	logs on Browns Beach
48	9.6-12.2	10.2	start of trees
49	5.0-6.2	7.2	logs on beach
50	9.0-11.2	8.1	start of vegetation
51	3.3-4.8	4.2	logs on beach
52	7.4-8.8	8.4	logs on beach

F Storm Hazard Results

Table 16: Estimated FCRP (m) for 0.0 m RSLR associated with 6.67%, 2%, 1%, 0.5% and 0.2% AEP (return periods of 15, 50, 100, 200 and 500 years). L, M and U indicate lower (5%), maximum likelihood and upper (95%) confidence estimates.

Trans #	Max in Hind-cast	99.8 %tile	# Events	6.7% AEP			2% AEP			1% AEP			0.5% AEP			0.2% AEP		
				L	M	U	L	M	U	L	M	U	L	M	U	L	M	U
1	5.7	4.2	59	4.5	5.0	5.8	4.6	5.3	6.8	4.7	5.5	7.5	4.7	5.6	8.4	4.7	5.9	9.7
2	5.7	4.2	55	4.5	5.0	5.8	4.6	5.3	6.8	4.7	5.4	7.4	4.7	5.6	8.3	4.7	5.8	9.5
3	3.7	3.0	64	3.3	3.6	4.1	3.3	3.7	4.5	3.3	3.7	4.6	3.3	3.8	4.8	3.3	3.8	5.0
4	4.3	3.6	62	3.8	4.1	4.7	3.9	4.2	5.1	3.9	4.3	5.3	3.9	4.3	5.5	3.9	4.4	5.7
5	4.0	3.4	62	3.7	3.9	4.4	3.7	4.0	4.6	3.7	4.0	4.7	3.7	4.1	4.8	3.7	4.1	4.9
6	4.0	3.2	70	3.6	3.8	4.2	3.6	3.9	4.4	3.6	3.9	4.5	3.6	4.0	4.5	3.6	4.0	4.6
7	3.0	2.4	86	2.6	2.9	3.4	2.6	3.0	3.9	2.7	3.1	4.2	2.7	3.1	4.5	2.7	3.2	4.9
8	2.7	2.2	77	2.4	2.6	3.0	2.4	2.7	3.3	2.4	2.7	3.4	2.4	2.8	3.6	2.4	2.8	3.8
9	3.5	2.7	76	3.0	3.3	3.7	3.1	3.4	3.9	3.1	3.4	4.1	3.1	3.5	4.2	3.1	3.5	4.4
10	2.8	2.2	77	2.4	2.7	3.0	2.5	2.7	3.3	2.5	2.8	3.5	2.5	2.8	3.6	2.5	2.9	3.8
11	2.7	2.1	75	2.4	2.6	2.9	2.4	2.6	3.1	2.4	2.7	3.2	2.4	2.7	3.3	2.4	2.7	3.4
12	3.0	2.3	81	2.6	2.8	3.2	2.6	2.9	3.5	2.6	3.0	3.7	2.7	3.0	3.9	2.7	3.1	4.2
13	2.7	2.2	83	2.4	2.6	3.1	2.4	2.7	3.5	2.4	2.8	3.8	2.4	2.8	4.0	2.4	2.9	4.4
14	2.9	2.2	81	2.4	2.7	3.3	2.5	2.8	3.6	2.5	2.9	3.8	2.5	2.9	4.0	2.5	2.9	4.3
16	2.9	2.3	83	2.5	2.8	3.1	2.6	2.9	3.5	2.6	2.9	3.6	2.6	3.0	3.8	2.6	3.0	4.1
18	2.7	2.1	72	2.3	2.6	3.0	2.4	2.7	3.3	2.4	2.7	3.5	2.4	2.7	3.7	2.4	2.8	3.9
19	2.7	2.1	80	2.3	2.6	2.9	2.4	2.6	3.1	2.4	2.7	3.2	2.4	2.7	3.3	2.4	2.7	3.5
20	3.1	2.4	78	2.7	2.9	3.2	2.7	3.0	3.5	2.7	3.1	3.6	2.8	3.1	3.7	2.8	3.2	3.9
22	2.8	2.2	78	2.5	2.7	3.1	2.5	2.8	3.3	2.5	2.8	3.4	2.5	2.8	3.5	2.5	2.9	3.6
24	2.6	2.1	78	2.3	2.5	2.9	2.3	2.6	3.2	2.3	2.6	3.4	2.3	2.7	3.6	2.3	2.7	3.8
25	3.0	2.3	76	2.6	2.8	3.1	2.7	2.9	3.4	2.7	3.0	3.5	2.7	3.0	3.6	2.7	3.0	3.7
26	3.0	2.3	87	2.6	2.8	3.2	2.6	2.9	3.5	2.6	3.0	3.7	2.6	3.0	3.8	2.6	3.0	4.1
27	2.7	2.1	78	2.3	2.6	3.1	2.3	2.7	3.5	2.4	2.8	3.9	2.4	2.8	4.2	2.4	2.9	4.7
28	3.1	2.4	84	2.7	2.9	3.2	2.7	3.0	3.5	2.7	3.0	3.6	2.7	3.1	3.8	2.8	3.1	3.9
29	2.7	2.2	77	2.4	2.6	3.0	2.4	2.7	3.2	2.4	2.7	3.3	2.4	2.7	3.4	2.4	2.8	3.6
30	3.1	2.5	84	2.7	3.0	3.3	2.8	3.1	3.7	2.8	3.1	3.9	2.8	3.2	4.0	2.8	3.2	4.3
31	2.7	2.2	81	2.4	2.6	3.0	2.4	2.7	3.3	2.4	2.8	3.5	2.5	2.8	3.8	2.5	2.9	4.0
32	3.3	2.4	78	2.7	3.0	3.7	2.7	3.3	4.5	2.8	3.4	5.1	2.8	3.5	5.7	2.8	3.7	6.7
33	5.2	3.8	62	4.1	4.5	5.3	4.2	4.9	6.4	4.2	5.0	7.1	4.3	5.2	8.1	4.3	5.5	9.7
34	3.2	2.4	75	2.8	3.0	3.5	2.8	3.2	3.8	2.8	3.2	4.0	2.8	3.3	4.2	2.8	3.3	4.4
35	2.8	2.3	71	2.5	2.7	3.1	2.5	2.8	3.4	2.5	2.9	3.6	2.5	2.9	3.8	2.5	2.9	4.0
36	3.8	3.1	70	3.4	3.6	4.1	3.4	3.8	4.5	3.4	3.8	4.8	3.4	3.9	5.0	3.4	4.0	5.4
37	4.8	3.7	63	4.0	4.4	5.1	4.1	4.6	6.1	4.1	4.8	6.7	4.1	4.9	7.5	4.1	5.1	8.8
38	7.6	5.3	50	5.7	6.4	7.7	5.8	6.9	9.7	5.9	7.2	11.4	5.9	7.5	13.5	6.0	8.0	17.3
39	7.7	5.3	44	6.0	6.7	7.9	6.1	7.2	9.2	6.2	7.4	10.0	6.3	7.6	10.9	6.3	7.9	12.1
40	10.4	7.6	65	8.5	9.4	11.0	8.7	10.0	12.6	8.7	10.2	13.6	8.8	10.5	14.7	8.8	10.8	16.2
41	9.6	6.4	40	6.8	7.8	10.5	6.9	8.7	16.0	7.0	9.4	21.6	7.0	10.1	30.2	7.1	11.3	48.9
42	5.8	4.2	80	4.7	5.2	6.4	4.8	5.6	7.8	4.8	5.9	8.8	4.8	6.1	10.1	4.9	6.4	12.3
43	6.7	4.9	74	5.7	6.2	6.9	5.8	6.4	7.5	5.8	6.5	7.7	5.8	6.6	8.0	5.9	6.7	8.3
44	5.3	3.7	80	4.2	4.9	6.2	4.3	5.3	7.5	4.4	5.4	8.3	4.4	5.6	9.2	4.4	5.8	10.7
45	5.0	3.7	62	4.0	4.4	5.0	4.1	4.6	5.7	4.1	4.8	6.2	4.2	4.9	6.8	4.2	5.1	7.7
46	6.1	4.3	51	4.7	5.2	6.3	4.8	5.6	7.8	4.8	5.9	9.0	4.8	6.1	10.4	4.9	6.5	12.9
47	8.3	5.7	43	6.3	7.0	8.2	6.4	7.5	9.8	6.5	7.8	10.9	6.6	8.1	12.3	6.6	8.5	14.4
48	12.2	8.4	35	9.3	10.6	13.1	9.5	11.4	16.2	9.5	11.8	18.2	9.6	12.2	20.6	9.6	12.7	24.2
49	6.2	4.4	55	4.8	5.3	6.1	4.9	5.6	7.2	5.0	5.8	8.0	5.0	6.0	8.9	5.1	6.3	10.3
50	11.2	8.2	39	8.7	9.8	12.3	8.8	10.6	16.9	8.9	11.2	21.2	9.0	11.9	27.2	9.0	12.8	39.4
51	4.8	3.9	66	4.2	4.5	4.9	4.3	4.6	5.2	4.3	4.7	5.4	4.3	4.8	5.6	4.3	4.8	5.9
52	8.8	6.7	45	7.2	7.9	9.2	7.4	8.4	10.9	7.4	8.7	12.1	7.5	8.9	13.6	7.5	9.3	16.0

Table 17: Estimated FCRP (m) for 0.5 m RSLR associated with 6.67%, 2%, 1%, 0.5% and 0.2% AEP (return periods of 15, 50, 100, 200 and 500 years). L, M and U indicate lower (5%), maximum likelihood and upper (95%) confidence estimates.

Trans #	Max in Hind-cast	99.8 %tile	# Events	6.7% AEP			2% AEP			1% AEP			0.5% AEP			0.2% AEP		
				L	M	U	L	M	U	L	M	U	L	M	U	L	M	U
1	6.5	4.9	58	5.3	5.8	6.7	5.4	6.1	8.0	5.4	6.3	8.9	5.4	6.5	10.1	5.5	6.8	11.9
2	7.8	5.7	45	6.2	6.8	7.9	6.3	7.2	9.3	6.3	7.5	10.4	6.4	7.7	11.6	6.4	8.0	13.6
3	4.2	3.6	75	3.9	4.0	4.3	3.9	4.1	4.5	3.9	4.2	4.6	3.9	4.2	4.7	3.9	4.2	4.8
4	4.8	4.1	62	4.3	4.6	5.2	4.4	4.7	5.6	4.4	4.8	5.8	4.4	4.8	6.0	4.4	4.9	6.2
5	4.6	4.0	62	4.2	4.5	4.9	4.3	4.6	5.1	4.3	4.6	5.2	4.3	4.6	5.3	4.3	4.6	5.5
6	5.0	3.8	75	4.2	4.6	5.3	4.3	4.9	5.9	4.3	5.0	6.3	4.4	5.1	6.7	4.4	5.2	7.2
7	3.2	2.9	100	3.0	3.1	3.3	3.0	3.2	3.4	3.1	3.2	3.4	3.1	3.2	3.5	3.1	3.2	3.5
8	3.2	2.7	77	2.9	3.1	3.5	2.9	3.2	3.8	2.9	3.2	3.9	2.9	3.3	4.1	2.9	3.3	4.3
9	4.0	3.2	76	3.5	3.8	4.2	3.6	3.9	4.4	3.6	3.9	4.6	3.6	4.0	4.7	3.6	4.0	4.9
10	3.3	2.7	82	3.0	3.2	3.5	3.0	3.2	3.8	3.0	3.3	3.9	3.0	3.3	4.1	3.0	3.4	4.3
11	3.2	2.6	76	2.9	3.1	3.4	2.9	3.1	3.6	2.9	3.2	3.7	2.9	3.2	3.9	2.9	3.2	4.0
12	3.5	2.8	81	3.1	3.3	3.7	3.1	3.4	4.0	3.1	3.5	4.2	3.2	3.5	4.4	3.2	3.6	4.7
13	3.2	2.7	84	2.9	3.1	3.5	2.9	3.2	3.8	2.9	3.2	4.0	2.9	3.2	4.2	2.9	3.3	4.5
14	3.3	2.8	78	3.0	3.2	3.6	3.0	3.3	3.8	3.0	3.3	3.9	3.0	3.3	4.0	3.0	3.4	4.2
16	3.4	2.8	83	3.0	3.3	3.6	3.1	3.4	4.0	3.1	3.4	4.1	3.1	3.5	4.3	3.1	3.5	4.6
18	3.1	2.6	70	2.8	3.0	3.4	2.8	3.1	3.6	2.9	3.1	3.7	2.9	3.2	3.9	2.9	3.2	4.0
19	3.1	2.6	80	2.8	3.0	3.3	2.9	3.1	3.5	2.9	3.1	3.6	2.9	3.1	3.7	2.9	3.2	3.8
20	3.6	2.9	73	3.2	3.4	3.7	3.2	3.5	3.9	3.2	3.5	4.0	3.2	3.6	4.1	3.3	3.6	4.3
22	3.3	2.7	77	3.0	3.2	3.6	3.0	3.3	3.8	3.0	3.3	3.9	3.0	3.4	4.1	3.0	3.4	4.2
24	3.1	2.6	73	2.8	3.0	3.3	2.8	3.1	3.6	2.8	3.1	3.7	2.8	3.1	3.8	2.9	3.2	3.9
25	3.5	2.8	77	3.1	3.3	3.6	3.2	3.4	3.9	3.2	3.5	4.0	3.2	3.5	4.1	3.2	3.5	4.2
26	3.1	2.8	94	3.0	3.0	3.2	3.0	3.1	3.2	3.0	3.1	3.2	3.0	3.1	3.2	3.0	3.1	3.2
27	3.4	2.7	74	3.0	3.2	3.6	3.0	3.3	3.8	3.1	3.4	3.9	3.1	3.4	4.0	3.1	3.4	4.1
28	3.3	2.8	96	3.1	3.2	3.4	3.1	3.2	3.5	3.1	3.3	3.5	3.1	3.3	3.6	3.1	3.3	3.6
29	3.1	2.6	91	2.8	3.0	3.3	2.8	3.1	3.6	2.9	3.2	3.8	2.9	3.2	4.1	2.9	3.3	4.4
30	3.8	3.0	83	3.2	3.5	4.1	3.3	3.7	4.6	3.3	3.8	5.0	3.4	3.9	5.4	3.4	4.1	6.1
31	3.5	2.7	80	3.1	3.4	4.0	3.1	3.5	4.5	3.1	3.6	4.8	3.1	3.7	5.2	3.1	3.8	5.7
32	3.9	3.1	84	3.4	3.7	4.1	3.5	3.8	4.4	3.5	3.9	4.6	3.5	3.9	4.8	3.5	4.0	5.0
33	5.8	4.2	61	4.9	5.5	6.5	4.9	5.7	7.2	4.9	5.8	7.5	5.0	5.9	7.9	5.0	5.9	8.3
34	3.7	2.9	75	3.3	3.5	4.0	3.3	3.7	4.3	3.3	3.7	4.5	3.3	3.8	4.7	3.3	3.8	5.0
35	3.6	2.9	69	3.2	3.5	3.8	3.2	3.5	4.1	3.3	3.6	4.2	3.3	3.6	4.3	3.3	3.6	4.4
36	4.8	3.6	70	3.9	4.2	4.9	4.0	4.5	5.7	4.0	4.7	6.4	4.0	4.9	7.1	4.1	5.1	8.4
37	5.5	4.3	61	4.6	5.0	5.8	4.7	5.3	6.7	4.7	5.4	7.4	4.7	5.6	8.2	4.8	5.8	9.5
38	8.2	5.9	48	6.4	7.0	8.3	6.5	7.5	10.1	6.6	7.8	11.5	6.6	8.2	13.3	6.7	8.6	16.3
39	8.3	6.0	47	6.5	7.2	8.7	6.6	7.8	11.0	6.6	8.1	12.9	6.7	8.5	15.4	6.7	9.0	19.8
40	10.9	8.1	69	9.0	9.9	11.4	9.1	10.4	13.1	9.2	10.7	14.3	9.2	11.0	15.5	9.3	11.3	17.4
41	10.3	7.0	38	7.5	8.5	10.8	7.6	9.3	15.0	7.7	9.9	19.0	7.8	10.5	24.6	7.8	11.4	35.9
42	7.3	5.2	84	5.9	6.6	7.9	6.0	7.1	9.2	6.1	7.3	10.1	6.2	7.5	11.1	6.2	7.8	12.7
43	7.3	5.9	65	6.4	7.0	8.1	6.5	7.3	9.1	6.5	7.4	9.7	6.5	7.6	10.4	6.5	7.7	11.3
44	6.3	4.9	69	5.5	6.0	6.7	5.6	6.2	7.1	5.6	6.2	7.4	5.6	6.3	7.6	5.7	6.4	7.8
45	5.8	4.4	60	4.7	5.1	5.8	4.8	5.4	6.6	4.8	5.5	7.3	4.9	5.7	8.0	4.9	5.9	9.1
46	6.7	4.8	53	5.2	5.7	6.7	5.3	6.1	8.1	5.3	6.3	9.2	5.4	6.6	10.5	5.4	6.9	12.8
47	8.9	6.1	41	6.7	7.5	8.8	6.9	8.1	10.7	7.0	8.4	12.0	7.0	8.7	13.7	7.1	9.2	16.3
48	12.7	9.3	36	9.9	10.9	13.2	10.0	11.8	17.3	10.1	12.3	20.8	10.1	12.9	25.6	10.2	13.7	34.8
49	6.8	5.0	55	5.4	5.8	6.6	5.5	6.2	7.7	5.5	6.4	8.6	5.5	6.6	9.6	5.6	6.9	11.4
50	11.7	8.7	39	9.2	10.3	12.8	9.3	11.1	17.4	9.4	11.7	21.7	9.5	12.4	27.7	9.5	13.3	39.9
51	5.3	4.4	66	4.7	5.0	5.4	4.8	5.1	5.8	4.8	5.2	6.0	4.8	5.3	6.2	4.8	5.4	6.5
52	9.3	7.2	45	7.7	8.4	9.7	7.9	8.9	11.4	7.9	9.2	12.6	8.0	9.4	14.1	8.0	9.8	16.5

Table 18: Estimated FCRP (m) for 1.0 m RSLR associated with 6.67%, 2%, 1%, 0.5% and 0.2% AEP (return periods of 15, 50, 100, 200 and 500 years). L, M and U indicate lower (5%), maximum likelihood and upper (95%) confidence estimates.

Trans #	Max in Hind-cast	99.8 %tile	# Events	6.7% AEP			2% AEP			1% AEP			0.5% AEP			0.2% AEP		
				L	M	U	L	M	U	L	M	U	L	M	U	L	M	U
1	7.4	5.7	55	6.1	6.6	7.7	6.2	7.0	9.0	6.2	7.2	10.0	6.3	7.4	11.2	6.3	7.7	13.1
2	8.9	6.6	46	7.0	7.7	8.9	7.2	8.2	10.8	7.2	8.5	12.2	7.3	8.8	14.0	7.3	9.3	17.0
3	4.7	4.0	65	4.3	4.6	5.0	4.3	4.6	5.3	4.3	4.7	5.4	4.3	4.7	5.6	4.3	4.7	5.7
4	5.3	4.6	63	4.8	5.1	5.7	4.9	5.3	6.1	4.9	5.3	6.4	4.9	5.3	6.6	4.9	5.4	6.8
5	5.5	4.5	56	4.8	5.1	5.6	4.9	5.3	6.0	4.9	5.4	6.3	4.9	5.4	6.6	4.9	5.5	6.9
6	5.5	4.4	77	4.8	5.2	5.7	4.9	5.4	6.1	4.9	5.4	6.4	4.9	5.5	6.6	5.0	5.6	6.9
7	3.8	3.2	79	3.4	3.7	4.3	3.5	3.9	5.0	3.5	4.0	5.6	3.5	4.1	6.2	3.5	4.3	7.3
8	3.7	3.2	79	3.4	3.6	3.9	3.4	3.6	4.2	3.4	3.7	4.3	3.4	3.7	4.4	3.4	3.7	4.6
9	4.4	3.6	77	4.0	4.2	4.5	4.0	4.3	4.7	4.0	4.3	4.8	4.0	4.4	4.9	4.0	4.4	5.1
10	3.8	3.2	81	3.5	3.7	4.0	3.5	3.7	4.3	3.5	3.8	4.4	3.5	3.8	4.5	3.5	3.9	4.7
11	3.7	3.1	76	3.4	3.6	3.9	3.4	3.6	4.1	3.4	3.7	4.2	3.4	3.7	4.4	3.4	3.7	4.5
12	3.8	3.3	91	3.5	3.6	3.8	3.5	3.7	4.0	3.5	3.7	4.1	3.5	3.8	4.1	3.6	3.8	4.2
13	3.7	3.1	81	3.3	3.6	4.0	3.4	3.7	4.4	3.4	3.7	4.6	3.4	3.7	4.8	3.4	3.8	5.1
14	3.6	3.2	95	3.4	3.5	3.8	3.4	3.6	4.0	3.4	3.6	4.2	3.4	3.7	4.3	3.4	3.7	4.5
16	4.2	3.3	80	3.8	4.1	4.6	3.8	4.2	4.9	3.8	4.2	5.0	3.8	4.3	5.1	3.8	4.3	5.3
18	3.6	3.1	70	3.3	3.5	3.9	3.3	3.6	4.2	3.3	3.6	4.3	3.3	3.7	4.5	3.3	3.7	4.6
19	3.6	3.1	82	3.3	3.5	3.9	3.3	3.6	4.1	3.3	3.6	4.3	3.3	3.7	4.4	3.3	3.7	4.6
20	3.8	3.3	92	3.5	3.6	3.9	3.5	3.7	4.0	3.5	3.7	4.1	3.5	3.8	4.2	3.5	3.8	4.4
22	3.7	3.2	77	3.4	3.6	3.9	3.5	3.6	4.0	3.5	3.7	4.0	3.5	3.7	4.1	3.5	3.7	4.1
24	3.7	3.1	73	3.3	3.5	3.9	3.4	3.6	4.2	3.4	3.7	4.3	3.4	3.7	4.4	3.4	3.7	4.6
25	3.9	3.3	77	3.6	3.8	4.1	3.6	3.9	4.2	3.6	3.9	4.3	3.7	3.9	4.4	3.7	4.0	4.5
26	3.6	3.1	75	3.3	3.5	3.8	3.3	3.6	4.1	3.3	3.6	4.2	3.3	3.6	4.3	3.3	3.6	4.5
27	3.6	3.2	98	3.4	3.5	3.7	3.4	3.6	3.8	3.4	3.6	3.8	3.4	3.6	3.8	3.4	3.6	3.9
28	3.6	3.1	121	3.3	3.5	3.7	3.3	3.5	4.0	3.3	3.6	4.1	3.3	3.6	4.3	3.4	3.7	4.5
29	3.6	3.1	74	3.3	3.5	3.9	3.3	3.6	4.2	3.3	3.7	4.4	3.3	3.7	4.6	3.4	3.7	4.8
30	4.3	3.6	86	3.9	4.1	4.6	3.9	4.3	4.9	4.0	4.3	5.1	4.0	4.4	5.2	4.0	4.4	5.5
31	4.0	3.4	92	3.6	3.9	4.5	3.6	4.1	5.1	3.7	4.1	5.5	3.7	4.2	5.9	3.7	4.3	6.6
32	4.4	3.6	85	3.9	4.2	4.6	4.0	4.3	5.0	4.0	4.4	5.2	4.0	4.4	5.5	4.0	4.5	5.8
33	6.8	5.8	57	6.2	6.6	7.2	6.3	6.8	7.7	6.3	6.8	8.0	6.3	6.9	8.2	6.3	6.9	8.6
34	4.2	3.4	76	3.8	4.0	4.5	3.8	4.2	4.9	3.8	4.2	5.1	3.8	4.3	5.3	3.8	4.3	5.6
35	4.1	3.5	70	3.7	4.0	4.3	3.8	4.0	4.6	3.8	4.1	4.7	3.8	4.1	4.8	3.8	4.1	5.0
36	5.3	4.1	69	4.7	5.1	5.7	4.7	5.2	6.0	4.8	5.3	6.1	4.8	5.3	6.3	4.8	5.4	6.4
37	6.2	4.9	60	5.2	5.6	6.4	5.3	5.9	7.3	5.3	6.0	8.0	5.3	6.2	8.8	5.4	6.4	10.1
38	8.9	6.5	48	7.0	7.7	9.0	7.1	8.2	11.0	7.2	8.5	12.6	7.2	8.9	14.6	7.3	9.3	18.1
39	9.0	6.5	48	7.1	7.9	9.3	7.2	8.4	11.2	7.3	8.7	12.5	7.3	9.0	14.0	7.4	9.3	16.4
40	11.4	8.7	66	9.5	10.5	12.2	9.7	11.0	14.1	9.7	11.3	15.3	9.8	11.6	16.7	9.8	11.9	18.8
41	11.0	7.7	38	8.2	9.2	11.6	8.3	10.1	16.3	8.3	10.7	20.8	8.4	11.3	27.3	8.5	12.3	40.7
42	8.2	6.7	71	7.4	7.9	8.9	7.4	8.1	9.5	7.5	8.2	9.8	7.5	8.3	10.1	7.5	8.4	10.5
43	7.8	6.7	62	7.2	7.7	8.4	7.2	7.8	8.8	7.2	7.8	9.0	7.2	7.9	9.2	7.2	7.9	9.4
44	7.0	5.8	66	6.3	6.7	7.5	6.3	6.9	8.0	6.4	7.0	8.2	6.4	7.0	8.5	6.4	7.1	8.8
45	6.3	4.9	60	5.2	5.6	6.3	5.3	5.9	7.1	5.3	6.0	7.8	5.4	6.2	8.5	5.4	6.4	9.6
46	7.2	5.2	51	5.7	6.2	7.2	5.8	6.6	8.5	5.8	6.8	9.5	5.8	7.1	10.6	5.9	7.4	12.5
47	9.4	6.5	41	7.0	7.9	9.6	7.2	8.6	12.3	7.2	9.0	14.6	7.3	9.4	17.5	7.3	10.1	22.8
48	13.2	9.8	38	10.3	11.4	14.0	10.4	12.3	18.8	10.5	12.9	23.3	10.6	13.6	29.7	10.6	14.5	42.6
49	7.3	5.5	56	5.9	6.3	7.1	6.0	6.7	8.2	6.0	6.9	9.1	6.1	7.1	10.0	6.1	7.4	11.7
50	12.2	9.2	39	9.7	10.8	13.3	9.8	11.6	17.9	9.9	12.2	22.2	10.0	12.9	28.2	10.0	13.8	40.4
51	5.9	4.9	66	5.3	5.5	5.9	5.3	5.7	6.3	5.3	5.8	6.6	5.4	5.8	6.8	5.4	5.9	7.1
52	9.8	7.7	45	8.2	8.9	10.2	8.4	9.4	11.9	8.4	9.7	13.1	8.5	9.9	14.6	8.5	10.3	17.0

Table 19: Estimated FCRP (m) for 2.0 m RSLR associated with 6.67%, 2%, 1%, 0.5% and 0.2% AEP (return periods of 15, 50, 100, 200 and 500 years). L, M and U indicate lower (5%), maximum likelihood and upper (95%) confidence estimates.

Trans #	Max in Hind-cast	99.8 %tile	# Events	6.7% AEP			2% AEP			1% AEP			0.5% AEP			0.2% AEP		
				L	M	U	L	M	U	L	M	U	L	M	U	L	M	U
1	9.4	7.2	47	7.7	8.3	9.3	7.8	8.7	10.7	7.9	9.0	11.6	7.9	9.2	12.6	8.0	9.5	14.3
2	10.3	7.8	46	8.3	9.0	10.4	8.4	9.6	12.5	8.5	9.9	14.1	8.5	10.3	16.3	8.6	10.8	20.0
3	5.4	4.9	90	5.1	5.3	5.4	5.2	5.3	5.6	5.2	5.4	5.7	5.2	5.4	5.8	5.2	5.5	5.9
4	6.3	5.6	63	5.8	6.1	6.7	5.9	6.3	7.1	5.9	6.3	7.4	5.9	6.3	7.6	5.9	6.4	7.8
5	6.5	5.7	60	6.0	6.3	7.0	6.0	6.5	7.5	6.0	6.5	7.7	6.0	6.6	8.0	6.0	6.6	8.4
6	6.1	5.4	74	5.8	6.0	6.4	5.8	6.1	6.6	5.8	6.1	6.7	5.8	6.1	6.8	5.8	6.2	6.8
7	5.7	4.7	89	5.1	5.5	6.4	5.1	5.7	7.0	5.2	5.8	7.3	5.2	5.8	7.7	5.2	5.9	8.1
8	4.7	4.1	76	4.3	4.5	4.9	4.4	4.6	5.2	4.4	4.7	5.4	4.4	4.7	5.5	4.4	4.7	5.7
9	5.4	4.6	81	4.9	5.1	5.5	4.9	5.3	5.9	5.0	5.3	6.0	5.0	5.4	6.2	5.0	5.4	6.4
10	4.7	4.1	78	4.3	4.6	4.9	4.4	4.7	5.2	4.4	4.7	5.4	4.4	4.8	5.6	4.4	4.8	5.9
11	4.8	4.2	82	4.4	4.6	5.0	4.4	4.7	5.3	4.5	4.8	5.5	4.5	4.8	5.6	4.5	4.9	5.9
12	4.6	4.2	79	4.4	4.5	4.7	4.4	4.5	4.8	4.4	4.6	4.8	4.4	4.6	4.9	4.4	4.6	4.9
13	4.7	4.1	80	4.3	4.6	5.0	4.4	4.7	5.4	4.4	4.7	5.6	4.4	4.7	5.8	4.4	4.8	6.1
14	5.0	4.1	72	4.4	4.8	5.6	4.5	5.0	6.5	4.5	5.1	7.1	4.5	5.3	7.9	4.5	5.4	9.1
16	5.2	4.5	76	4.9	5.1	5.4	4.9	5.2	5.7	4.9	5.2	5.8	4.9	5.3	5.9	4.9	5.3	6.0
18	4.7	4.2	70	4.4	4.6	5.0	4.4	4.7	5.3	4.4	4.7	5.4	4.4	4.8	5.6	4.4	4.8	5.8
19	5.0	4.1	82	4.3	4.7	5.4	4.4	5.0	6.5	4.4	5.1	7.3	4.5	5.3	8.4	4.5	5.6	10.3
20	4.8	4.2	78	4.4	4.6	4.9	4.4	4.7	5.2	4.5	4.7	5.3	4.5	4.8	5.5	4.5	4.8	5.6
22	4.6	4.1	76	4.3	4.5	4.9	4.4	4.6	5.2	4.4	4.7	5.3	4.4	4.7	5.4	4.4	4.7	5.6
24	4.7	4.1	75	4.3	4.5	4.9	4.4	4.6	5.1	4.4	4.7	5.2	4.4	4.7	5.4	4.4	4.7	5.5
25	4.9	4.3	75	4.6	4.8	5.1	4.6	4.9	5.3	4.6	4.9	5.4	4.6	4.9	5.5	4.6	5.0	5.6
26	4.7	4.1	76	4.3	4.5	4.9	4.4	4.6	5.1	4.4	4.6	5.2	4.4	4.7	5.4	4.4	4.7	5.5
27	4.6	4.1	79	4.3	4.5	4.9	4.3	4.6	5.2	4.3	4.6	5.5	4.3	4.7	5.7	4.3	4.7	6.0
28	4.8	4.4	84	4.8	4.8	4.8	4.8	4.8	4.8	4.8	4.8	4.8	4.8	4.8	4.8	4.8	4.8	4.8
29	4.6	4.1	77	4.3	4.5	4.9	4.3	4.6	5.2	4.3	4.6	5.4	4.3	4.7	5.6	4.3	4.7	5.8
30	5.3	4.6	82	4.9	5.1	5.6	4.9	5.3	5.9	5.0	5.3	6.1	5.0	5.4	6.3	5.0	5.4	6.6
31	5.0	4.4	92	4.6	4.9	5.5	4.6	5.1	6.2	4.7	5.2	6.6	4.7	5.2	7.2	4.7	5.4	8.0
32	5.5	4.7	86	5.0	5.3	5.7	5.1	5.4	6.1	5.1	5.5	6.2	5.1	5.5	6.4	5.1	5.6	6.6
33	8.9	6.7	59	7.2	7.8	9.0	7.3	8.3	10.7	7.4	8.6	12.0	7.4	8.9	13.7	7.5	9.3	16.6
34	5.2	4.5	78	4.8	5.0	5.5	4.8	5.2	5.8	4.8	5.2	6.1	4.8	5.3	6.3	4.8	5.3	6.5
35	5.1	4.5	71	4.7	5.0	5.3	4.8	5.0	5.6	4.8	5.1	5.7	4.8	5.1	5.8	4.8	5.1	6.0
36	6.6	5.5	62	5.9	6.2	6.7	6.0	6.4	7.1	6.0	6.5	7.3	6.0	6.5	7.5	6.1	6.6	7.8
37	7.7	6.3	56	6.7	7.0	7.7	6.8	7.3	8.4	6.8	7.5	8.8	6.8	7.6	9.3	6.9	7.8	10.1
38	10.3	7.8	42	8.4	9.1	10.2	8.5	9.5	11.7	8.6	9.8	12.7	8.7	10.1	13.9	8.7	10.4	15.7
39	10.4	7.8	62	8.3	9.1	10.6	8.5	9.7	13.1	8.5	10.1	15.1	8.6	10.6	17.7	8.7	11.2	22.6
40	12.4	9.6	70	10.6	11.6	13.5	10.7	12.1	15.2	10.8	12.4	16.2	10.8	12.6	17.3	10.9	12.9	18.8
41	12.3	8.9	37	9.3	10.4	12.8	9.5	11.3	17.5	9.5	11.9	21.8	9.6	12.5	28.1	9.6	13.5	40.8
42	11.7	9.2	71	10.1	10.9	12.3	10.2	11.3	13.6	10.3	11.6	14.4	10.3	11.8	15.2	10.3	12.0	16.4
43	10.4	7.8	50	8.4	9.1	10.5	8.5	9.7	12.4	8.6	10.0	13.9	8.7	10.4	15.7	8.7	10.8	18.7
44	8.6	7.1	62	7.5	8.3	10.3	7.5	8.7	12.7	7.6	8.9	14.4	7.6	9.1	16.6	7.6	9.4	20.3
45	7.3	5.9	60	6.2	6.6	7.3	6.3	6.9	8.1	6.3	7.0	8.8	6.4	7.2	9.5	6.4	7.4	10.6
46	8.2	6.2	51	6.7	7.2	8.0	6.9	7.6	8.9	6.9	7.8	9.5	7.0	8.0	10.1	7.0	8.2	11.0
47	10.4	7.3	47	7.7	8.5	10.4	7.9	9.3	14.3	7.9	9.9	18.2	8.0	10.6	24.2	8.1	11.7	37.1
48	14.1	10.8	38	11.3	12.4	14.9	11.5	13.3	19.6	11.5	13.9	24.0	11.6	14.5	30.1	11.6	15.5	42.4
49	8.3	6.8	70	7.2	7.6	8.4	7.3	7.9	9.2	7.4	8.1	9.8	7.4	8.3	10.4	7.4	8.5	11.4
50	13.2	10.2	39	10.7	11.8	14.3	10.8	12.6	18.9	10.9	13.2	23.2	11.0	13.9	29.2	11.0	14.8	41.4
51	7.0	6.0	67	6.3	6.6	7.0	6.4	6.7	7.4	6.4	6.8	7.6	6.4	6.9	7.9	6.5	7.0	8.2
52	10.8	8.7	45	9.2	9.9	11.2	9.4	10.4	12.9	9.4	10.7	14.1	9.5	10.9	15.6	9.5	11.3	18.0

G Hydrodynamic Model Description

The model, RiCOM, is based on the 3-dimensional shallow water equations which are derived from the Reynolds-averaged Navier-Stokes equations by using the hydrostatic assumption and the Boussinesq approximation. For incompressible flows the continuity equation (incompressibility constraint) is

$$\nabla \cdot \mathbf{u} + \frac{\partial w}{\partial z} = 0, \quad (4)$$

and the momentum equation expressed in nonconservative form is

$$\frac{D\mathbf{u}}{Dt} + f\hat{\mathbf{z}} \times \mathbf{u} + g\nabla\eta - \frac{\partial}{\partial z}(A_v \frac{\partial \mathbf{u}}{\partial z}) - \nabla \cdot (A_h \nabla \mathbf{u}) = 0, \quad (5)$$

where the coordinate directions (x, y, z) are aligned in the east, north, and vertical directions; $\mathbf{u}(x, y, z, t)$ is the horizontal velocity with components (u, v) ; $w(x, y, z, t)$ is the vertical velocity; f is the Coriolis parameter; $\hat{\mathbf{z}}$ is the upward unit vector; $\eta(x, y, t)$ is the distance from a reference elevation (mean sea level in this case) to the free surface; g is the gravitational acceleration; A_v and A_h are the kinematic vertical and horizontal viscosities, respectively; and ∇ is the horizontal gradient operator $(\partial/\partial x, \partial/\partial y)$.

The free surface equation is derived by vertically-integrating the continuity equation and using the kinematic free surface and bottom boundary conditions:

$$\frac{\partial \eta}{\partial t} + \nabla \cdot \left(\int_h^n \mathbf{u} dz \right) = 0, \quad (6)$$

where $h(x, y)$ is the bottom elevation measured from a reference elevation such that $H(x, y, t)$ is the total water depth given by $H = \eta - h$.

In this study, the vertically integrated 2-dimensional shallow water equations are used. The continuity equation is the same as the free surface equation given by (6), and the momentum equation is given by the vertical integral of (5). The continuity equation is

$$\frac{\partial \eta}{\partial t} + \nabla \cdot (H\mathbf{u}) = 0 \quad (7)$$

and the momentum equation expressed in nonconservative form is

$$\frac{d\mathbf{u}}{dt} + f\hat{\mathbf{z}} \times \mathbf{u} + g\nabla\eta + \frac{\tau_b}{\rho H} = 0 \quad (8)$$

where $\mathbf{u}(x, y, t)$ is now the depth-averaged horizontal velocity with components (u, v) ; $h(x, y)$ is the water depth measured from a reference elevation; $H(x, y, t)$ is the total water depth, $H = \eta - h$; and ρ is a reference density. The bottom stress τ_b is given by

$$\frac{\tau_b}{\rho} = C_D |\mathbf{u}| \mathbf{u} = \gamma H \mathbf{u} \quad (z = h), \quad (9)$$

where C_D is a bottom drag coefficient, and γ is defined by this equation.

Lateral boundary conditions for (4) - (6) generally fall into two categories: conditions at open (sea) boundaries and conditions at solid (land) boundaries. At open boundaries sea level η , radiation conditions, or a combination of these two are generally set. For this study, radiation conditions are used. At land boundaries, the normal component of velocity vanishes so that $(\mathbf{u} \cdot \hat{\mathbf{n}}) = 0$ where $\hat{\mathbf{n}}$ is the unit normal.

G.1 Time discretization

The equations are discretized in time using a semi-implicit method such that some of the terms in the equations are treated implicitly and some terms explicitly. The equations are evaluated in the time interval $\Delta t = t^{n+1} - t^n$ where the superscript denotes the time level. The distance through the time interval is given by the weight θ . Using this approximation, the free surface equation becomes

$$\frac{\eta^{n+1} - \eta^n}{\Delta t} + \nabla \cdot [\theta H^{n+1} \mathbf{u}^{n+1} + (1 - \theta) H^n \mathbf{u}^n] = 0 \quad (10)$$

The material derivative in the momentum equation is approximated using Eulerian-Lagrangian methods (ELM) or semi-Lagrangian methods (SLM) which take advantage of the simplicity of Eulerian methods and the enhanced stability and accuracy of Lagrangian methods. With ELM, only the term at time level n in the material derivative is evaluated at the foot of the trajectory. With SLM, all terms evaluated at time level n are evaluated at the foot of the trajectory so the entire equation is treated in a Lagrangian sense.

Using an ELM approach, the momentum equation becomes

$$\frac{\mathbf{u}^{n+1} - \mathbf{u}^*}{\Delta t} + \gamma \mathbf{u}^{n+1} + f \hat{\mathbf{z}} \times \mathbf{u}^m = g \nabla [\theta \eta^{n+1} + (1 - \theta) \eta^n] \quad (11)$$

where the superscripts $n + 1$ and n denote variables evaluated at the fixed nodes in the Eulerian grid at times t^{n+1} and t^n , respectively. At each time step, the velocity is integrated backwards with respect to time to determine where a particle starts at time t^n in order to arrive at a grid node at time t^{n+1} . This point is referred to as the foot of the trajectory. The superscript $*$ denotes a variable evaluated at the foot of the trajectory. The material derivative, the first term, thus has a very simple form.

The proper choice of tracking and interpolation methods is critical for maintaining accuracy with SLM and ELM approximations. Here, a power-series approach in time is used to calculate the trajectory and the global-quadratic interpolation method is used to evaluate the velocity at the foot of the trajectory [41].

Note that the viscosity term is treated implicitly to remove stability constraints whereas the horizontal viscosity term is neglected. The Coriolis term is integrated using a 3rd-order Adams-Bashforth scheme that is both efficient and avoids any major stability constraints [42].

G.2 Space discretization

The governing equations, (10) and (11), are approximated in space using finite element methods. The interpolation functions on each element are a piecewise constant approximation for sea level, η , and a linear approximation for velocity such that the normal velocity is constant on each edge. This element is known as the RT_0 element, the Raviart-Thomas element of lowest order.

Both the continuity equation and free surface equation reduce to a finite volume approximation using the RT_0 element. The free surface equation can be written in a finite volume form that conserves mass both locally and globally,

$$A_e \frac{\eta_e^{n+1} - \eta_e^n}{\Delta t} = \int_{\Gamma_e} [\theta(H^{n+1}u_n^{n+1}) + (1 - \theta)(H^n u_n^n)] d\Gamma_e, \quad (12)$$

where subscript e denotes the value for a specific element, subscript n denotes a normal component, A is the area in the x-y plane, and Γ_e is the bounding surface along the edges of the element. The last term has been converted from a volume divergence to a surface integral using the Gauss Divergence Theorem.

Likewise, the momentum equation becomes

$$\mathbf{A}\mathbf{u}_n^{n+1} = \mathbf{G} - g\theta\Delta t\Delta\eta^{n+1}\mathbf{Z}, \quad (13)$$

where \mathbf{A} is a block tridiagonal matrix that contains the mass matrix and the implicit terms arising from the vertical component of stress, \mathbf{u}_n is the vector of normal velocity on each edge, \mathbf{G} contains all the explicit terms and the known component of the implicit terms, and the last term is the implicit part of the surface pressure gradient term such that $\Delta\eta$ is a vector of the difference in element values across an edge and \mathbf{Z} is a vector of depth increments. The mass matrix is lumped using the technique for finite element node point integration (FE-NPI) described in [43]. This is equivalent to discretising the pressure gradient term using the distance between element centroids as measured orthogonal to an element edge.

The tridiagonal matrix at each velocity node can be inverted and u_n^{n+1} substituted into the free surface equation (12) to derive a discrete form of a wave equation that has only η at the $n + 1$ time level. Typically, η^{n+1} is solved for first, followed by a calculation of \mathbf{u}_n^{n+1} from (13). This method provides an efficient means to solve the equations. The specific forms of the matrices are shown in detail in [43].

G.3 Wetting and drying algorithm

Note that in the free surface equation and the discrete wave equation, water depth H is a factor in all the side flux terms. When $H = 0$ (i.e. the side is dry), there is automatically no water flux through that side. When all sides of an element are dry, the water level is stationary in time. Hence, wetting and drying can be implemented as a linear problem without any special treatment but are limited by the Courant number.

However, RiCOM now uses a nonlinear approach. Writing the free-surface equation in terms of finite volumes

$$\mathbf{V}_i(\eta_i^{n+1}) = \mathbf{V}_i(\eta_i^n) - \Delta t \sum_{l=1}^{S_i} s_{i,l} A_j^n [\theta u_j^{n+1} + (1 - \theta) u_j^n] \quad (14)$$

where $\mathbf{V}_i(\eta_i^n)$ is the volume in the i th column delimited by the free surface η^n , Δt is the time step size, $s_{i,l}$ is a sign function to identify the positive normal direction, θ is the implicitness factor, and u_j^n is the normal velocity on side j and time t^n .

Solving the momentum equation for u_j^{n+1} and substituting into (14), the resulting discrete wave equation can be written in compact form as

$$\mathbf{V}(\zeta) + \mathbf{T}\zeta = \mathbf{b} \quad (15)$$

where $\zeta_i = \eta_i^{n+1}$, $\mathbf{V}_i(\zeta) = \mathbf{V}_i(\eta_i^{n+1})$, and \mathbf{T} is the pressure gradient flux matrix.

Note that if the surface elevation is greater than the depth at any of the vertices of the element, the method reduces to the linear method. Otherwise, $\mathbf{V}(\eta)$ is a nonlinear function of η . An efficient Newton-type

algorithm for solving 15 is given by [44]

$$[\mathbf{P}(\zeta^m) + \mathbf{T}]\Delta\zeta^{m+1} = [\mathbf{V}(\zeta^m) + \mathbf{T}\zeta^m - \mathbf{b}] \quad (16)$$

where m is the iteration index, \mathbf{P} is the wetted area, and $\Delta\zeta^{m+1} = \zeta^{m+1} - \zeta^m$. In practice, this formulation converges rapidly so presents little overhead.